A Realisable Non–Linear Eddy Viscosity/Diffusivity Model for confined swirling flows

W. P. Jones
Imperial College London
Exhibition Road, London SW7 2AZ, UK

D. Lentini
Dipartimento di Meccanica e Aeronautica
Università degli Studi di Roma "La Sapienza"
Via Eudossiana 18, I–00184 Roma RM

Revised version, November 2007

Submitted to *Int. J. Heat Fluid Flow*

Corresponding author: D. Lentini

- tel: +39 0644585281
- fax: +39 06483729
- e–mail: diego.lentini@uniroma1.it

Abstract

A Non–Linear Eddy Viscosity/Diffusivity Model for turbulent flows is presented, featuring quadratic constitutive relationships for both Reynolds stresses and scalar fluxes. Model coefficients are defined by enforcing compliance with fundamental experimental evidence, and realisability of both the velocity and scalar fields, which is achieved by making coefficients depend upon an appropriately defined strain parameter. The model is also shown to satisfy joint–realisability. The model is extensively tested against experimental results for confined swirling flows, encompassing a wide range of values of the swirl number, momentum and density ratios. The results unambiguously indicate a remarkable, uniform improvement over standard modelling. Further, previous work on the subject of nonlinear models is reviewed.

1 Introduction

Non–Linear Eddy Viscosity Models (NLEVMs) appear as potential candidates to replace the well–tried k–ϵ model [20, 21] (with minor re–optimisation of the model constants as in [25]) as a 'workhorse' for the computation of turbulent flows. The k–ϵ and other linear eddy viscosity models are known to exhibit fundamental shortcomings, particularly in their inability to reproduce flows featuring recirculation and/or swirl, streamline curvature and secondary flows in non–circular ducts. Similar deficiencies are evident in flows involving scalar transport related in particular to the largely underestimated ratio of stream wise to transverse turbulent fluxes in heated/cooled channel or pipe flows and scalar fluctuations in buoyant flows that are also poorly reproduced. To correct this behaviour, non–linear models, here termed Non–Linear Eddy Diffusivity Models (NLEDMs), have been proposed. However, finding a suitable replacement for the standard k–ϵ model appears to be a major challenge; despite the above mentioned weaknesses, it nonetheless features undeniable virtues. These are related to its relative ease of use and robustness and to the fact that it is well-calibrated, so that it leads to acceptable results in many cases. This is in spite of the fact that while a term–by–term analysis of the model undoubtedly reveals inadequacies, the resulting negative impact on the quality of predictions is limited, due to compensating errors. A plethora of NLEVMs and (to a smaller extent) NLEDMs have been proposed in recent years. Such a proliferation is clearly a consequence of the large number of undetermined coefficients appearing in the non–linear expansions of Reynolds stresses and scalar fluxes, which can be specified according to different criteria. A categorisation of these models can be attempted, based on the following criteria:

(a) possible inclusion of higher–order derivatives.

(b) choice of variables to identify turbulent velocity and length scales.

(c) order of the polynomial expansion.

(d) relationship to second–moment models.

As far as item (a) is concerned, it can be observed that by far the vast majority of non–linear models adopt forms which only feature the first derivatives of the mean velocity components and of the mean scalar. However, a small number of NLEVMs, [63, 19] start from a form including the second–derivatives of the mean velocity components. The latter choice, although supposedly involving some advantage raises the order of the resulting RANS equations above that of the original Navier-Stokes equation with the consequence that boundary conditions are required for the mean velocity components and their spatial gradients.

Item (b) also features two options, with one being overwhelmingly more popular than the other. In fact, whereas practically all models choose the square root of the turbulent kinetic energy $\sqrt{k}$ as a turbulent velocity scale, either the mechanical dissipation rate ϵ or a (pseudo)–vorticity ω can be used to construct a turbulent time scale, with the latter approach representing an extension of the (linear) k–ω model [51, 74]. The vast majority of non–linear models adopt ϵ as the second variable,

whilst a few prefer ω [74, 1, 35, 60]. One–equation NLEVMs, involving only an equation for k, have also been proposed [61, 62].

The nearly unanimous consensus above is not replicated for the two remaining items. In particular, as far as item (c) is concerned, NLEVMs have been proposed adopting quadratic [63, 12, 53, 54, 61, 32, 13, 49, 44, 73, 11, 3], cubic [8, 56, 28, 69, 1, 35, 39, 60], or even quartic (though incomplete) [7, 69] constitutive relationships for the Reynolds stress. In contrast practically all the proposed NLEDMs [26, 17, 2, 23, 41, 47, 48, 3, 38, 67] belong to the quadratic family.

Lastly, item (d) refers to the methodology adopted in formulating NLEVMs and NLEDMs. While some authors simply postulate a non–linear expression for turbulent stresses and/or fluxes, and determine the coefficients by imposing appropriate conditions, others recover a non–linear expression by simplifying second–moment closure models. In particular, Algebraic Stress Models (ASMs) assume that the anisotropy tensor is conserved along a streamline (though a different condition has also been proposed [50] to account for curvature effects), and that the rate of change and diffusion of the anisotropy is linearly related to the rate of change and diffusion of the turbulence kinetic energy. This approach, initiated by Rodi [45, 46], leads to implicit forms for the Reynolds stresses. The resulting expressions are rather complex, and cannot be strictly classified as NLEVMs; furthermore ASMs are often reported to give convergence problems in numerical solutions. Gatski and Speziale [12, 64] and Girimaji [14, 15], by adopting a non–linear form in an appropriate tensor basis, recover an explicit non–linear expression, termed an Explicit Algebraic Stress Model (EASM), see also [40, 13, 23, 11, 70]. On the basis of their close relationship to second–moment closures the authors claim these to be more powerful than ordinary NLEVMs. However, it has to be said that a full tensor basis requires five terms; when fewer terms are used, as is usually the case, the resulting model amounts rather to a least–square fit. Furthermore singular expressions can result in same situations, thereby requiring a 'regularization' of the expressions for the stresses [12, 13], which then depart from those of the parent second–moment model. Other realisability constraints related to EASMs are discussed by Durbin and Petterson–Reif [10] and Weis *et al.* [72].

A similar distinction can be drawn for scalar transport between those in which a non–linear expression for the scalar fluxes is simply postulated and those in which a similar form is obtained as a result of simplifications to second–moment closures for the scalar fluxes. Such simplifications lead to implicit algebraic expression for the latter; again, by adopting an appropriate basis, the model can be expressed in explicit form, sometimes termed an Explicit Algebraic Heat flux Model (EAHM), [71, 42]. The full basis in this case requires ten terms and the development of such a full model has not yet been attempted. Thus current models can be considered as least–square fits to full EAHMs. As for the Reynold stresses singularities can arise for the scalar fluxes and 'regularization' is then required. An alternative widely used expression for the scalar fluxes is the Generalised Gradient Diffusion Hypothesis (GGDH), stemming from application of a higher–order model [9] to heat fluxes [26], which also conserves some relation to second–moment models. It has been used extensively [17, 2, 47, 67]; a higher–order version (HOGGDH) has also been proposed [38].

The near–wall behaviour of non–linear models have been addressed by a number of authors [23, 35, 44, 50, 3, 42]. Non–linear models have also been extended to deal with high–speed flows [39], two–phase flows [33, 34, 75], buoyant flows [73, 59], fluids exhibiting very small (such as liquid metals) or large (liquids) Prandtl numbers, [2, 71], or even viscoelastic behaviour, [36, 37]. This serves to emphasise the practical importance currently attached to non–linear constitutive equations. A critical point in the derivation of non–linear models is the determination of the model coefficients. Compliance with experiments, realisability, and criteria borrowed from thermodynamics have been used. Incidentally, the circumstance that the modelled equations can switch their nature from parabolic to hyperbolic due to an inappropriate choice of the model coefficients was recognised by Weigand *et al.* [71].

In the present work non-linear constitutive equations, involving quadratic forms, are devised to allow both the Reynolds stresses and scalar fluxes to be determined. A quadratic form is selected in order to depart relatively little from the well–tried standard k–ϵ model and also because, in previous work, the effect of higher–order terms proved to be relatively small [1]. As in all similar approaches the present formulation involves a significant number of undetermined parameters. However, it is shown that the imposition of realisability constraints - positivity of the normal stresses and satisfaction of Schwarz's inequality by the shear stresses and compliance with extremum principles for scalar quantities - results in a substantial reduction in the number of free parameters. The remaining free constants and parameters are then determined by recourse to measurements in simple canonical shear flows. The enforcement of realisability constraints on the Reynolds stresses is achieved mainly through consideration of thin shear flows and mixing layers and, while realisable results are not guaranteed under all general strain conditions, this is clearly a prerequisite to ensuring realisability in more complex flows. None of the currently available Non-Linear Eddy Diffusivity Models (NLEDM) appear to take account of extremum principles, a consequence of which is that the maximum and minimum values of a strictly conserved scalar quantity arising in any steady solution must lie on the boundaries of the solution domain. Satisfaction of this constraint is of paramount importance in many practical applications and a failure to do so can have catastrophic consequences in computations; species mass fractions less than zero and greater than unity can arise and, for heat transfer problems, temperature profiles may violate the second law. In the present paper a condition on the model coefficients is explicitly enforced to ensure compliance with extremum principles. The resulting complete model, termed a Non-Linear Eddy Viscosity and Diffusivity Model (NLEVDM), is also shown to satisfy joint–realisability.

Section 2 presents the proposed form of the constitutive relationship for the Reynolds stresses, and discuss the criteria adopted to identify the NLEVM coefficients. These are defined as a function of an appropriate strain parameter, with the aim of preventing the occurrence of unphysical situations. Similarly, Section 3 presents the form of the constitutive relationships for scalar fluxes, and discusses the criteria adopted to identify the NLEDM coefficients, which are also prescribed as a function of the previously defined strain parameter, again in order to ensure physically realizable solutions. The performance of the proposed models is investigated in Section 4. The accurate prediction of flows in combustion chamber and furnaces,

in which swirl is routinely adopted, and more generally in devices involving heat and/or mass transfer, calls for improved modelling of both Reynolds stresses and scalar fluxes. Accordingly, the models are applied to a range of confined swirling flows, covering a range of swirl numbers and momentum and density ratios; both inert and reacting flows are considered. In the test cases considered the details of the flow in the vicinity of the walls do not play a significant role - attention is focused on measurements taken well inside the flow. Accordingly, a wall–function approach is adopted in order to save computer time. The results of the computations are compared extensively with measurements of mean velocity and the components of the Reynolds stress and scalar fluxes, thereby enabling an accurately evaluation of the performance of the models. Finally, conclusions are drawn in Section 5.

2 Non–Linear Eddy Viscosity Model (NLEVM)

In formulating constitutive relationships for stress it is conventional to separate the velocity gradient $\partial u_i/\partial x_j$ into a symmetric part - the rate of deformation, $S_{ij} = \frac{1}{2}\left(\partial u_i/\partial x_j + \partial u_j/\partial x_i\right)$ – and antisymmetric part – the rotation tensor, $\Omega_{ij} = \frac{1}{2}\left(\partial u_i/\partial x_j - \partial u_j/\partial x_i\right)$. The reasoning behind this separation is that the stress in a fluid continuum is independent of fluid rotation and the stress then depends only on the rate of deformation; a solid body rotation of a fluid element does not induce a stress. However the Reynolds stresses originate from the convection terms and as a consequence they are not invariant under rotation. Under these circumstances the separation of the velocity gradient into rate of deformation and rotation appears to offer little advantage and is therefore not adopted. To formulate a constitutive equation we first write:

$$\widetilde{u_i'' u_j''} = \widetilde{u_i'' u_j''}\left(k, \epsilon, \frac{\partial u_i}{\partial x_j}\right) \tag{1}$$

where nothing has been omitted from the argument of equation (1). The Cayley–Hamilton theorem, [31] can now be used to write the following most general expression for $\widetilde{u_i'' u_j''}$:

$$\begin{aligned}\widetilde{u_i'' u_j''} \;=\; & a\delta_{ij} + b\left(\frac{\partial \tilde{u}_i}{\partial x_j} + \frac{\partial \tilde{u}_j}{\partial x_i}\right) + c\left(\frac{\partial \tilde{u}_i}{\partial x_k}\frac{\partial \tilde{u}_k}{\partial x_j} + \frac{\partial \tilde{u}_j}{\partial x_k}\frac{\partial \tilde{u}_k}{\partial x_i}\right) \\ & + d\frac{\partial \tilde{u}_i}{\partial x_k}\frac{\partial \tilde{u}_j}{\partial x_k} + e\,\frac{\partial \tilde{u}_k}{\partial x_i}\frac{\partial \tilde{u}_k}{\partial x_j}\end{aligned} \tag{2}$$

where a, b, c, d, e are functions of k, ϵ and the first, second and third invariants of $\partial u_i/\partial x_j$.

Equation (2) is used as a basis for constructing a constitutive relationship for the Reynolds stresses, hopefully more powerful than standard eddy viscosity models. The result is a Non-Linear Eddy Viscosity Model (NLEVM). If account is taken of dimensional homogeneity, symmetry and the fact that $\widetilde{u_i'' u_i''} = 2k$ then the following

expression can be constructed [52, 55]:

$$\widetilde{u_i'' u_j''} = \frac{1}{3}\left[2\,k - 2\,\alpha_1 \frac{k^2}{\epsilon}\frac{\partial \tilde{u_k}}{\partial x_k} - 2\,\alpha_2 \frac{k^3}{\epsilon^2}\frac{\partial \tilde{u_l}}{\partial x_k}\frac{\partial \tilde{u_k}}{\partial x_l} - (\alpha_3 + \alpha_4)\frac{k^3}{\epsilon^2}\frac{\partial \tilde{u_l}}{\partial x_k}\frac{\partial \tilde{u_l}}{\partial x_k}\right]\delta_{ij} + \\ + \alpha_1 \frac{k^2}{\epsilon}\left(\frac{\partial \tilde{u_i}}{\partial x_j} + \frac{\partial \tilde{u_j}}{\partial x_i}\right) + \alpha_2 \frac{k^3}{\epsilon^2}\left(\frac{\partial \tilde{u_i}}{\partial x_k}\frac{\partial \tilde{u_k}}{\partial x_j} + \frac{\partial \tilde{u_j}}{\partial x_k}\frac{\partial \tilde{u_k}}{\partial x_i}\right) + \\ + \alpha_3 \frac{k^3}{\epsilon^2}\frac{\partial \tilde{u_i}}{\partial x_k}\frac{\partial \tilde{u_j}}{\partial x_k} + \alpha_4 \frac{k^3}{\epsilon^2}\frac{\partial \tilde{u_k}}{\partial x_i}\frac{\partial \tilde{u_k}}{\partial x_j} \tag{3}$$

where the $\alpha' s$ are functions of the invariants. The quantity contained within [ ] on the *rhs* of equation (3) is chosen to ensure that both sides of the equation contract to $2k$.

The isotropic contribution to the stress in equation (3) can be adsorbed into the definition of pressure so that when substituted into the momentum equation the result is:

$$\frac{\partial \overline{\rho}\,\tilde{u}_i}{\partial t} + \frac{\partial \overline{\rho}\,\tilde{u}_l\,\tilde{u}_i}{\partial x_l} = -\frac{\partial \overline{p}^*}{\partial x_i} + \frac{\partial}{\partial x_l}\left[\mu\left(\frac{\partial \tilde{u_i}}{\partial x_l} + \frac{\partial u_l}{\partial x_i}\right)\right] - \\ - \frac{\partial}{\partial x_l}\overline{\rho}\left[\alpha_1 \frac{k^2}{\epsilon}\left(\frac{\partial \tilde{u_i}}{\partial x_l} + \frac{\partial \tilde{u_l}}{\partial x_i}\right) + \alpha_2 \frac{k^3}{\epsilon^2}\left(\frac{\partial \tilde{u_i}}{\partial x_k}\frac{\partial \tilde{u_k}}{\partial x_l} + \frac{\partial \tilde{u_l}}{\partial x_k}\frac{\partial \tilde{u_k}}{\partial x_i}\right) + \right. \\ \left. + \alpha_3 \frac{k^3}{\epsilon^2}\frac{\partial \tilde{u_i}}{\partial x_k}\frac{\partial \tilde{u_l}}{\partial x_k} + \alpha_4 \frac{k^3}{\epsilon^2}\frac{\partial \tilde{u_k}}{\partial x_i}\frac{\partial \tilde{u_k}}{\partial x_l}\right] + \overline{\rho}\,g_i \tag{4}$$

where p^* is the pseudo–pressure.

The values of k and ϵ are obtained from the standard form of the $k-\epsilon$ model with the constant values $C\epsilon_1 = 1.44$; $C\epsilon_2 = 1.92$; $\sigma_k = 1.0$ and $\sigma_\epsilon = 1.3$. The only modification required is to the turbulence energy production rate:

$$P = -\widetilde{u_m'' u_n''}\frac{\partial \tilde{u}_m}{\partial x_n} \tag{5}$$

which is evaluated using Eq. (3) so that:

$$P = -\frac{1}{3}\left[2\,\tilde{k} - 2\,\alpha_1 \frac{\tilde{k}^2}{\tilde{\epsilon}}\frac{\partial \tilde{u_k}}{\partial x_k} - 2\,\alpha_2 \frac{\tilde{k}^3}{\tilde{\epsilon}^2}\frac{\partial \tilde{u_l}}{\partial x_k}\frac{\partial \tilde{u_k}}{\partial x_l} - (\alpha_3 + \alpha_4)\frac{\tilde{k}^3}{\tilde{\epsilon}^2}\frac{\partial \tilde{u_l}}{\partial x_k}\frac{\partial \tilde{u_l}}{\partial x_k}\right]\frac{\partial \tilde{u}_m}{\partial x_m} - \\ - \left[\alpha_1 \frac{\tilde{k}^2}{\tilde{\epsilon}}\left(\frac{\partial \tilde{u_m}}{\partial x_n} + \frac{\partial \tilde{u_n}}{\partial x_m}\right) + \alpha_2 \frac{\tilde{k}^3}{\tilde{\epsilon}^2}\left(\frac{\partial \tilde{u_m}}{\partial x_k}\frac{\partial \tilde{u_k}}{\partial x_n} + \frac{\partial \tilde{u_n}}{\partial x_k}\frac{\partial \tilde{u_k}}{\partial x_m}\right) + \right. \\ \left. + \alpha_3 \frac{\tilde{k}^3}{\tilde{\epsilon}^2}\frac{\partial \tilde{u_m}}{\partial x_k}\frac{\partial \tilde{u_n}}{\partial x_k} + \alpha_4 \frac{\tilde{k}^3}{\tilde{\epsilon}^2}\frac{\partial \tilde{u_k}}{\partial x_m}\frac{\partial \tilde{u_k}}{\partial x_n}\right]\frac{\partial \tilde{u}_m}{\partial x_n} \tag{6}$$

The problem is now the determination of the model coefficients, α_1, α_2, α_3 and α_4. As an aid to this a dimensionless strain parameter, A is introduced:

$$A = \frac{\tilde{k}}{\tilde{\epsilon}}\left(\frac{\partial \tilde{u_k}}{\partial x_l}\frac{\partial \tilde{u_k}}{\partial x_l}\right)^{1/2} \tag{7}$$

To determine the coefficients the following information is used:

1. As suggested by previous work it is presumed that $c_\mu (\equiv -\alpha_1) \rightarrow 0.09$ as $A \rightarrow 0$.

2. The measurements of anisotropy obtained in the low strain nearly homogeneous shear flows of [4], see Appendix A.

3. Positivity of the Reynolds normal stresses.

4. Satisfaction of Schwarz's inequality for the Reynolds shear stresses.

If equation (3) is applied, in conjunction with the turbulence kinetic energy equation, to nearly homogeneous shear flows then the following expressions can be derived for the components of the isotropy tensor, b_{ij}

$$b_{12} = \frac{\widetilde{u''v''}}{2k} = \frac{\alpha_1}{2} A \tag{8}$$

$$b_{11} = \frac{\widetilde{u''^2}}{2\tilde{k}} - \frac{1}{3} = \frac{2\alpha_3 - \alpha_4}{6} A^2 \tag{9}$$

$$b_{22} = \frac{\widetilde{v''^2}}{2\tilde{k}} - \frac{1}{3} = \frac{-\alpha_3 + 2\alpha_4}{6} A^2 \tag{10}$$

$$b_{33} = \frac{\widetilde{w''^2}}{2\tilde{k}} - \frac{1}{3} = -\frac{\alpha_3 + \alpha_4}{6} A^2 \tag{11}$$

Equations (8) to (11) can be rearranged to yield:

$$-\alpha_1 = c_\mu = -\frac{2\, b_{12}}{A} \tag{12}$$

$$\alpha_3 = \left(\frac{4\, b_{11} + 2\, b_{22}}{A^2} \right) \tag{13}$$

$$\alpha_4 = \left(\frac{2\, b_{11} + 4\, b_{22}}{A^2} \right) \tag{14}$$

From Eq. (9–11) it is seen that normal anisotropies for $A = 0$ are identically zero, irrespective of the values of the model coefficients.

In the nearly homogeneous shear flow of [4] the mean strain parameter A is found to have value around 2.9 and the values of the components of the anisotropy tensor are found to be approximately constant with values $b_{11} \approx 0.137$ and $b_{22} \approx -0.088$. If these are inserted into equations (13) and (14) then the following values result:

$$\alpha_3 = 0.04395$$

$$\alpha_4 = -0.0093$$

However these constant values are only appropriate in this particular flow and α_3 and α_4 must be at least a function of A if negative normal stresses are to be avoided

in general. For example, for an arbitrary value of the strain parameter A, Equations (9 – 11) with the α's constant give:

$$\frac{\widetilde{u''^2}}{k} = \frac{2}{3} + 0.0324A^2 \tag{15}$$

$$\frac{\widetilde{v''^2}}{k} = \frac{2}{3} - 0.02085A^2 \tag{16}$$

$$\frac{\widetilde{w''^2}}{k} = \frac{2}{3} - 0.01775A^2 \tag{17}$$

While $\widetilde{u''^2}$ is always positive both $\widetilde{v''^2}$ and $\widetilde{w''^2}$ will become negative at high values of mean strain. The most critical situation is for the transverse component where negative values arise for:

$$A > \left(\frac{2/3}{0.02085}\right)^{1/2} = 5.65$$

To avoid this behaviour it is necessary to assume that α_3 and α_4 be, rather than constants, functions of the strain parameter, and in particular that they decrease at least as fast as A^{-2} for large values of A. It is thus tentatively assumed that:

$$\alpha_3 = \left(\frac{\alpha_3}{[c_\mu(A)]^2}\right)\Bigg|_{A=2.9} [c_\mu(A)]^2 = c_3\,[c_\mu(A)]^2 \tag{18}$$

and

$$\alpha_4 = \left(\frac{\alpha_4}{[c_\mu(A)]^2}\right)\Bigg|_{A=2.9} [c_\mu(A)]^2 = c_4\,[c_\mu(A)]^2 \tag{19}$$

where $c_3 \approx 3.6$ and $c_4 \approx -0.75$ as experimental results [4] for $A = 2.9$ indicate a corresponding $c_\mu = 0.111$.

2.1 Positivity of normal stresses

If equations (18–19) are substituted into equations (9–11) then in order to prevent $\widetilde{v''^2}$ and $\widetilde{w''^2}$ attaining negative values it is easy to show that the function $c_\mu(A)$ must obey the constraint:

$$c_\mu(A) < \frac{1}{A}\sqrt{\frac{1}{0.5\,c_3 - c_4}} \approx \frac{0.626}{A} \tag{20}$$

2.2 Schwarz's inequality

The Reynolds shear stress can be expressed, Equation (8), as:

$$\frac{\left|\widetilde{u''v''}\right|}{k} = A \cdot c_\mu(A) \tag{21}$$

and Schwarz's inequality requires that the ratio

$$\frac{(\widetilde{u''v''})^2}{\widetilde{u''^2}\widetilde{v''^2}} = \frac{9[c_\mu(A)\cdot A]^2}{\{2+(2c_3-c_4)\,[c_\mu(A)\cdot A]^2\}\,\{2+(2c_4-c_3)\,[c_\mu(A)\cdot A]^2\}} \tag{22}$$

be less than unity, resulting in the condition:

$$\left(5c_3c_4 - 2\left[{c_3}^2+{c_4}^2\right]\right)[c_\mu(A)\cdot\ A]^4 + (2\,[c_3+c_4])\,[c_\mu(A)\cdot A]^2 + 4 > 0 \tag{23}$$

The roots of the associated equation are then:

$$[c_\mu(A)\cdot A]^2 = \frac{-\left(2\,[c_3+c_4]\right) \mp \sqrt{\left(2\,[c_3+c_4]\right)^2 - 16\left(5c_3c_4 - 2\,[{c_3}^2+{c_4}^2]\right)}}{2\left(5c_3c_4 - 2\,[{c_3}^2+{c_4}^2]\right)} \tag{24}$$

The only physical solution results in the constraint

$$c_\mu(A) < \frac{1}{A}\sqrt{\frac{-\left(2\,[c_3+c_4]\right) - \sqrt{\left(2\,[c_3+c_4]\right)^2 - 16\left(5c_3c_4 - 2\,[{c_3}^2+{c_4}^2]\right)}}{2\left(5c_3c_4 - 2\,[{c_3}^2+{c_4}^2]\right)}} \approx \frac{0.525}{A} \tag{25}$$

2.3 Coefficient α_2

The coefficient α_2 is as yet undetermined, since it multiplies a term which is zero in thin shear layers. Its determination then requires consideration of more complex flows. Shih *et al.* [54] utilises Rapid Distortion Theory (RDT) to recover a relationship among the coefficients, but RDT is known to have little relevance to practical flows and so the approach is not adopted here. Instead α_2 is provisionally assigned a value of zero. This can be relaxed later if necessary.

2.4 Proposed NLEVM form

The only outstanding issue is the evaluation of α_1 or equivalently c_μ. A number of authors have proposed different expressions for c_μ as a function of a strain parameter, *e.g.* [54, 30], with a general feature being a value slightly above that of the standard $k-\epsilon$ model, *ie* $c_\mu = 0.09$, for moderate strain rates, (A less than 3), and an asymptotic decay as the inverse of the strain parameter. Although the former specification has some justification, e.g., experiments at $A = 2.9$ indicate $c_\mu = 0.111$ - see Appendix A - it has been found in the present investigation that adopting $c_\mu > 0.09$ invariably leads to an excessive centreline velocity decay in jets. For this reason the following form is proposed for c_μ $(= -\alpha_1)$ as a function of the strain parameter:

$$\begin{array}{rcll} c_\mu & = & c_{\mu,0} \;=\; 0.09 & \text{for} \quad A \le A^* \\ & = & c_{\mu,0} \;+\; a_\mu\,(A - A^*)^3 & \text{for} \quad A^* \le A \le A^{**} \\ & = & b_\mu/A & \text{for} \quad A > A^{**} \end{array} \tag{26}$$

where to satisfy constraints (20) and (25) the following values have been selected:

$$A^* = 4 \qquad\qquad A^{**} = 5$$

The coefficients a_μ and b_μ are determined by requiring that the first and second derivatives of c_μ be continuous at A^* and A^{**} leading to:

$$a_\mu = -0.0056 \qquad\qquad b_\mu = 0.422$$

In summary the NLEVM coefficients are:

$$\alpha_1 = -c_\mu(A), \qquad \alpha_2 = 0, \qquad \alpha_3 = c_3\,[c_\mu(A)]^2, \qquad \alpha_4 = c_4\,[c_\mu(A)]^2 \tag{27}$$

with $c_3 = 3.6$ and $c_4 = -0.75$. The functional dependence of c_μ on A given by equation (26) is plotted in Figure (1), together with the constraints (20) and (25), with the latter being more stringent. Both are both shown to be satisfied. Figure (2) shows the correlation coefficient R_{uv}, ie, the square root of Equation (22) resulting from the proposed model; it is shown to remain bounded with a value well below unity in all cases, thus ensuring realisability. It is worth noting that the standard k–ϵ model fails to obey this constraint for A larger than about 7. As a check of the performance of the proposed model, the anisotropy in the high strain nearly homogeneous shear flow of Harris *et al.*, [18] (see Appendix B) for which $A = 5.5$, is considered. The representative experimentally determined values are:

$$b_{11} = 0.168, \qquad b_{22} = -0.134, \qquad b_{33} = -0.034 \tag{28}$$

compared with the predicted values:

$$b_{11} = 0.236, \qquad b_{22} = -0.151, \qquad b_{33} = -0.085 \tag{29}$$

As is evident the anisotropies are somewhat over predicted. This could be corrected, but requires a more complex form than (18) and (19) for the coefficients α_3 and α_4 (ie, c_3 and c_4 function of A, rather than constant). Such an extension is not pursued in the present context.

3 Non–Linear Eddy Diffusivity Model (NLEDM)

An approach parallelling that adopted in Sec. 2 is adopted for the scalar flux. If the scalar flux is presumed to depend only on the turbulence energy and dissipation rates and the mean velocity and scalar gradients then, analogous to equation (2), the following general expression, [31], can be written:

$$-\widetilde{u_i'' \xi''} \;=\; \beta_1 \frac{\tilde{k}^2}{\tilde{\epsilon}} \frac{\partial \tilde{\xi}}{\partial x_i} \;+\; \frac{\tilde{k}^3}{\tilde{\epsilon}^2} \left(\beta_2 \frac{\partial \tilde{u_i}}{\partial x_k} \;+\; \beta_3 \frac{\partial \tilde{u_k}}{\partial x_i} \right) \frac{\partial \tilde{\xi}}{\partial x_k} \tag{30}$$

where ξ represents a scalar quantity and the turbulent scalar flux is now prescribed as a function of both the mean velocity and scalar gradients.

As in equation (3) the model coefficients are in principle functions of the invariants of $\partial u_i/\partial x_j$ and $\partial \xi/\partial x_i$. However an approach similar to that followed for the $\alpha's$ will be adopted to determine the three model coefficients, β_1, β_2 and β_3. The criteria selected to evaluate them in the course of the present research is described below.

First, all solutions of the exact equation for a strictly conserved scalar variable satisfy extremum principles, [43]; the magnitude of any local extrema present in the initial conditions must decay with time. A consequence of this is that the maximum and minimum values of the scalar in any resulting steady solution will occur on the boundaries of the solution domain. The satisfaction of this condition is clearly desirable in any model and can be used to establish constraints on the values of the coefficients. The precise value of the coefficients are determined by enforcing compliance of the model with measurements of the stream wise and transverse components of the scalar flux in equilibrium shear layers.

The equation describing the mean value of a strictly conserved scalar, with the scalar flux given by equation (30) can be written in the form:

$$\rho \frac{\partial \tilde{\xi}}{\partial t} \; + \; \rho \, \tilde{u}_l \frac{\partial \tilde{\xi}}{\partial x_l} \; = \; \frac{\partial}{\partial x_l} \left[\left(\frac{\mu}{\sigma} \delta_{kl} + \Gamma_{kl} \right) \frac{\partial \tilde{\xi}}{\partial x_k} \right] \tag{31}$$

with:

$$\Gamma_{kl} = \overline{\rho} \frac{k^2}{\epsilon} \left(\beta_1 \delta_{kl} + \beta_2 \frac{k}{\epsilon} \frac{\partial \tilde{u}_l}{\partial x_k} + \beta_3 \frac{k}{\epsilon} \frac{\partial \tilde{u}_k}{\partial x_l} \right) \tag{32}$$

Equation (31) can now be used to evaluate the incremental change in ξ with time at any position within the solution domain, *viz*:

$$\begin{aligned} \xi(t+dt) &= \xi(t) + \frac{\partial \xi}{\partial t} dt \\ &= \xi(t) + \left(\frac{1}{\rho} \frac{\partial}{\partial x_l} \left[\left(\frac{\mu}{\sigma} \delta_{kl} + \Gamma_{kl} \right) \frac{\partial \tilde{\xi}}{\partial x_k} \right] - \tilde{u}_l \frac{\partial \tilde{\xi}}{\partial x_l} \right) dt \end{aligned} \tag{33}$$

To ensure conformity with the extremum principle the equation (31) can first be written in principal axes whereby Γ_{ij} becomes:

$$\Gamma_{\alpha\alpha} = \rho \frac{k^2}{\epsilon} \left[\beta_1 + (\beta_2 + \beta_3) \frac{k}{\epsilon} \frac{\partial \tilde{u_\alpha}}{\partial x_\alpha} \right] \tag{34}$$

with no summation implied on α.

At an extrema $\partial \xi / \partial x_i = 0 \; \forall \; i$ so that the change in ξ over a time interval dt at the extrema, for high turbulence Reynolds numbers, is given by:

$$\begin{aligned} \xi(t+dt) &= \xi(t) + \frac{\partial \xi}{\partial t} dt \\ &= \xi(t) + \textstyle\sum_{\alpha=1}^{3} \Gamma_{\alpha\alpha} \dfrac{\partial^2 \xi}{\partial x_\alpha \partial x_\alpha} dt \end{aligned} \tag{35}$$

Satisfaction of the solutions of equation (31) with the extremum principle then requires:

$$\Gamma_{\alpha\alpha} \geq 0 \qquad \alpha = 1, 2, 3 \tag{36}$$

This clearly imposes conditions on the values of β_1, β_2 and β_3. In general the coefficients must satisfy:

$$\beta_1 + (\beta_2 + \beta_3) \, A \geq 0 \tag{37}$$

To develop matters further it will be presumed that $\beta_1 > 0$ and that $\beta_2 = -\beta_3$. This latter choice is made purely on the grounds of simplicity and the presumption can be relaxed later if found to be necessary. The conditions imposed by equation (36) are then automatically satisfied.

To determine the values of the two coefficients the model will be applied to a two-dimensional equilibrium thin shear layer. In two-dimensions the components of the scalar flux are:

$$-\widetilde{u''\xi''} = \frac{k^2}{\epsilon}\left\{\beta_1\frac{\partial\tilde{\xi}}{\partial x} + \beta_2\frac{k}{\epsilon}\left[\left(\frac{\partial\tilde{u}}{\partial x}\frac{\partial\tilde{\xi}}{\partial x} + \frac{\partial\tilde{u}}{\partial y}\frac{\partial\tilde{\xi}}{\partial y}\right) - \left(\frac{\partial\tilde{u}}{\partial x}\frac{\partial\tilde{\xi}}{\partial x} + \frac{\partial\tilde{v}}{\partial x}\frac{\partial\tilde{\xi}}{\partial y}\right)\right]\right\} \tag{38}$$

$$-\widetilde{v''\xi''} = \frac{k^2}{\epsilon}\left\{\beta_1\frac{\partial\tilde{\xi}}{\partial y} + \beta_2\frac{k}{\epsilon}\left[\left(\frac{\partial\tilde{v}}{\partial x}\frac{\partial\tilde{\xi}}{\partial x} + \frac{\partial\tilde{v}}{\partial y}\frac{\partial\tilde{\xi}}{\partial y}\right) - \left(\frac{\partial\tilde{u}}{\partial y}\frac{\partial\tilde{\xi}}{\partial x} + \frac{\partial\tilde{v}}{\partial y}\frac{\partial\tilde{\xi}}{\partial y}\right)\right]\right\} \tag{39}$$

In a thin shear layer $\partial\tilde{u}/\partial x$, $\partial\tilde{v}/\partial x$ and $\partial\tilde{v}/\partial y$ are negligible compared with $\partial\tilde{u}/\partial y$ while $\partial\tilde{\xi}/\partial x$ is negligibly small relative to $\partial\tilde{\xi}/\partial y$. Thus

$$-\widetilde{u''\xi''} \;\simeq\; \beta_2\frac{\tilde{k}^3}{\tilde{\epsilon}^2}\frac{\partial\tilde{u}}{\partial y}\frac{\partial\tilde{\xi}}{\partial y} \tag{40}$$

$$-\widetilde{v''\xi''} \;\simeq\; \beta_1\frac{\tilde{k}^2}{\tilde{\epsilon}}\frac{\partial\tilde{\xi}}{\partial y} \tag{41}$$

In equilibrium shear layers it is known that experimental measurements of the y–component of the scalar flux are well reproduced by the expression:

$$-\widetilde{v''\xi''} = \frac{c_\mu}{\sigma_t}\frac{k^2}{\epsilon}\frac{\partial\tilde{\xi}}{\partial y} \tag{42}$$

with $C_\mu = 0.09$ and $\sigma_t = 0.7$. Thus to make Eq. (42) consistent with Eq. (41):

$$\beta_1 = \frac{c_\mu}{\sigma_t} \tag{43}$$

The relationship (42) is relevant to measurements at relatively low strain. However, in the framework of the present model it is assumed that its validity can be carried over a wider range of strain rates by adopting c_μ as a function of the strain rate parameter, A as defined by Eq. (26). With this proviso the coefficient β_1 is presumed given by:

$$\beta_1 = \frac{c_\mu(A)}{\sigma_t} \tag{44}$$

This function is plotted, as a function of the strain parameter A, in Fig. 3.

To determine β_2 use will be made of the experimental observation that the ratio of the two components of the scalar fluxes is approximately constant in near equilibrium flows; namely

$$\left(\frac{\widetilde{u''\xi''}}{\widetilde{v''\xi''}}\right)_{exp} \approx 2 \tag{45}$$

Combining equations (40) and (41) gives for this ratio:

$$\begin{pmatrix} \widetilde{u''\xi''} \\ \widetilde{v''\xi''} \end{pmatrix} = \frac{\beta_2}{\beta_1} \frac{k}{\epsilon} \frac{\partial \tilde{u}}{\partial y} \tag{46}$$

For an equilibrium flow the velocity gradient can be replaced by the strain parameter, Eq. (7) so that equation (46) can be written as:

$$\beta_2 = -2 \frac{\beta_1}{A} \tag{47}$$

However this would entail $\beta_2 \to \infty$ for $A \to 0$. A more cautious choice can be obtained if use is made of the finding that:

$$\frac{\sqrt{c_\mu}\, k\, \partial \tilde{u}/\partial y}{\epsilon} \simeq 1 \tag{48}$$

so that in equilibrium flows equation (46) can also be written:

$$\beta_2 = -2\beta_1 \sqrt{C_\mu} \tag{49}$$

As above it is assumed that the validity of equation (49) can be carried over to a wider range of strain rates by adopting c_μ as a function of the strain rate parameter so that:

$$\beta_2 = -2 \frac{[c_\mu(A)]^{3/2}}{\sigma_t} \tag{50}$$

The coefficient β_2 is also plotted in Fig. 3 as a function of the strain parameter. Finally the third coefficient is determined as

$$\beta_3(A) = -\beta_2(A) \tag{51}$$

Note that adopting Eq. (30) to represent the scalar fluxes entails that the production term in the scalar variance equation:

$$P_{\widetilde{\xi''^2}} \;=\; -\,2\,\widetilde{u_k''\xi''}\,\frac{\partial \tilde{\xi}}{\partial x_k} \tag{52}$$

must be expanded as

$$P_{\widetilde{\xi''^2}} = +2\beta_1 \frac{k^2}{\epsilon} \frac{\partial \tilde{\xi}}{\partial x_l} \frac{\partial \tilde{\xi}}{\partial x_l} + 2\frac{k^3}{\epsilon^2} \left(\beta_2 \frac{\partial \tilde{u_l}}{\partial x_k} + \beta_3 \frac{\partial \tilde{u_k}}{\partial x_l} \right) \frac{\partial \tilde{\xi}}{\partial x_k} \frac{\partial \tilde{\xi}}{\partial x_l} \tag{53}$$

though with the condition equation (51) the second term on the *rhs* turns out to be identically zero.

3.1 Joint realisability

It will now be checked that the above NLEDM satisfies another crucial requirement of the closure approximation if solutions are to have physical significance.
Schwarz's inequality for the stream wise and transverse Reynolds fluxes requires

$$(\widetilde{u''\xi''})^2 \;\leq\; \widetilde{u''^2} \cdot \widetilde{\xi''^2} \tag{54}$$

$$(\widetilde{v''\xi''})^2 \;\leq\; \widetilde{v''^2} \cdot \widetilde{\xi''^2} \tag{55}$$

where $\widetilde{\xi''^2}$ is the scalar variance. In a mixing layer with a single non zero component of the velocity gradient, the normal components of interest of the Reynolds stress can be expressed, according to the NLEVM, by Equations (15,16). As far as the scalar variance is concerned, in an equilibrium mixing layer this can be obtained from a balance between the scalar production and dissipation rates, which with the linear relaxation model leads to:

$$2\beta_1 \frac{k^2}{\epsilon}\left(\frac{\partial\tilde{\xi}}{\partial y}\right)^2 = C_d \frac{\epsilon\,\widetilde{\xi''^2}}{k} \tag{56}$$

where C_d is a model constant with the commonly accepted value

$$C_d \;=\; 2.0$$

This leads to the following expression for the scalar variance:

$$\widetilde{\xi''^2} = 2\frac{\beta_1(A)}{C_d}\frac{k^3}{\epsilon^2}\left(\frac{\partial\tilde{\xi}}{\partial y}\right)^2 \tag{57}$$

Then, with consideration of Equations. (40), (41), (15) and (16), Schwarz's inequalities can be recast as:

$$[\beta_2(A)]^2 \frac{\tilde{k}^6}{\tilde{\epsilon}^4}\left(\frac{\partial\tilde{u}}{\partial y}\right)^2\left(\frac{\partial\tilde{\xi}}{\partial y}\right)^2 \;\leq\; \left\{\frac{2}{3} \;+\; \frac{1}{3}(2c_3 - c_4)\cdot[c_\mu(A)\cdot A]^2\right\}\cdot 2\,\frac{\beta_1(A)}{C_d}\,\frac{\tilde{k}^4}{\tilde{\epsilon}^2}\left(\frac{\partial\tilde{\xi}}{\partial y}\right)^2 \tag{58}$$

$$[\beta_1(A)]^2 \frac{\tilde{k}^4}{\tilde{\epsilon}^2}\left(\frac{\partial\tilde{\xi}}{\partial y}\right)^2 \;\leq\; \left\{\frac{2}{3} \;+\; \frac{1}{3}(2c_4 - c_3)\cdot[c_\mu(A)\cdot A]^2\right\}\cdot 2\,\frac{\beta_1(A)}{C_d}\,\frac{\tilde{k}^4}{\tilde{\epsilon}^2}\left(\frac{\partial\tilde{\xi}}{\partial y}\right)^2 \tag{59}$$

After some manipulation Equations. (59) and (58) result in the respective constraints,

$$|\beta_1(A)| \;\leq\; \sqrt{\frac{2}{C_d}\left\{\frac{2}{3} \;+\; \frac{1}{3}(2c_4 - c_3)\cdot[c_\mu(A)\cdot A]^2\right\}} \tag{60}$$

$$|\beta_2(A)| \;<\; \frac{1}{A}\sqrt{\frac{2}{C_d}\,\beta_1(A)\left\{\frac{2}{3} \;+\; \frac{1}{3}(2c_3 - c_4)\cdot[c_\mu(A)\cdot A]^2\right\}} \tag{61}$$

The correlation coefficients between u and ξ and between v and ξ:

$$R_{u\xi} = \frac{\left|\widetilde{u''\xi''}\right|}{\left[\widetilde{u''^2} \cdot \widetilde{\xi''^2}\right]^{1/2}} \tag{62}$$

$$R_{v\xi} = \frac{\left|\widetilde{v''\xi''}\right|}{\left[\widetilde{v''^2} \cdot \widetilde{\xi''^2}\right]^{1/2}} \tag{63}$$

are plotted in Fig. 4 for $0 \leq A \leq 10$ in the fully and for the present choice of the coefficients and indicate that the model under consideration ensures realisable solutions in this respect under all circumstances. It can be noted that the correlation coefficients can attain quite high values for highly strained flows. While such high A's are likely to occur [1] rarely in statistically stationary flows they may well occur during transients, particularly for an injudicious choice of initial conditions. The model formulated should prevent the appearance of unphysical and potentially destabilising solutions in these circumstances.

4 Test cases

In this Section the performance of the closures formulated in section 2 and 3 is investigated through application to swirling flows and comparison of the results with experimental data. In order to characterise the different test cases three dimensionless groups are considered. The strength of swirl is characterised by the swirl number, defined as:

$$S = \frac{1}{R_e} \frac{\int_0^{R_e} \overline{\rho}\, r^2\, \tilde{u}\, \tilde{w}\, dr}{\int_0^{R_e} \overline{\rho}\, r\, \tilde{u}^2\, dr} \tag{64}$$

where R_e denotes the radius of the inlet duct. Swirl number accordingly represents the ratio of the axial flux of angular momentum to the axial flux of linear momentum ($\tilde{u}$ and $\tilde{w}$ denote the stream wise and tangential mean velocity components). The swirl number has a major effect on determining the flow pattern in purely swirling flows [5, 6, 68, 29]: with increasing S, the jet spreads progressively outwards, until for a critical value of around 0.6 recirculation sets on, with the appearance of a toroidal reverse flow region. The critical value may be different for flows subjected to very large density variations, see Section 4.2.

For flows featuring a central jet surrounded by a swirling co-flow (as in one of the test cases considered) an axial momentum ratio is also defined:

$$J = \frac{\int_0^{R_j} \overline{\rho}\, r\, \tilde{u}^2\, dr}{\int_{R_j}^{R_e} \overline{\rho}\, r\, \tilde{u}^2\, dr} \tag{65}$$

[1] In the near wall region of a fully turbulent boundary layer $A \approx 3.3$

where R_j is the radius of the centre jet nozzle. The presence of a central, non-swirling jet can suppress or displace the recirculation region for high values of swirl numbers, S.

In combusting flows the density varies over a wide range due to both temperature and molar mass changes, the latter being due to varying fluid composition. Inert flows may also experience variable density effects, in this case either because of differing molar masses or temperatures of the inflowing central jet and co-flow fluids. It is then useful to introduce a density ratio:

$$\Upsilon = \frac{\rho_j}{\rho_o} \tag{66}$$

where the subscript j denotes conditions in the central nozzle and where the subscript o indicates conditions in the incoming (swirling) co-flow. In combusting flows oxidiser it generally enters as a co-flow. The density ratio strongly affects the mixing of the jet and the swirling co-flow.

In choosing the appropriate test cases for comparison, attention has been directed to ensure that they:

- include both inert and reacting flows (ie, jets and flames);
- encompass a range of swirl numbers;
- encompass a range of axial momentum ratios;
- encompass a range of density ratios;
- that detailed measurements of both mean quantities and second–moments (Reynolds stresses and scalar fluxes) are available;
- that measurements are reported at several downstream stations.

With these considerations in mind two test cases have been identified:

1. inert jets issuing into swirling air [57, 58], with a swirl number $S = 2.25$, momentum ratios J spanning the range from 0.032 to 0.475 and density ratios Υ covering the range 0.228, 1 and 1.52;
2. swirling hydrogen/air flames [65], with swirl numbers $S = 0.02$, 0.6 and associated momentum ratios $J = 36.8$, 0.412 respectively, while the density ratio Υ is 0.069.

These test cases are discussed in detail in the next two subsections. Numerical simulation are performed by means of the finite–volume code BOFFIN [22].

4.1 Swirling jets (So *et al.* 1984, 1987)

An extensive experimental study on (inert) jets injected into co-flowing swirling air is reported by So *et al.* [57, 58]. The swirl number is fixed at 2.25, while the momentum ratio number is varied between 0.032 and 0.475 in the test cases selected

for comparison in the present investigation; the density ratio assumes the values 0.228, 1.0, 1.52 through use of different jet fluids. A schematic of the test rig is shown in Figure (5). The jet nozzle comprises a sudden expansion 12.7 mm upstream of the discharge plane, introduced in order to ensure that the jet flow is fully turbulent even for jet Reynolds numbers close to the transitional value. The jet diameter at the discharge plane is $D_j = 8.73$ mm and this is taken as a reference length for these test cases. The nozzle is surrounded by an annulus of inner diameter 53.18 mm and outer diameter $D_o = 125$ mm through which swirling air flows. The swirl is generated by a flat vane swirler with vanes at an angle of 66^o giving a swirl number of 2.25. The Reynolds number of the co-flowing swirling air is maintained constant in all cases with a value of 54900 (based on the average velocity across the tube of diameter D_o). Both the central jet and annulus flow issue into a duct of diameter $D_o = 125$ mm.

In the numerical simulations reported below, the inflow boundary conditions are estimated on the basis of velocity measurements taken at an axial location close to the discharge plane. Not all of the large number of conditions measured provide suitable test cases, either because there are insufficient measurements available or that negative stream wise velocities are reported very close to the inlet plane. Accordingly the cases that are retained for validation are labelled as follows

- air jets (unity density ratio):
  - $u_j = 25.4$ m/s, resulting in $Re_j = 14380$, $J = 0.068$ (case 31);
  - $u_j = 66.8$ m/s, $Re_j = 37820$, $J = 0.475$ (case 32);
- helium/air jets (with two different compositions):
  - $\Upsilon = 0.228$, $Re_j = 2970$, $u_j = 36.5$ m/s, $J = 0.032$ (case 42);
- carbon dioxide jets, $\Upsilon = 1.52$:
  - $u_j = 25.4$ m/s, $Re_j = 28430$, $J = 0.104$ (case 51);
  - $u_j = 54.0$ m/s, $Re_j = 60440$, $J = 0.472$ (case 52).

where u_j denotes the jet bulk velocity. It is to be noted that the inflowing helium/air jet is fully turbulent in spite of the relatively low jet Reynolds number as a result of the upstream sudden expansion of the nozzle.

For the simulations inflow profiles are derived from measurements taken at station $x/D_j = 1$ for cases 31, 32, 51 and 52, and at station $x/D_j = 3$ for case 42. There are no measurements of the mean and rms profiles of the radial velocity component at these stations. The mean radial velocity is thus presumed to be negligible while the rms is set equal to that of the tangential component. The turbulence energy dissipation rate at the inflow boundary is specified on the basis of estimated dissipation length scales. The sensitivity of predictions to the specified dissipation rates at inflow boundaries is small for all the flows presently considered. Providing sensible values are chosen the only major influence is on the predicted length of

the potential core. In all cases the computed results to be presented were obtained using a 150×100 grid in the axial and radial directions respectively. The grid is slightly stretched, with grid expansion ratios of 1.015 in the axial direction (1.02 for case 31) and 1.02 in the radial one. Computations with finer and coarser grids have demonstrated that the results described below are definitely grid–independent.

Figures (6)–(10) show, for each case, the radial profiles of the stream wise and tangential mean velocities and the two corresponding rms velocities, at several axial stations. Results are presented against a radial coordinate, made dimensionless with respect to both jet diameter D_j (lower scale) and the external diameter D_o (upper scale). Test cases 31 and 32 are constant–density, hence only a comparison with the results obtained with the standard k–ϵ and NLEVM considered. The remaining cases involve variable–density and results with a full range of models is shown. The results compared correspond to: k–ϵ; k–ϵ for velocity with NLEDM for the scalar; NLEVM for the velocities with k–ϵ for the scalar and the complete model, ie, NLEVM with NLEDM. As is evident the model used for the scalar flux appears to exert very little influence on the velocities, both mean and rms but this is almost certainly due to the density ratios under consideration being relatively close to unity.

Due to the relatively limited density variations, averages are indicated with the over bar conventionally associated with Reynolds averaging, while the computational results imply Favre–averages (density weighted averages). The difference is generally found to be quite small for the velocity components; as an illustration measurements, ([24]) in an helium–air mixing layer with a density ratio as small as 0.138 exhibit a difference between the density weighted and unweighted mean velocities of less than 1%. The difference can however be more substantial for scalar quantities.

Since the main purpose is to compare the results obtained with the various models (and space limitations prevent a more detailed discussion) the comparisons are reported in the following concise form for each of the different cases:

Case 31:
- $\overline{u}$ appears to be greatly improved by NLEVM, especially close to the axis in the near field. The standard k–ϵ greatly over predicts the initial velocity decay rate on the centreline, while predicting too high velocities at the last measuring station. The NLEVM appears to correctly reproduce the observed trends, resulting in an improved agreement also off–axis at downstream stations;
- $\overline{w}$ results are more or less the same for both k–ϵ and NLEVM, the former performing somewhat better in the near field, the latter in the far field;
- $(\overline{u'^2})^{1/2}$ is uniformly improved with NLEVM compared with the $k-\epsilon$ model
- $(\overline{w'^2})^{1/2}$ same as above.

Case 32:
- $\overline{u}$ appears to be somewhat improved by NLEVM, both in the near and far fields;
- $\overline{w}$ is about the same for the two models;
- $(\overline{u'^2})^{1/2}$ is better reproduced by NLEVM, except at the axis in the near field (where neither models perform particularly well);
- $(\overline{w'^2})^{1/2}$ is also generally better with NLEVM, except at the axis in the near field.

Case 42: $\overline{u}$ the performance of k–ϵ and NLEVM is comparable, the former being somewhat better at the axis, the latter off–axis, but both models fail to reproduce the recirculation bubble located around $r/D_j = 2$;

$\overline{w}$ is somewhat better predicted by NLEVM in the far field;

$(\overline{u'^2})^{1/2}$ is better predicted with NLEVM, best with NLEVM and NLEDM;

$(\overline{w'^2})^{1/2}$ same as above.

Case 51: $\overline{u}$ is markedly better with NLEVM;

$\overline{w}$ is somewhat better predicted by NLEVM;

$(\overline{u'^2})^{1/2}$ is markedly better predicted by NLEVM, especially in the near field;

$(\overline{w'^2})^{1/2}$ is slightly better predicted by NLEVM at station $x/D_j = 20$, somewhat worse at $x/D_j = 40$.

Case 52: $\overline{u}$ is again markedly better with NLEVM (though in the near field NLEDM give a somewhat reduced level of agreement at the axis);

$\overline{w}$ is also somewhat better predicted by NLEVM;

$(\overline{u'^2})^{1/2}$ poorly predicted by both models, nonetheless NLEVM appears to give somewhat better agreement off–axis;

$(\overline{w'^2})^{1/2}$ is somewhat better predicted by NLEVM at station $x/D_j = 20$, slightly worse at $x/D_j = 40$.

Taken together the results obtained with the proposed non linear eddy viscosity and diffusivity models appear, on the whole, to be encouraging. As noted by So *et al.*, [58], an efficient mixing enhancement by swirl requires that the heavier fluid is injected from the central pipe (ie, as a jet, case 51 and 52) because in this case the jet fluid is pushed radially outward by centrifugal force. In the reverse situation (lighter jet fluid, case 42), the jet tends instead to be confined close to the centreline, thereby inhibiting mixing of the two streams.

4.2 Swirling flame (Stårner and Bilger, 1986)

The experiments carried out by Stårner and Bilger at the University of Sydney [65], see also [66], represent the only test case known to the authors of a swirling flow involving scalar mixing, which report detailed measurements of all three components of the scalar flux together with the mean scalar. Even in these very detailed experiments there is a lack of certain information for validation, as radial profiles of mean mixture fraction are not reported. The test rig is sketched in Figure (11). Hydrogen is injected through the central nozzle of inner diameter 9.9 mm at a bulk velocity of 139 m/s (with a maximum at the centreline of 177.1 m/s), giving a jet Reynolds number of 13000. Air is supplied *via* a surrounding annulus (inner diameter 10.72 mm, outer diameter 18.4 mm) with a swirling motion (generated by vanes at 45^o to the axial direction; see below for bulk velocity); a further outer region (inner diameter 19.1 mm, bounded by a square duct of 305 mm side) supplies unswirled air at a bulk velocity $u_e = 12$ m/s. Two operating conditions are considered, an

essentially non–swirling case with $S = 0.02$ (when the bulk velocity of swirling air is limited to 4 m/s), and a swirling one with $S = 0.60$ (bulk velocity of swirling air 37.8 m/s). The latter value of S usually corresponds to the onset of recirculation; however, in the present configuration no flow reversal is observed.

Measurements include, for the swirling case, inflow profiles (at $x/D_j = 0.2$) of the three mean velocity components, and their intensity, so that inflow boundary conditions are unambiguous. Similar profiles are not available for the non swirling case, giving rise to some uncertainty in the inflow conditions to be applied. In the present simulations the inflow velocity profile for $S = 0.02$ is obtained from the corresponding swirling one, by scaling all velocities in the annulus by a factor 4/37.8. Turbulence energy dissipation rate inflow profiles are, as previously, specified in terms of estimate length scales. For combustion a thermo-chemical closure model based on the conserved scalar approach with a presumed β-pdf is adopted to describe hydrogen-air combustion. As for the previous case predictions are shown for the following model combinations: standard k–ϵ; k–ϵ+NLEDM; NLEVM+k–ϵ and NLEVM + NLEDM. A 150×100 grid in the axial and radial directions is again used with a moderate grid expansion ratios (1.002 in the axial direction, 1.012 in the radial one).

The inverse centreline velocity, expressed in the form:

$$\frac{\overline{u_{0j}}}{\overline{u_0}} = \frac{\left[\overline{u_{CL}} - \overline{u_e}\right]_{x=0}}{\left[\overline{u_{CL}} - \overline{u_e}\right]_x}$$

is plotted in Figure 12.

The results for the full range of modelling options considered above are shown. Experiments indicate that the centreline velocity of the swirling flame has an initial decay rate much steeper than the corresponding non swirling flame. Predictions by the standard k–ϵ show that this effect is poorly reproduced in the simulations, this being one of its well–known deficiencies. Instead, predictions by the NLEVM show that this model is able to reproduce the behaviour for swirling flows quite correctly, thus marking an important improvement over standard modelling. As far as scalar transport modelling is concerned, it is seen to play a minor role as far as the velocity field is concerned, at least in this case. However, the results obtained with the combined NLEVM and NLEDM exhibit significant difference for swirling and non swirling flow in the far field. Unfortunately, measurements of the non swirling case are limited to the region up to $x/D = 40$, and do not shed light on the issue.

Figures (13) and (14) display radial profiles taken at three axial stations located at $x/D_j = 26$, 40, 80, for the swirling case only. Results are presented in Cartesian form, rather than axisymmetric, to illustrate the asymmetry in some of Reynolds stress and scalar flux components as well as experimental scatter. Figure (13a) shows radial profiles of the dimensionless mean stream wise excess velocity, ie, the quantity

$$\frac{\overline{u_0}}{\overline{u_{0j}}} = \frac{\left[\overline{u} - \overline{u_e}\right]_{r,x}}{\left[\overline{u_{CL}} - \overline{u_e}\right]_{x=0}} = \frac{\left[\overline{u} - \overline{u_e}\right]_{r,x}}{165.1}$$

A markedly improved prediction by NLEVM is evident near the centreline, especially at the first station, consistently with the results of Figure (12). In a similar fashion,

Figure (13b) shows comparisons for the tangential velocity components in the form

$$\frac{\overline{w}}{\overline{u_{0j}}} \;=\; \frac{[\overline{w}]_{r,x}}{[\overline{u_{CL}} \,-\, \overline{u_e}]_{x=0}} \;=\; \frac{[\overline{w}]_{r,x}}{165.1}$$

In this latter case the predictions with k–ϵ and NLEVM are about the same accuracy compared with measurements with a somewhat unclear effect of scalar transport modelling.

Figure (14) displays the components of the Reynolds stress tensor. In particular, Figures (14a–c) show results for the normal components, while Figures (14d–f) show the corresponding shear stress profiles. The normal components are more accurately reproduced by the NLEVM, this being a possible key to the markedly improved results shown in Figure (13a) with the model. Predictions for the shear stresses $\widetilde{u''v''}$ and $\widetilde{v''w''}$ do not show significant difference with the two models though $\widetilde{u''w''}$, which is predicted to be identically zero by the k–ϵ model, is at least qualitatively reproduced by NLEVM. Predictions for $\widetilde{u''v''}$ and $\widetilde{u''w''}$ by NLEVM and NLEDM show a small kink at the centreline at downstream stations, of unclear origin.

Figure (15) displays radial profiles of the stream wise, radial and tangential components of the scalar flux vector, respectively, ie, those quantities which are the primary focus of the NLEDM. The predictions of the stream-wise scalar flux with the standard k–ϵ model are seen to grossly underestimate this component, and further do not show any sign of the double–peaked structure reported in the experiments. The nonlinear models in contrast do reproduce both the experimentally observed order of magnitude and trends. The differences between the computational resulting from the NLEDM for the scalar fluxes but with the k–ϵ retained for the Reynolds stresses and those arising from the full non linear model are seen to be relatively minor. The greatly improved performance of the NLEDM is almost certainly a consequence of ensuring that the condition corresponding to equation (45) is satisfied in equilibrium shear flows. The differences between the predictions with the linear and the nonlinear models is much smaller for the radial component of the scalar flux. Predictions with the nonlinear models look somewhat better at the first station, while experimental uncertainties (as apparent from asymmetry of measurements) preclude a thorough comparison at the second station; at the third station the performance of both models is similar. As far as the tangential component of the scalar flux is concerned, the behaviour is somewhat puzzling. The experiments show positive values of $\widetilde{w''\xi''}$ for $r > 0$ with some lack of asymmetry in the profiles evident near $r = 0$. In an axisymmetric flow of the type being considered $\widetilde{w''\xi''}$ should be zero at $r = 0$. The k–ϵ model, as anticipated, returns identically zero values of this component while the nonlinear non linear diffusivity model predicts nonzero values of roughly the correct magnitude *but with the wrong sign* over most radial positions. Only in the outermost part of the flow field (beyond $r/D \sim 3$) are the predicted and measured fluxes the same sign, albeit small in magnitude. The reasons for these discrepancies are at this stage unclear. In the downstream regions of the flow only gradients in the radial direction are significant and, given $\beta_1 > 0$ and $\beta_2 < 0$ with both $\frac{\partial \tilde{w}}{\partial r}$ and $\frac{\tilde{w}}{r}$ positive in the region close to $r = 0$ then the predicted profiles are consistent with the equations given in Appendix C. In any event the tangential

flux is anticipated to play a minor role in combustors with a close-to-axisymmetric geometry.

The mean mixture fraction field is now considered. Unfortunately, measured radial profiles of mean mixture fraction are not available with the only information reported being the centreline decay, shown in Figure (16). It is seen that nonlinear models reproduce the initial decay of scalar concentration somewhat better , while the reverse is true further downstream. The initial trend is consistent with the observed initial improvement in stream-wise and radial scalar fluxes brought about by nonlinear models. The downstream trend is less easily explained in the absence of radial mean scalar measurements. In summary it can be said that for scalar fluxes the proposed nonlinear model results in significantly improved performance in the upstream part of the flow, while further downstream results are closer to those given by standard models.

5 Conclusions

A Non–Linear Eddy Viscosity/Diffusivity Model for turbulent flows has been formulated, featuring quadratic constitutive relationships for both Reynolds stresses and scalar fluxes. The model coefficients have been determined by enforcing compliance with experimental data obtained in simple and generic turbulent flows and by ensuring that the model generates realisable solutions for both the velocity and scalar fields. This is achieved, in part, by making the coefficients depend upon an appropriately defined strain parameter.

The resulting models have been applied to a wide range of swirling jet flows and flames for which extensive experimental data is available. A comparison of the computational results with this data suggests that the formulated models lead to significantly improved (and substantially improved in some cases) predictions compared with those that can be achieved with the standard k–ϵ model. However, some areas remain in which further investigations are desirable. These are related to:

1. the far–field behaviour of the models - see Figure (12).
2. the degradation of the centre-line mean conserved scalar with NLEDM for swirling flames (despite greatly improved scalar flux profiles) - see Figure (16).

A major positive feature of the proposed model form is that it appears to be robust and gives rise to smooth and rapidly converging simulations; a feature almost certainly due to the 'realisable' nature of the formulation. Further work should involve evaluating the performance of the model under a wider range of flow conditions, i.e., not restricted to confined swirling flows.

Acknowledgments

Research supported by the BRITE–EURAM Project 'Advanced burner design methodology for efficient and clean gas fired commercial and industrial boilers' (MECBURN), Contract no. BRPR–CT 98–0782.

References

[1] Abdon, A. and Sundén, B., "Numerical investigation of impingement heat transfer using linear and non–linear turbulence models", *Num. Heat Transf. A* 40:563–578, 2001.

[2] Abe, K. and Suga, K., "Towards the development of a Reynolds–averaged algebraic turbulent scalar–flux model", *Int. J. Heat Fluid Flow* 22:19–29, 2001.

[3] Abe, K., Jang, Y.–J. and Leschziner, M.A., "An investigation of wall–anisotropy expressions and length–scale equations for non–linear eddy–viscosity model", *Int. J. Heat Fluid Flow* 24:181–198, 2003.

[4] Champagne, F.H., Harris, V.G. and Corrsin, S., "Experiments on nearly homogeneous turbulent shear flow", *J. Fluid. Mech.* 41:81–139, 1970.

[5] Chigier, N.A. and Chervinsky, A., "Experimental investigation of swirling vortex motion in jets", *J. Appl. Mech.* 34:443–451, 1967.

[6] Chigier, N.A., "Gas dynamics of swirling flow in combustion systems", *Astron. Acta* 17:387–395, 1972.

[7] Craft, T.J., Launder, B.E. and Suga, K., "A non–linear eddy viscosity model including sensitivity to stress anisotropy", *Tenth Symp. Turb. Shear Flows* 2, Pennsylvania State University, University Park, 1995, pp. 23/19–23/24.

[8] Craft, T.J., Launder, B.E. and Suga, K., "Development and application of a cubic eddy–viscosity model of turbulence", *J. Heat Fluid Flow* 17:108–115, 1996.

[9] Daly, B.J. and Harlow, F.H., "Transport equations in turbulence", *Phys. Fluids* 13:2634–2649, 1970.

[10] Durbin, P.A. and Petterson–Reif, B.A., "On algebraic second moment models", Center for Turbulence Research, Manuscript 175, Stanford, 1999.

[11] Fu, S. and Qian, W.Q., "Development of curvature sensitive nonlinear eddy–viscosity model", *AIAA J.* 40:2225–2233, 2002.

[12] Gatski, T.B. and Speziale, C.G., "On explicit algebraic stress models for complex turbulent flows", *J. Fluid Mech.* 254:59–78, 1993.

[13] Gatski, T.B. and Jongen, T., "Nonlinear eddy viscosity and algebraic stress models for solving complex turbulent flows", *Prog. Aerosp. Sci.* 36:655–682, 2000.

[14] Girimaji, S.S., "Full explicit and self–consistent algebraic Reynolds stress model", *Theor. Comput. Fluid Dynamics* 8:387–402, 1996.

[15] Girimaji, S.S., "Lower–dimensional manifold (algebraic) representation of Reynolds stress closure equations", *Theor. Comput. Fluid Dynamics* 14:259–281, 2001.

[16] Ha Minh, M.H., "The impact of turbulence modelling on the numerical predictions of flows", 13th Int. Conf. Num. Meth. Fluid Dyn., Napolitano, M. and Sabetta, F., Eds., Springer–Verlag, Berlin, 1993.

[17] Hanjalić, K., "Achievements and limitations in modelling and computation of buoyant turbulent flows and heat transfer", *10th Int. Heat Transfer Conf.*, Brighton, 1994.

[18] Harris, V.G., Graham, J.A.H. and Corrsin, S., "Further experiments in nearly homogeneous turbulent shear flow", *J. Fluid. Mech.* 81:657–687, 1977.

[19] Huang, Y.–N. and Rajagopal, K.R., "On a generalised nonlinear k–ϵ model for turbulence that models relaxation effects", *Theor. Comput. Fluid Dynamics* 8:275–288, 1996.

[20] Jones, W.P., "The prediction of laminarization with a 2–equation model of turbulence", Ph.D. Thesis, Imperial College, Univ. of London, 1971.

[21] Jones, W.P. and Launder, B.E., "The prediction of laminarization with a 2–equation model of turbulence", *Int. J. Heat Mass Transf.* 15:301–314, 1972.

[22] Jones, W.P., "BOFFIN: a computer program for flow and combustion in complex geometries", 1994.

[23] Knoell, J. and Taulbee, D.B., "A nonlinear stress–strain model for wall–bounded turbulent flows", *Int. J. Heat Fluid Flow* 22:402–408, 2001.

[24] LaRue, J.C. and Libby, P.A., "Measurements in the turbulent boundary layer with slot injection of helium", *Phys. Fluids* 20:192–202, 1977.

[25] Launder, B.E. and Spalding, D.B., "The numerical computation of turbulent flows", *Comp. Meth. Appl. Mech. Eng.* 3:269–289, 1974.

[26] Launder, B.E., "On the computation of convective heat transfer in complex turbulent flows", *J. Heat Transf.* 110:1112–1128, 1988.

[27] Launder, B.E., "Second–moment closure: present... and future?", *Int. J. Heat Fluid Flow* 10:282–300, 1989.

[28] Lien, F.S. and Leschziner, M.A., "Low–Reynolds–number eddy–viscosity modelling based on non–linear stress–strain/vorticity relations", in *Engineering Turbulence Modelling and Experiments 3* (Rodi, W. and Bergeles, G., Eds.), Elsevier, Amsterdam, 1996, pp. 91–100.

[29] Lilley, D.G., "Swirl flows in combustion: a review", *AIAA J.* 15:1063–1078, 1977.

[30] Loyau, H., Batten, P. and Leschziner, M.A., "Modelling shock/boundary–layer interaction with nonlinear eddy–viscosity closures", *Flow, Turb. Combust.* 60:257–282, 1998.

[31] Lumley, J.L., *Stochastic Tools in Turbulence*, Academic Press, New York, 1970.

[32] Luo, J. and Lakshminarayana, B., "Prediction of strongly curved turbulent duct flows with Reynolds stress models", *AIAA J.* 35:91–98, 1997.

[33] Mashayek, F. and Taulbee, D.B., "A four–equation model for prediction of gas–solid turbulent flows", *Num. Heat Transf. B* 41:95–116, 2002.

[34] Mashayek, F. and Taulbee, D.B., "Turbulent gas–solid flows, part II: explicit algebraic models", *Num. Heat Transf. B* 41:31–52, 2002.

[35] Merci, B., De Langhe, C., Vierendeels, J. and Dick, E., "A quasi–realizable cubic low–Reynolds eddy–viscosity turbulence model with a new dissipation rate equation", *Flow, Turb. Combust.* 66:133–157, 2001.

[36] Mompean, G., "On predicting abrupt contraction flows with differential and algebraic viscoelastic models", *Computers & Fluids* 31:935–956, 2002.

[37] Mompean, G., Thompson, R.L. and Souza Mendes, P.R., "A general transformation procedure for differential viscoelastic models", *J. Non–Newtonian Fluid Mech.* 111:151–174, 2003.

[38] Nagaoka, M. and Suga, K., "Application of a higher order GGDH heat flux model to three–dimensional turbulent U–bend duct heat transfer", *J. Heat Transfer* 125:200–203, 2003.

[39] Palaniswami, S., Goldberg, U., Peroomian, O. and Chacravarthy, S., "Prediction of axial and transverse injection into supersonic flow", *Flow Turb. Combust.* 66:37–55, 2001.

[40] Park, T.S. and Sung, H.J., "A nonlinear low–Reynolds–number k–ϵ model for turbulent separated and reattaching flows – (I) flow field computation", *Int. J. Heat Mass Transfer* 38:2657–2666, 1995.

[41] Park, T.S. and Sung, H.J., "Development of a near–wall turbulence model and application to jet impingement heat transfer", *Int. J. Heat Fluid Flow* 22:10–18, 2001.

[42] Park, T.S., Sung, H.J. and Suzuki, K., "Development of a nonlinear near–wall turbulence model for turbulent flow and heat transfer", *Int. J. Heat Fluid Flow* 24:29–40, 2003.

[43] Protter, M.H., *Maximum Principles in Differential Equations*, Prentice-Hall, New Jersey, 1967.

[44] Rahman, M.M., Rautaheimo, P. and Siikonen, T., "Modifications for an explicit algebraic stress model", *Int. J. Numer. Meth. Fluids* 35:221–245, 2001.

[45] Rodi, W., Ph.D. Thesis, Imperial College, Univ. of London, 1972.

[46] Rodi, W., "A new algebraic relation for calculating Reynolds stresses", *Z. Angew. Math. Mech.* 56:219–221 , 1976.

[47] Rokni, M. and Gatski, T.B., "Predicting turbulent convective heat transfer in fully developed duct flows", *Int. J. Heat Fluid Flow* 22:382–392, 2001.

[48] Rokni, M. and Sundén, B., "Calculation of turbulent fluid flow and heat transfer in ducts by a full Reynolds stress model", *Int. J. Numer. Meth. Fluids* 42:147–162, 2003.

[49] Rumsey, C.M., Gatski, T.B. and Morrison, J.H., "Turbulence model predictions of strongly curved flow in a U duct", *AIAA J.* 38:1394–1402, 2000.

[50] Rumsey, C.M., Gatski, T.B., Anderson, W.K. and Nielsen, E.J., "Isolating curvature effects in computing wall–bounded turbulent flows", *Int. J. Heat Fluid Flow* 22:573–582, 2001.

[51] Saffman, P.G., "A model for inhomogeneous turbulent flow", *Proc. Roy. Soc. London A* 317:417–433, 1970.

[52] Shih, T–H. and Lumley, J.L., "Remarks on turbulent constitutive relations", *Math. Comput. Modelling* 18:9–16, 1993.

[53] Shih, T–H., Zhu, J. and Lumley, J.L., "A realisable Reynolds stress algebraic equation model", NASA TM 105993, 1993.

[54] Shih, T–H., Zhu, J. and Lumley, J.L., "A new Reynolds stress algebraic equation model", *Comput. Meth. Appl. Mech. Engrg.* 125:287–302, 1995.

[55] Shih, T.–H., "Constitutive relations and realisability of single–point turbulence closures", in *Turbulence and Transition Modelling* (Hallbäck, M., Henningson, D.S., Johansson, A.V. and Alfredsson, H.P., Eds.), Kluwer, Dordrecht, 1996, pp. 155–192.

[56] Shih, T.–H., Zhu, J., Liou, W.W., Chen, K.H., Liu, N.S. and Lumley, J.L., "Modelling of turbulent swirling flows", in *Proc. 11th Symp. on Turbulent Shear Flow*, Grenoble, 1997, pp. 31.1–31.6.

[57] So, R.M.C., Ahmed, S.A. and Mongia, H.C., "An experimental investigation of gas jets in confined swirling air flow", NASA CR 3832, 1984.

[58] So, R.M.C. and Ahmed, S.A., "Behaviour of carbon dioxide jets in a confined swirling flow", *Int. J. Heat Fluid Flow* 8:171–176, 1987.

[59] So, R.M.C., Vimala, P., Jin, L.H., Zhao, C.Y. and Gatski, T.B., "Accounting for buoyancy effects in the explicit algebraic stress model: homogeneous turbulent shear flows", *Theor. Comput. Fluid Dynamics* 15:283–302, 2002.

[60] Song, B. Amano, R.S. and Liu, G.R., "On computation of complex turbulent flow by using non–linear k–ω model", *Num. Heat Transf. B* 39:421–434, 2001.

[61] Spalart, P.R. and Shur, M., "On the sensitization of turbulence models to rotation and curvature", *Aerosp. Sci. Tech.* 5:297–302, 1997.

[62] Spalart, P.R., "Strategies for turbulence modelling and simulations", *Int. J. Heat Fluid Flow* 21:252–263, 2000.

[63] Speziale, C.G., "On nonlinear K–l and K–ϵ models of turbulence", *J. Fluid Mech.* 178:459–475, 1987.

[64] Speziale, C.G., "Comparison of explicit and traditional algebraic stress models of turbulence", *AIAA J.* 35:1506–1509, 1997.

[65] Stårner, S.H. and Bilger, R.W., "Joint measurements of velocity and scalars in a turbulent diffusion flame with moderate swirl", *21st Symp. (Int.) on Combust.*, pp. 1569–1577, 1986.

[66] Stårner, S.H. and Bilger, R.W., "Further velocity measurements in a turbulent diffusion flame with moderate swirl", *Combust. Sci. and Tech.* 63:257–274, 1989.

[67] Suga, K., "Predicting turbulence and heat transfer in 3–D curved ducts by near–wall second moment closures", *Int. J. Heat Mass Transfer* 46:161–173, 2003.

[68] Syred, N. and Beér, J.M., "Combustion in swirling flows: a review", *Combust. Flame* 23:143–201, 1974.

[69] Wallin, S. and Johansson, A.V., "An explicit algebraic Reynolds stress model for incompressible and compressible turbulent flows", *J. Fluid Mech.* 403:89–132, 2000.

[70] Wallin, S. and Johansson, A.V., "Modelling streamline curvature effects in explicit algebraic Reynolds stress turbulence models", *Int. J. Heat Fluid Flow* 23:721–730, 2002.

[71] Weigand, B., Schwartzkoppf, T. and Sommer, T.P., "A numerical investigation of the heat transfer in a parallel plate channel with piecewise constant wall temperature boundary conditions", *J. Heat Transfer* 124:626–634, 2002.

[72] Weis, J. and Hutter, K., "On euclidean invariance of algebraic Reynolds stress models in turbulence", *J. Fluid Mech.* 476:63–68, 2003.

[73] Wen, J.X., Liu, F. and Lo, S., "Performance comparison of a buoyancy–modified turbulence model with three LRN turbulence models for a square cavity", *Num. Heat Transf. B* 39:257–276, 2001.

[74] Wilcox, D.C., *Turbulence modelling for CFD*, 2nd ed., DCW Industries, La Cañada, 1993.

[75] Zhou, L.X. and Gu, H.X., "Simulation of swirling gas–particle flows using a nonlinear k–ϵ–k_p two–phase turbulence model", *Powder Tech.* 128:47–55, 2002.

Appendix A

Champagne *et al.* [4] consider an equilibrium shear layer with mean velocity gradient

$$\left|\frac{\partial \tilde{u}}{\partial y}\right| \;=\; 12.9 \;\; \mathrm{s}^{-1}$$

The normal components of the Reynolds stress at the centreline can be recovered after the ratios

$$\frac{\sqrt{\overline{u'^2}}}{U_c} \;=\; 0.018, \quad \frac{\sqrt{\overline{v'^2}}}{U_c} \;=\; 0.013, \quad \frac{\sqrt{\overline{u'^2}}}{U_c} \;=\; 0.014$$

where $U_c = 12.4$ m s^{-1} is the mean centreline velocity. The turbulent kinetic energy then results as

$$k = 0.05297\mathrm{m}^2 \;\mathrm{s}^{-2}$$

while the viscous dissipation rate is estimated by the authors, on the basis of equilibrium between production and dissipation, to be

$$\epsilon = 0.235\mathrm{m}^2 \;\mathrm{s}^{-3}$$

The strain parameter for this case is accordingly identified as

$$A = \frac{k}{\epsilon}\left|\frac{\partial \tilde{u}}{\partial y}\right| = 2.908$$

The measured Reynolds shear stress is reported as

$$-\frac{\overline{u'v'}}{U_c^2} = 0.000111$$

and c_μ $(= -\alpha_1)$ can accordingly be determined, after equation (8) as

$$c_{\mu,1} = \frac{1}{A}\frac{\mid \overline{u'v'} \mid}{k} = \frac{1}{A}\frac{\overline{u'v'}}{U_c^2}\frac{U_c^2}{k} = 0.111$$

The anisotropies of the normal components are:

$$b_{11} = \frac{\overline{u'^2}}{2k} - \frac{1}{3} = 0.1369134, \quad b_{22} = \frac{\overline{v'^2}}{2k} - \frac{1}{3} = -0.08805032, \quad b_{33} = \frac{\overline{w'^2}}{2k} - \frac{1}{3} = -0.04886309$$

Appendix B

Harris *et al.* [18] consider a shear layer with $P/\overline{\epsilon} = 1.8$ and mean velocity gradient

$$\left|\frac{\partial \tilde{u}}{\partial y}\right| \;=\; 44.0 \;\; \mathrm{s}^{-1}$$

The normal components of the Reynolds stress are reported as

$$\sqrt{\overline{u'^2}} \;=\; 0.641 \;\; \mathrm{m} \;\; \mathrm{s}^{-1}, \quad \sqrt{\overline{v'^2}} \;=\; 0.404 \;\; \mathrm{m} \;\; \mathrm{s}^{-1}, \quad \sqrt{\overline{u'^2}} \;=\; 0.495 \;\; \mathrm{m} \;\; \mathrm{s}^{-1}$$

Accordingly, the turbulent kinetic energy is $k = 0.409561 \;\; \mathrm{m}^2 \;\; \mathrm{s}^{-2}$, while the viscous dissipation rate is estimated by the authors from the turbulent kinetic energy equation as

$$\epsilon = 3.28 \;\; \mathrm{m}^2 \;\; \mathrm{s}^{-3}$$

The strain parameter for this case is accordingly identified as

$$A = \frac{k}{\epsilon}\left|\frac{\partial \tilde{u}}{\partial y}\right| = 5.494$$

The measured Reynolds shear stress is reported as

$$-\,\overline{u'v'} \;=\; 0.1217 \;\; \mathrm{m}^2 \;\; \mathrm{s}^{-2}$$

and c_μ $(= -\alpha_1)$ can accordingly be determined, after equation (8) as

$$c_{\mu,2} = \frac{1}{A}\frac{|\,\overline{u'v'}\,|}{k} = 0.054085$$

The anisotropies of the normal components are

$$b_{11} = \frac{\overline{u'^2}}{2k} - \frac{1}{3} = 0.168278, \quad b_{22} = \frac{\overline{v'^2}}{2k} - \frac{1}{3} = -0.134076, \quad b_{33} = \frac{\overline{w'^2}}{2k} - \frac{1}{3} = -0.034202$$

Appendix C

The total (molecular plus turbulent) scalar flux is denoted as ζ, then

$$\zeta_i \;=\; \frac{\mu}{\sigma}\frac{\partial\tilde{\xi}}{\partial x_i} \;-\; \overline{\rho}\,\widetilde{u_i''\xi''}$$

with σ_ξ indicating the molecular Prandtl/Schmidt number. The i–th component of ζ can be modelled, following (30), in the form

$$\zeta_i \;=\; \left(\frac{\mu}{\sigma} \;+\; \beta_1\,\overline{\rho}\,\frac{k^2}{\epsilon}\right)\frac{\partial\tilde{\xi}}{\partial x_i} \;+\; \overline{\rho}\,\frac{k^3}{\epsilon^2}\left(\beta_2\,\frac{\partial\tilde{u_i}}{\partial x_k} \;+\; \beta_3\,\frac{\partial\tilde{u_k}}{\partial x_i}\right)\frac{\partial\tilde{\xi}}{\partial x_k}$$

and with a simple manipulation the scalar derivative can be taken out to give

$$\zeta_i \;=\; \left[\left(\frac{\mu}{\sigma} \;+\; \beta_1\,\overline{\rho}\,\frac{k^2}{\epsilon}\right)\delta_{ik} \;+\; \beta_2\,\overline{\rho}\,\frac{k^3}{\epsilon^2}\,\frac{\partial\tilde{u_i}}{\partial x_k} \;+\; \beta_3\,\overline{\rho}\,\frac{k^3}{\epsilon^2}\,\frac{\partial\tilde{u_k}}{\partial x_i}\right]\frac{\partial\tilde{\xi}}{\partial x_k}$$

with δ_{ik} indicating Kronecker's operator. This can be formally recast as the product of a suitably defined *tensorial* effective diffusivity Γ_{ik} and the mean scalar gradient vector:

$$\zeta_i \;=\; \Gamma_{ik}\,\frac{\partial\tilde{\xi}}{\partial x_k}$$

The components of Γ_{ik} turns out to be (in cylindrical coordinates x, θ, r, with corresponding velocity components u, v, w for ease of reference)

$$\Gamma_{xx} \;=\; \frac{\mu}{\sigma} \;+\; \beta_1\,\overline{\rho}\,\frac{k^2}{\epsilon} \;+\; (\beta_2 \;+\; \beta_3)\,\overline{\rho}\,\frac{k^3}{\epsilon^2}\,\frac{\partial\tilde{u}}{\partial x}$$

$$\Gamma_{xr} \;=\; +\,\beta_2\,\overline{\rho}\,\frac{k^3}{\epsilon^2}\,\frac{\partial\tilde{u}}{\partial r} \;+\; \beta_3\,\overline{\rho}\,\frac{k^3}{\epsilon^2}\,\frac{\partial\tilde{v}}{\partial x}$$

$$\Gamma_{x\theta} \;=\; +\,\beta_2\,\overline{\rho}\,\frac{k^3}{\epsilon^2}\,\frac{1}{r}\,\frac{\partial\tilde{u}}{\partial\theta} \;+\; \beta_3\,\overline{\rho}\,\frac{k^3}{\epsilon^2}\,\frac{\partial\tilde{w}}{\partial x}$$

$$\Gamma_{rx} \;=\; +\,\beta_2\,\overline{\rho}\,\frac{k^3}{\epsilon^2}\,\frac{\partial\tilde{v}}{\partial x} \;+\; \beta_3\,\overline{\rho}\,\frac{k^3}{\epsilon^2}\,\frac{\partial\tilde{u}}{\partial r}$$

$$\Gamma_{rr} \;=\; \frac{\mu}{\sigma} \;+\; \beta_1\,\overline{\rho}\,\frac{k^2}{\epsilon} \;+\; (\beta_2 \;+\; \beta_3)\,\overline{\rho}\,\frac{k^3}{\epsilon^2}\,\frac{\partial\tilde{v}}{\partial r}$$

$$\Gamma_{r\theta} \;=\; +\,\beta_2\,\overline{\rho}\,\frac{k^3}{\epsilon^2}\left(\frac{1}{r}\,\frac{\partial\tilde{v}}{\partial\theta} \;-\; \frac{\tilde{w}}{r}\right) \;+\; \beta_3\,\overline{\rho}\,\frac{k^3}{\epsilon^2}\,\frac{\partial\tilde{w}}{\partial r}$$

$$\Gamma_{\theta x} \;=\; +\,\beta_2\,\overline{\rho}\,\frac{k^3}{\epsilon^2}\,\frac{\partial\tilde{w}}{\partial x} \;+\; \beta_3\,\overline{\rho}\,\frac{k^3}{\epsilon^2}\,\frac{1}{r}\,\frac{\partial\tilde{u}}{\partial\theta}$$

$$\Gamma_{\theta r} \;=\; +\,\beta_2\,\overline{\rho}\,\frac{k^3}{\epsilon^2}\,\frac{\partial\tilde{w}}{\partial r} \;+\; \beta_3\,\overline{\rho}\,\frac{k^3}{\epsilon^2}\left(\frac{1}{r}\,\frac{\partial\tilde{v}}{\partial\theta} \;-\; \frac{\tilde{w}}{r}\right)$$

$$\Gamma_{\theta\theta} \;=\; \frac{\mu}{\sigma} \;+\; \beta_1\,\overline{\rho}\,\frac{k^2}{\epsilon} \;+\; (\beta_2 \;+\; \beta_3)\,\overline{\rho}\,\frac{k^3}{\epsilon^2}\,\left(\frac{1}{r}\,\frac{\partial\tilde{w}}{\partial\theta} \;+\; \frac{\tilde{v}}{r}\right)$$

The scalar diffusion term at the RHS of the mean scalar equation takes therefore the form

$$\begin{aligned}\frac{\partial\zeta_k}{\partial x_k} \;=\; & \frac{\partial}{\partial x}\left[\Gamma_{xx}\,\frac{\partial\tilde{\xi}}{\partial x} \;+\; \Gamma_{xr}\,\frac{\partial\tilde{\xi}}{\partial r} \;+\; \Gamma_{x\theta}\,\frac{1}{r}\,\frac{\partial\tilde{\xi}}{\partial\theta}\right] \;+ \\ & +\,\frac{1}{r}\,\frac{\partial}{\partial r}\left[r\,\left(\Gamma_{rx}\,\frac{\partial\tilde{\xi}}{\partial x} \;+\; \Gamma_{rr}\,\frac{\partial\tilde{\xi}}{\partial r} \;+\; \Gamma_{r\theta}\,\frac{1}{r}\,\frac{\partial\tilde{\xi}}{\partial\theta}\right)\right] \;+ \\ & +\,\frac{1}{r}\,\frac{\partial}{\partial\theta}\left[\Gamma_{\theta x}\,\frac{\partial\tilde{\xi}}{\partial x} \;+\; \Gamma_{\theta r}\,\frac{\partial\tilde{\xi}}{\partial r} \;+\; \Gamma_{\theta\theta}\,\frac{1}{r}\,\frac{\partial\tilde{\xi}}{\partial\theta}\right]\end{aligned}$$

This expression must be compared to the one holding when the standard gradient transport is adopted:

$$\frac{\partial\zeta_k}{\partial x_k} \;=\; \frac{\partial}{\partial x}\left(\Gamma\,\frac{\partial\tilde{\xi}}{\partial x}\right) \;+\; \frac{1}{r}\,\frac{\partial}{\partial r}\left(r\,\Gamma\,\frac{\partial\tilde{\xi}}{\partial r}\right) \;+\; \frac{1}{r}\,\frac{\partial}{\partial\theta}\left(\Gamma\,\frac{1}{r}\,\frac{\partial\tilde{\xi}}{\partial\theta}\right)$$

List of figure captions

1. Coefficient c_μ as a function of A: —— —— proposed form (NLEVM), — — — Schwarz's inequality constraint, — · — positivity constraint.

2. Correlation coefficient for shear stress. ———- k–ϵ, —— —— proposed form (NLEVM).

3. NLEDM coefficients β_1 and β_2 as a function of strain parameter A.

4. Velocity–scalar correlation coefficients.

5. Sketch of the experimental test rig of So et al. (1984, 1987). —— —— mean axial velocity profile at $x/D_j = 1$ (referring to case 31).

6. Case 31 (air jet in co-flowing air, $u_j = 25.4$ m/s), comparison of (top left) axial mean velocity, (top right) tangential mean velocity, (bottom left) axial rms velocity, (bottom right) tangential rms velocity at different transverse stations. □ measurements, ———- k–ϵ, —— —- NLEVM.

7. Case 32 (air jet in co-flowing air, $u_j = 66.8$ m/s), comparison of (top left) axial mean velocity, (top right) tangential mean velocity, (bottom left) axial rms velocity, (bottom right) tangential rms velocity at different transverse stations. □ measurements, ———- k–ϵ, —— —- NLEVM.

8. Case 42 (He/air jet in co-flowing air, $u_j = 36.5$ m/s), comparison of (top left) axial mean velocity, (top right) tangential mean velocity, (bottom left) axial rms velocity, (bottom right) tangential rms velocity at different transverse stations. □ measurements, ———- k–ϵ, — · — · — k–ϵ + NLEDM, —— —- NLEVM, — · · — · · — NLEVDM.

9. Case 51 (CO_2 jet in co-flowing air, $u_j = 25.4$ m/s), comparison of (top left) axial mean velocity, (top right) tangential mean velocity, (bottom left) axial rms velocity, (bottom right) tangential rms velocity at different transverse stations. □ measurements, ———- k–ϵ, — · — · — k–ϵ + NLEDM, —— —- NLEVM, — · · — · · — NLEVDM.

10. Case 52 (CO_2 jet in co-flowing air, $u_j = 54$ m/s), comparison of (top left) axial mean velocity, (top right) tangential mean velocity, (bottom left) axial rms velocity, (bottom right) tangential rms velocity at different transverse stations. □ measurements, ———- k–ϵ, — · — · — k–ϵ + NLEDM, —— —- NLEVM, — · · — · · — NLEVDM.

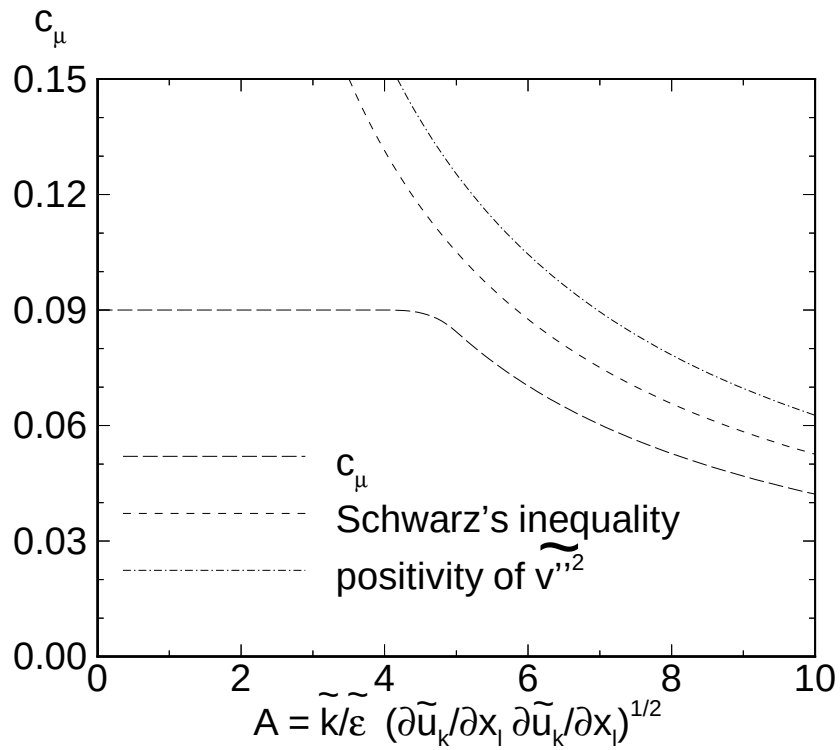

Figure 1: Variation of C_μ with strain

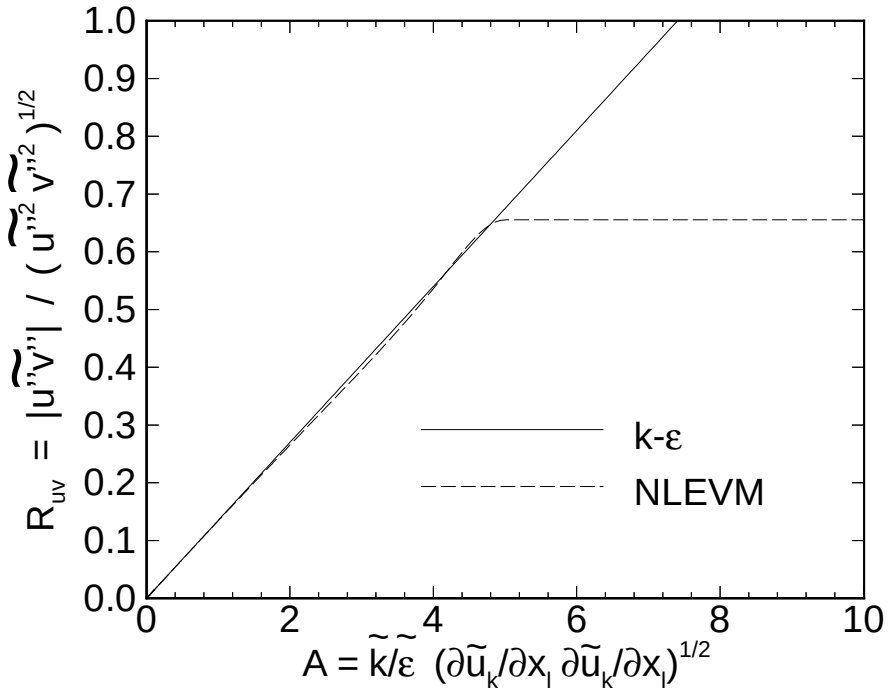

Figure 2:

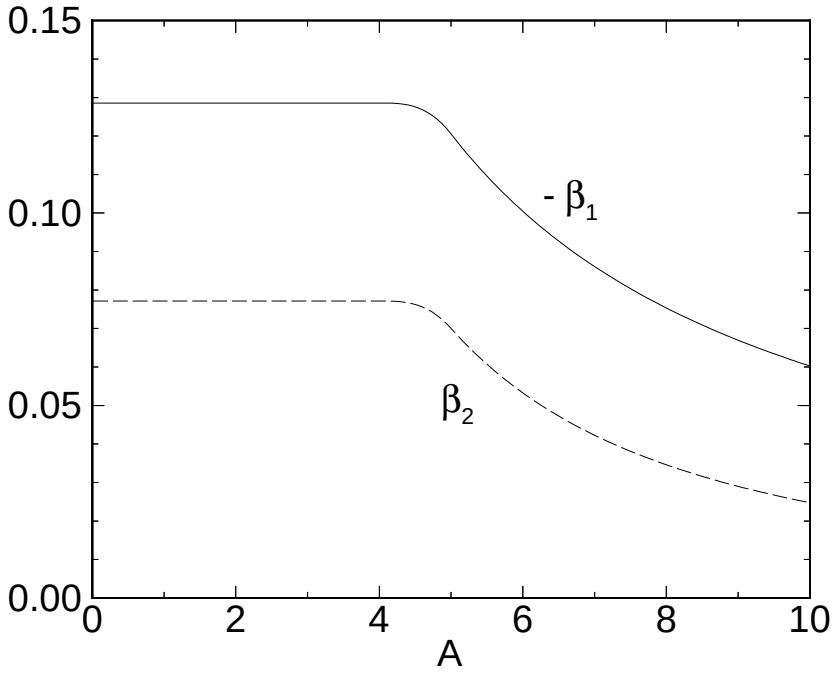

Figure 3:

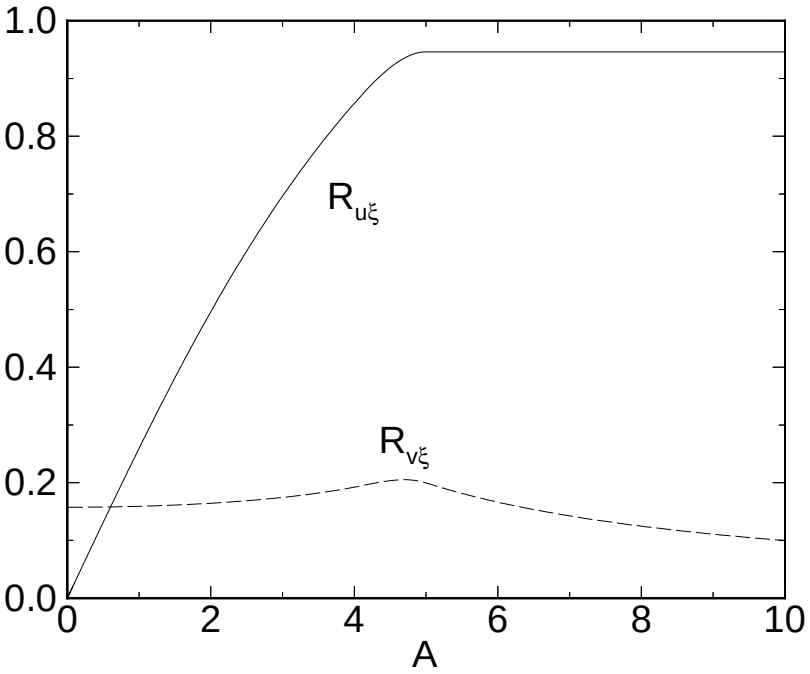

Figure 4:

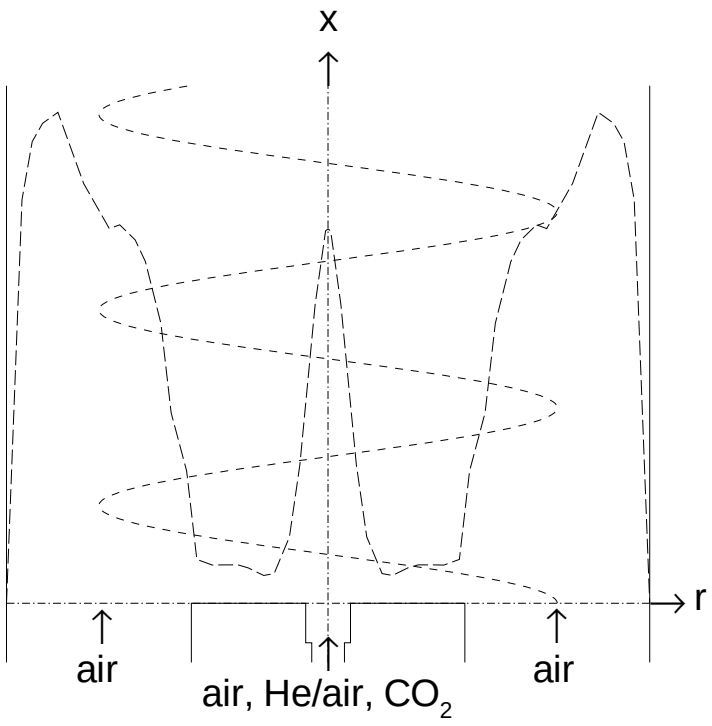

Figure 5:

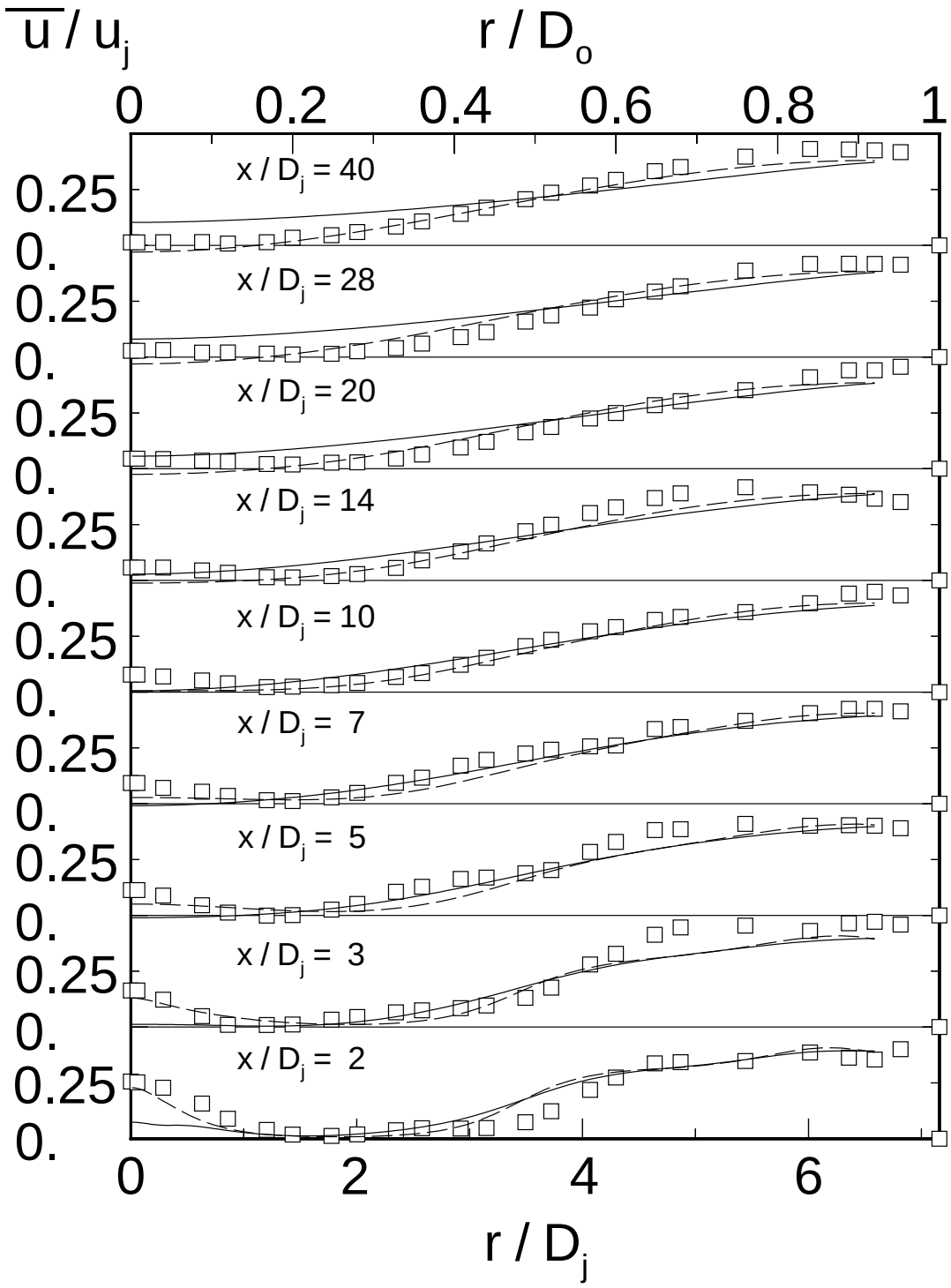

Figure 6: (TOP LEFT)

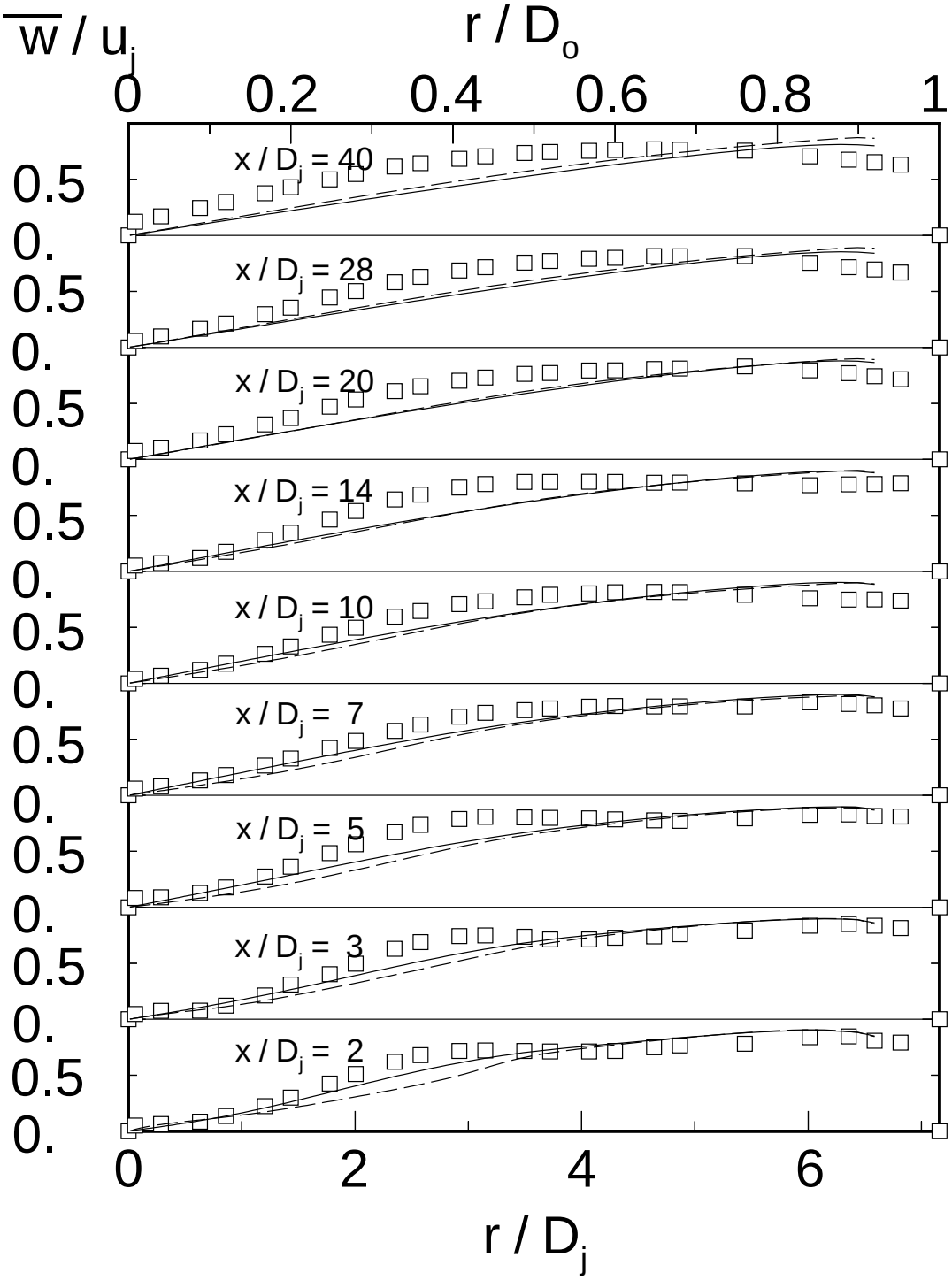

Figure 6: (TOP RIGHT)

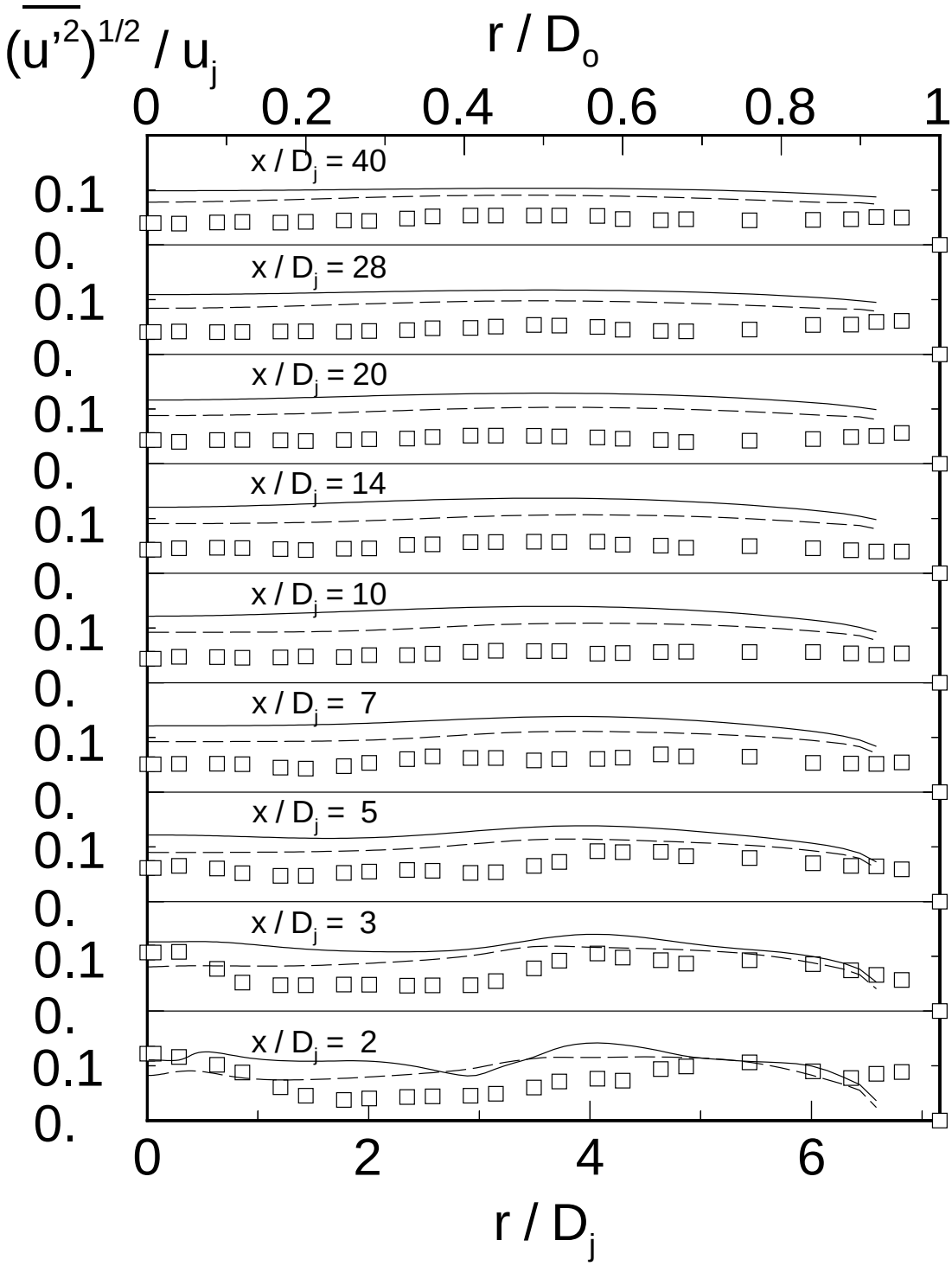

Figure 6: (BOTTOM LEFT)

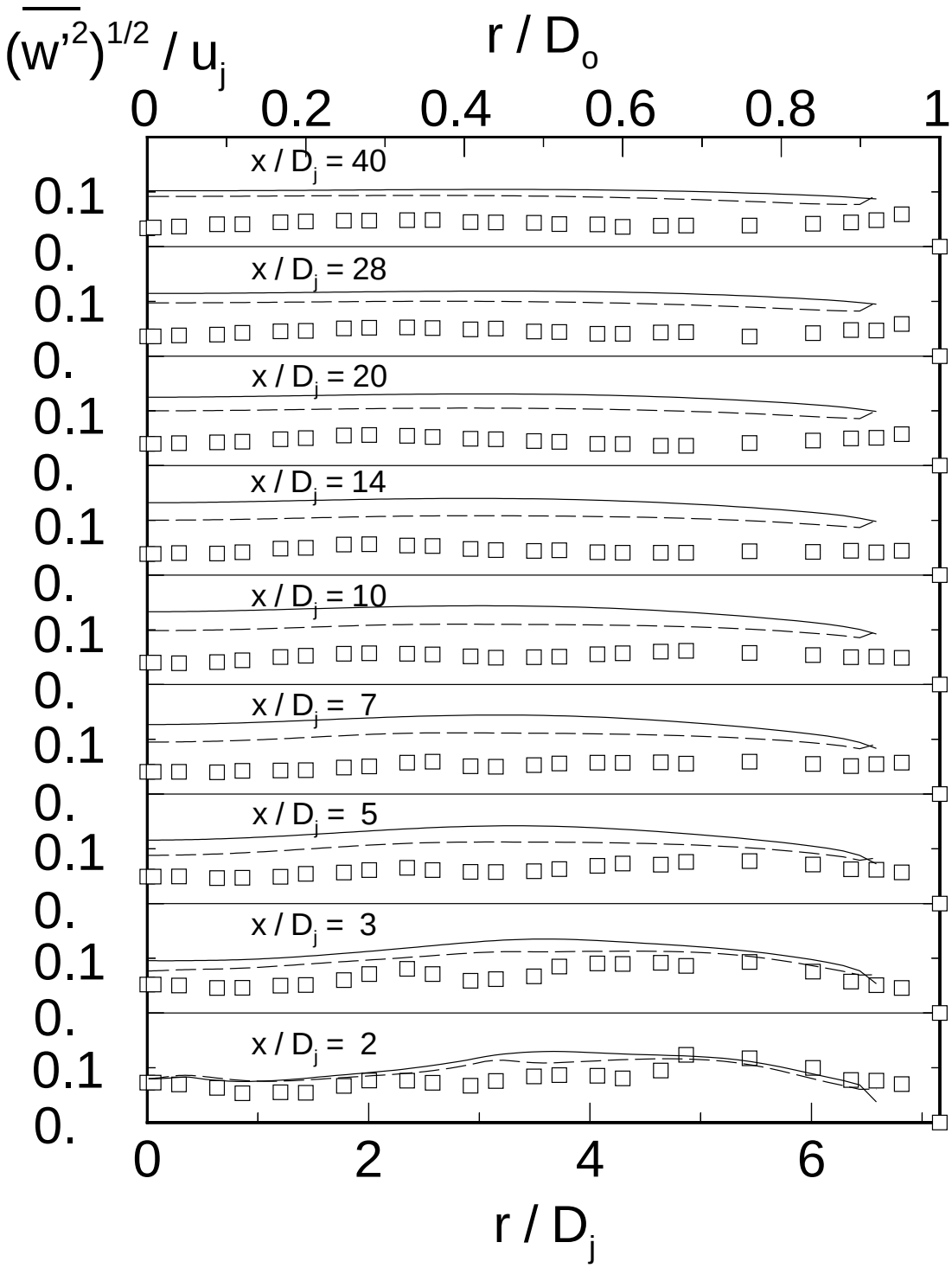

Figure 6: (BOTTOM RIGHT)

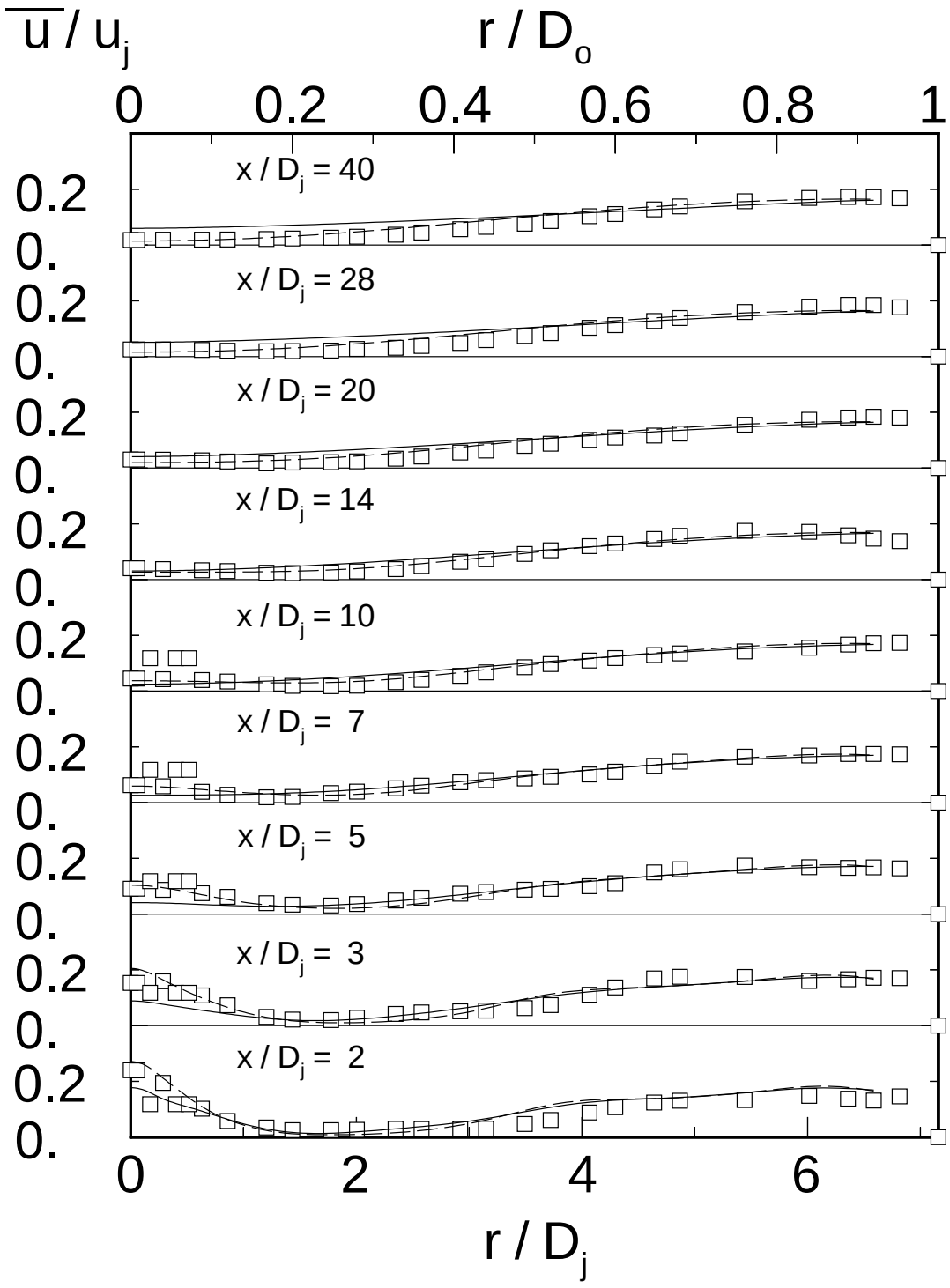

Figure 7: (TOP LEFT)

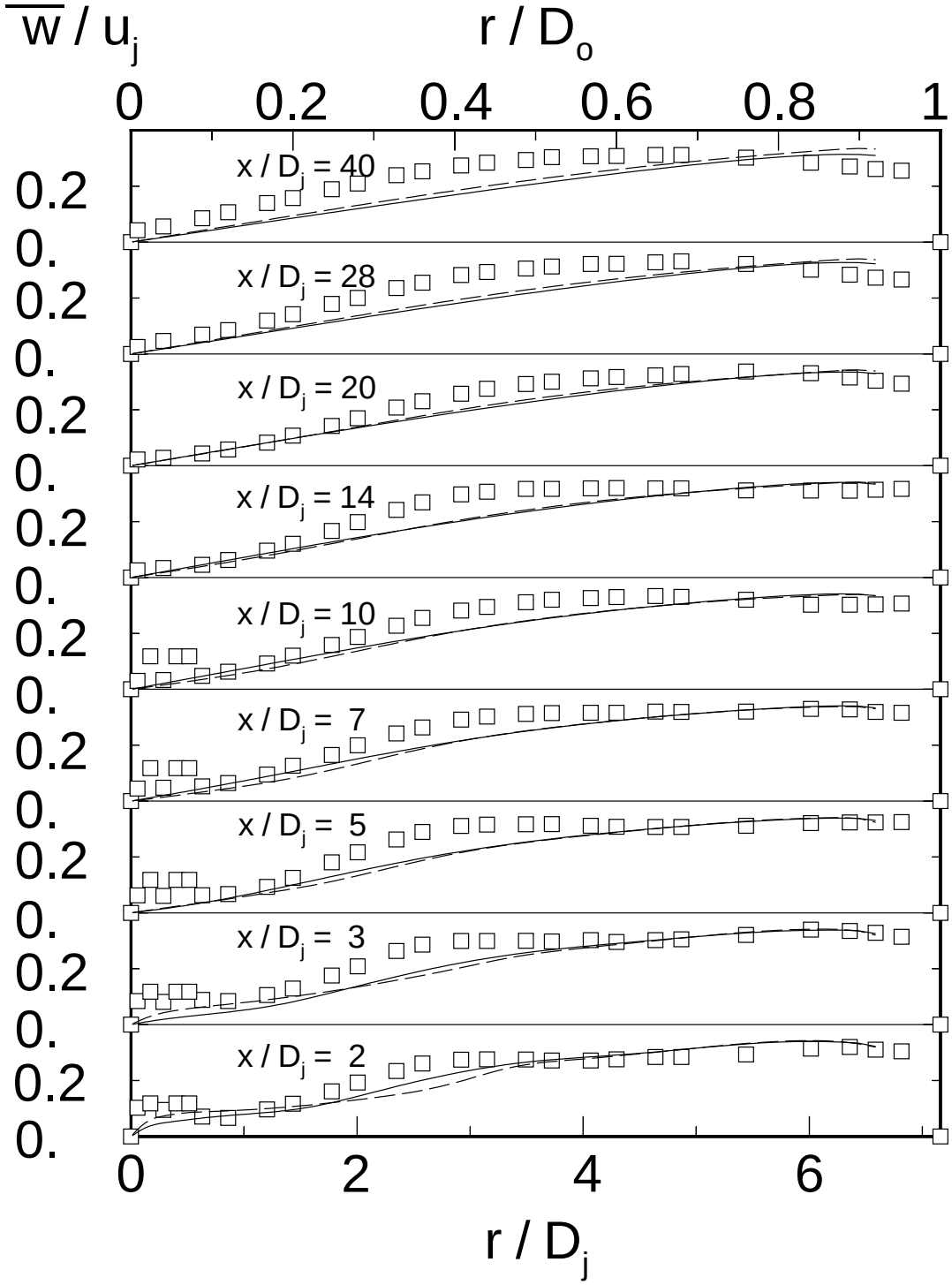

Figure 7: (TOP RIGHT)

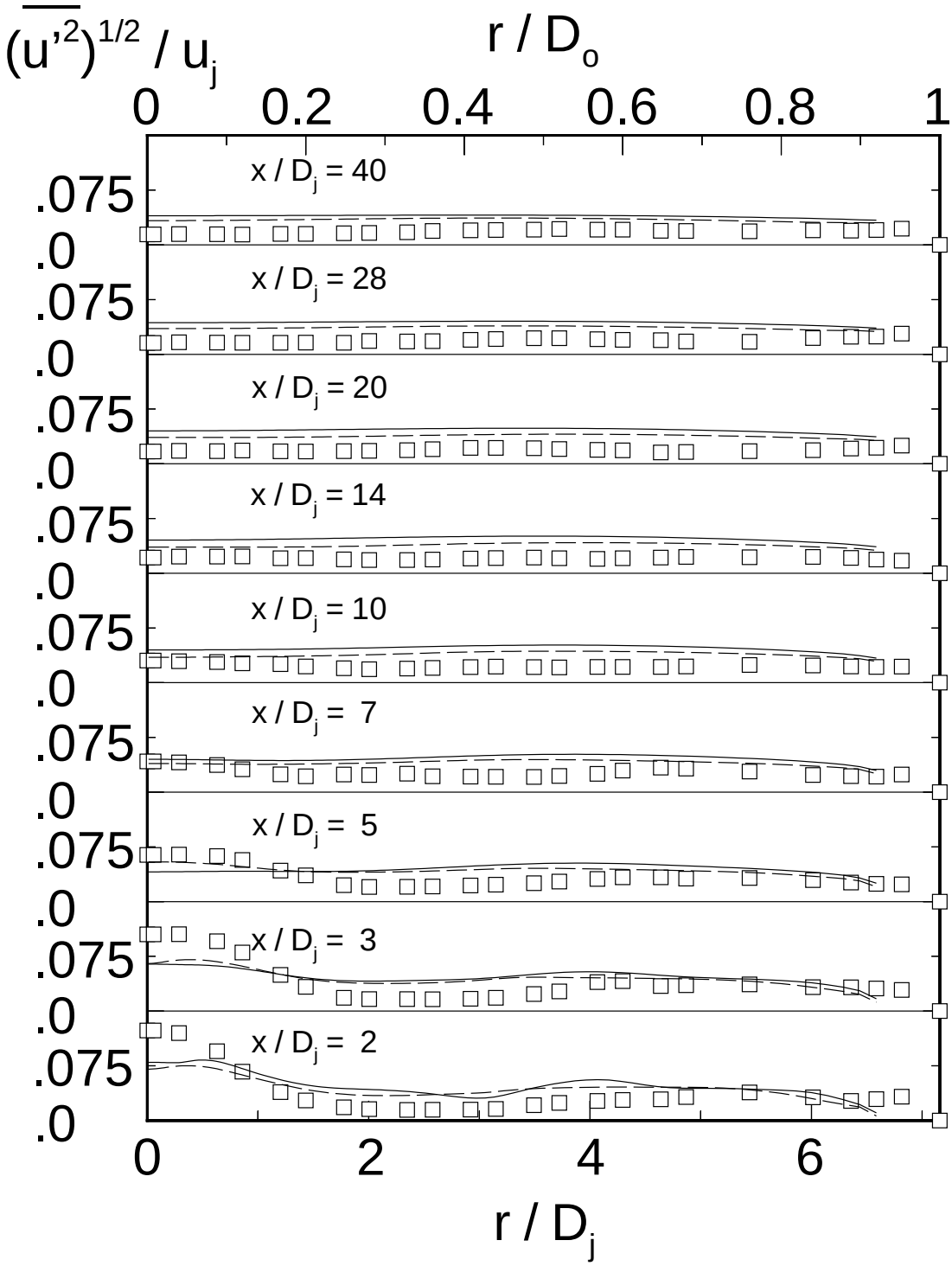

Figure 7: (BOTTOM LEFT)

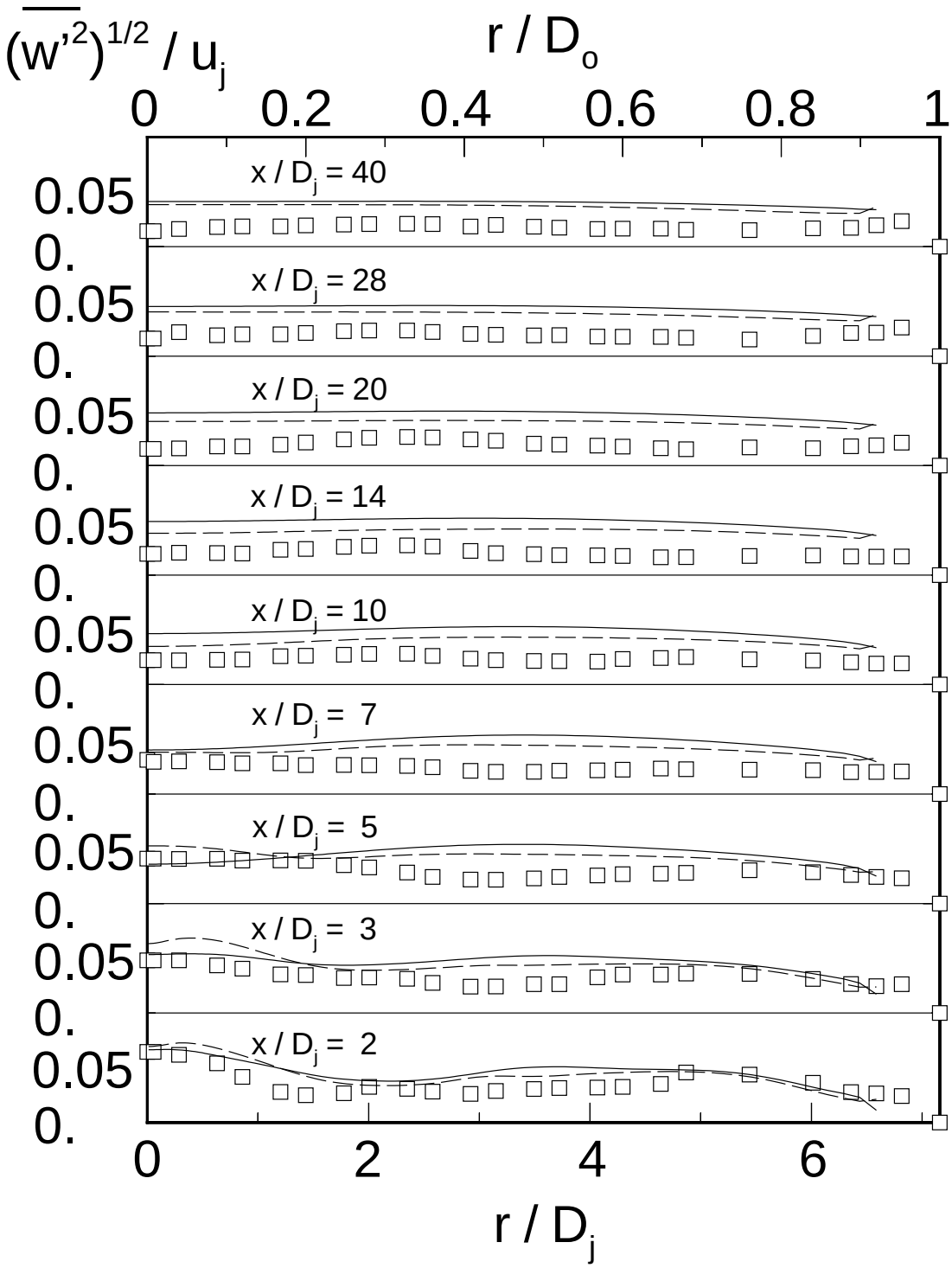

Figure 7: (BOTTOM RIGHT)

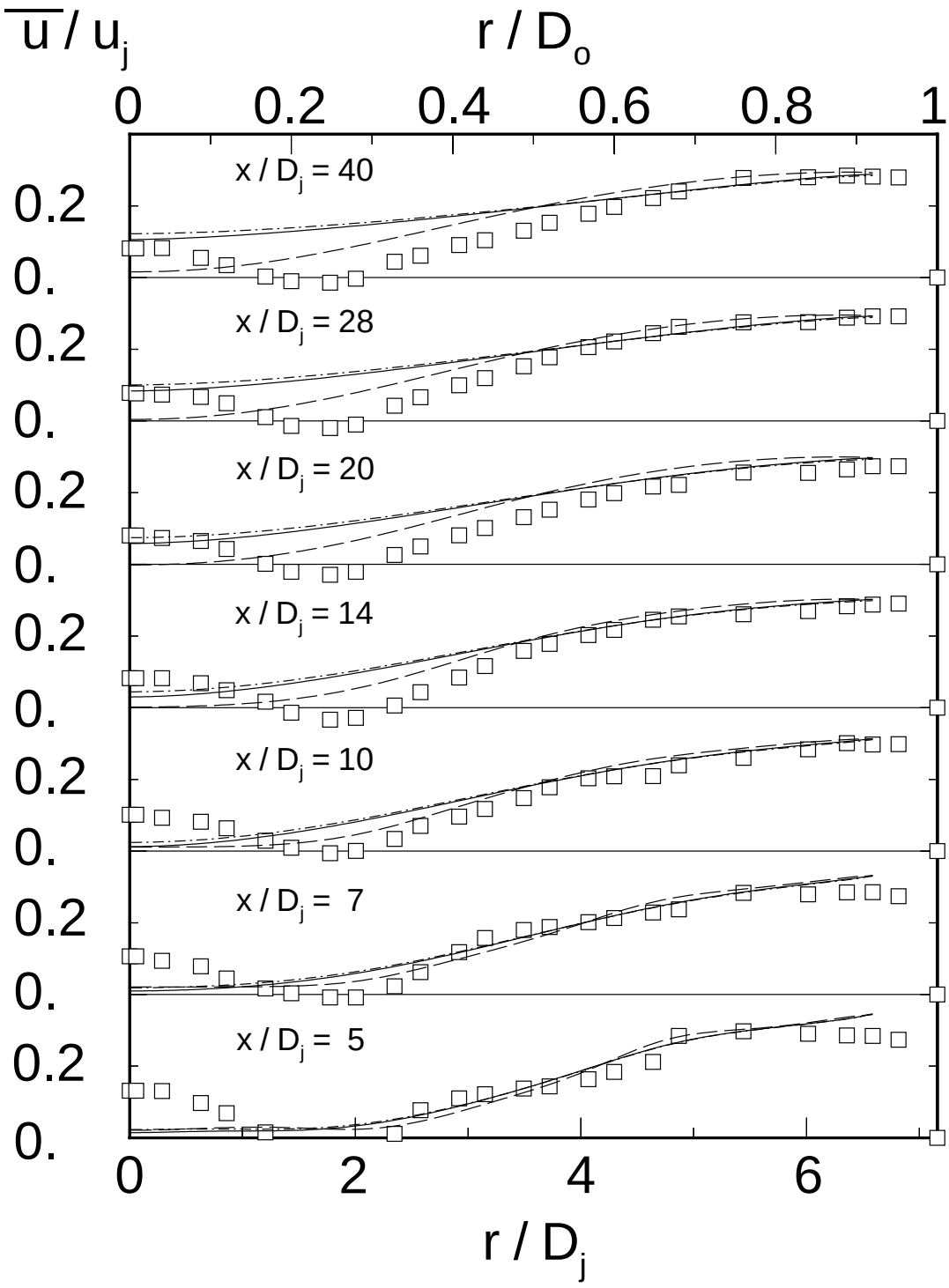

Figure 8: (TOP LEFT)

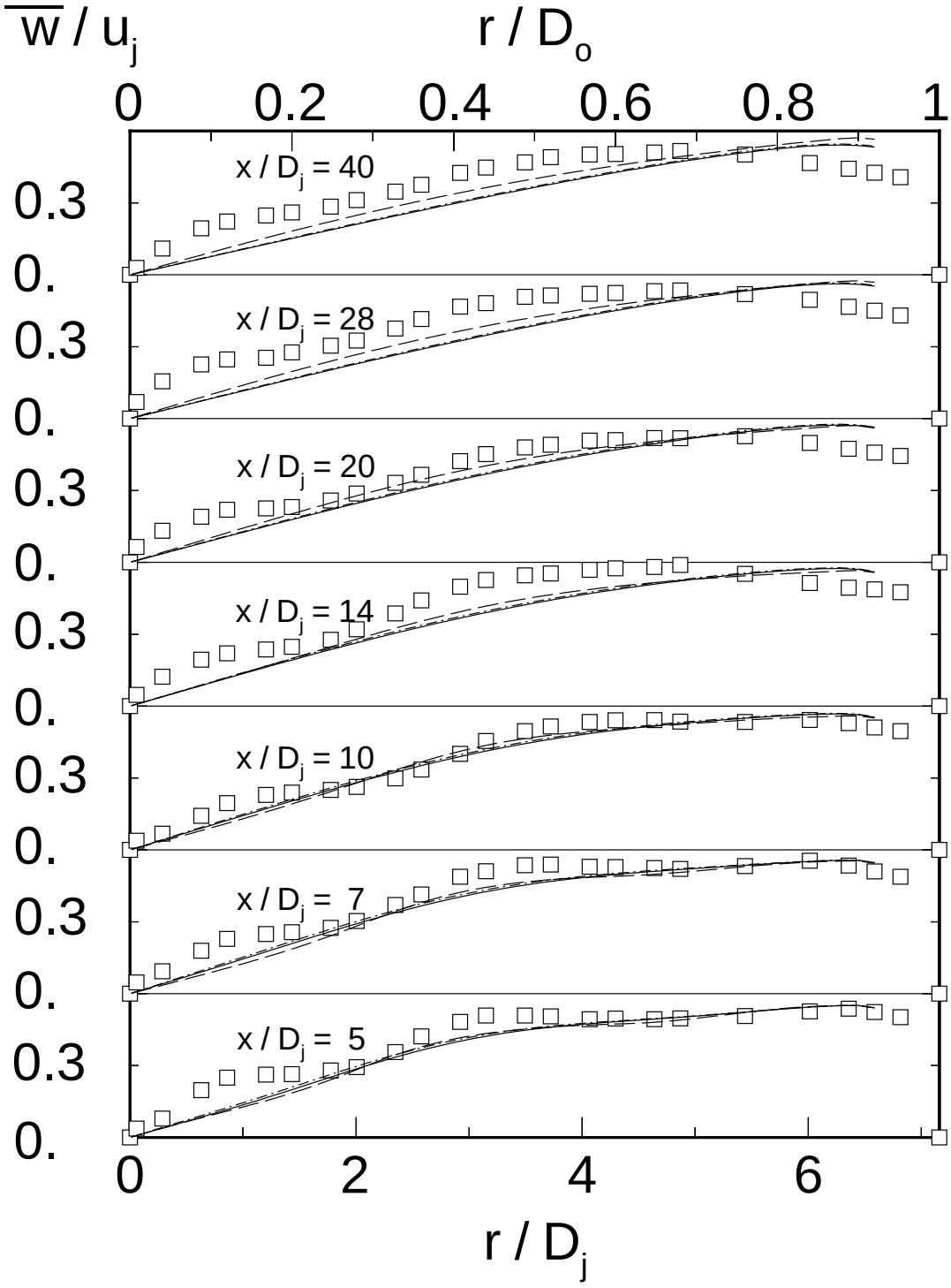

Figure 8: (TOP RIGHT)

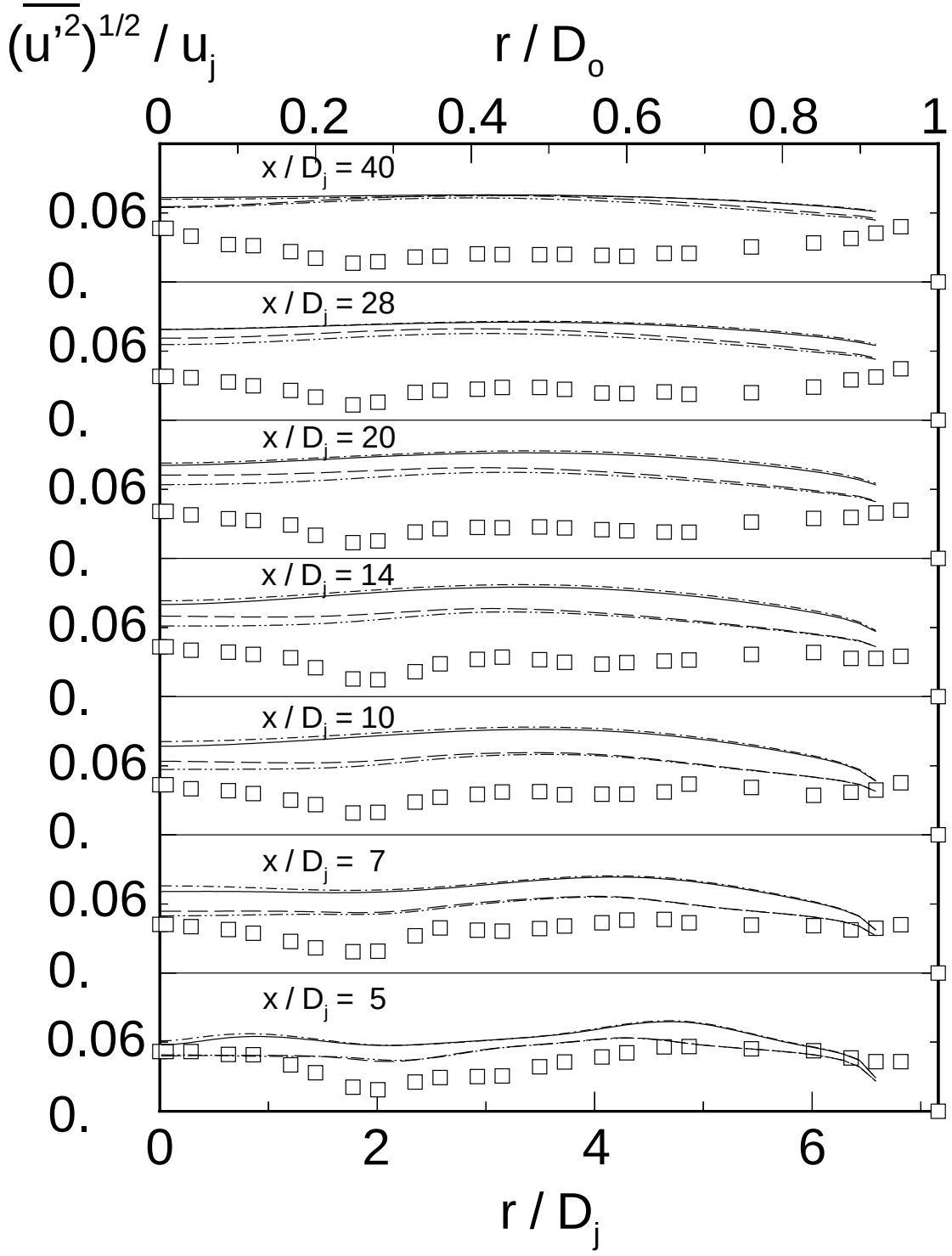

Figure 8: (BOTTOM LEFT)

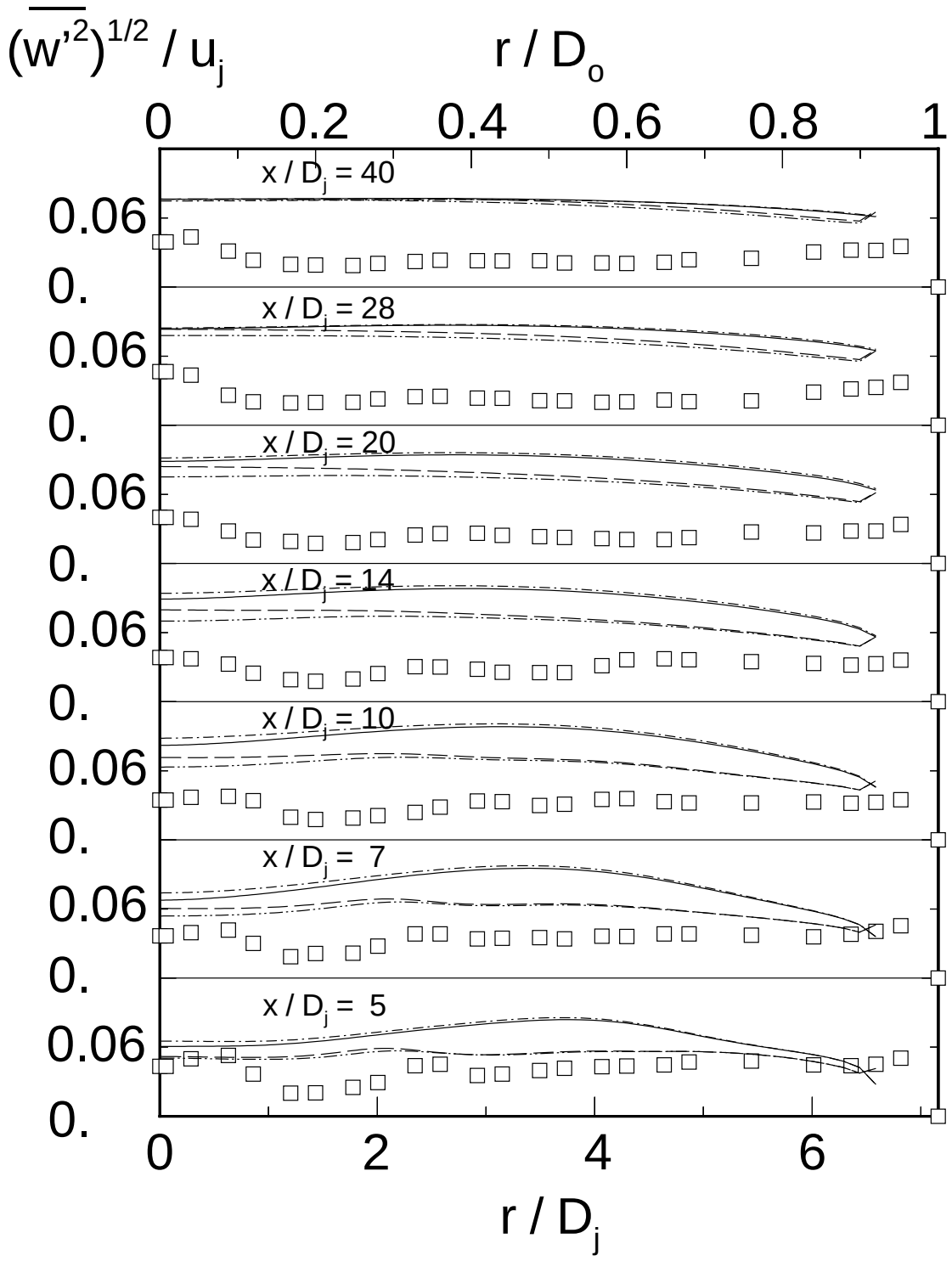

Figure 8: (BOTTOM RIGHT)

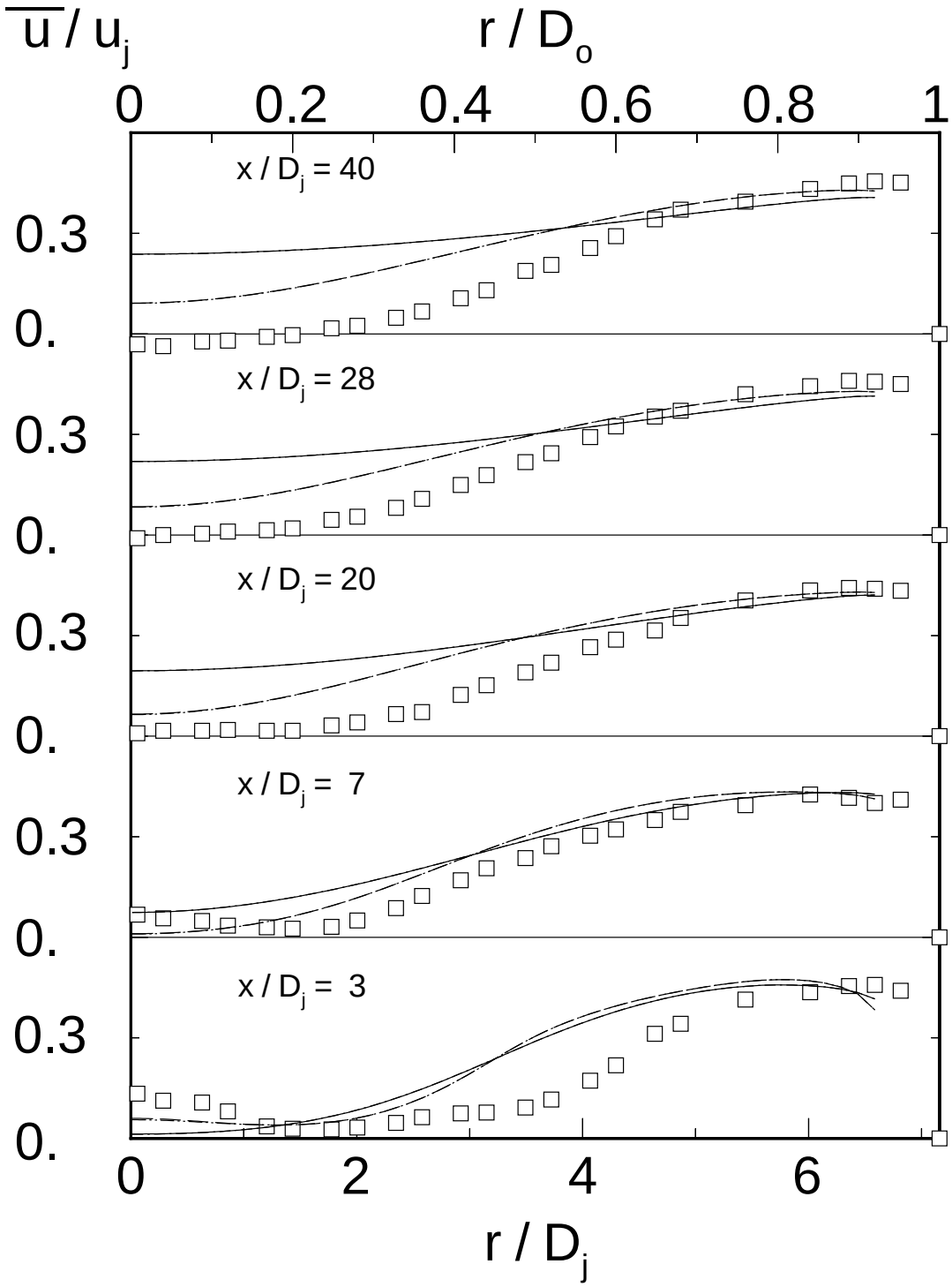

Figure 9: (TOP LEFT)

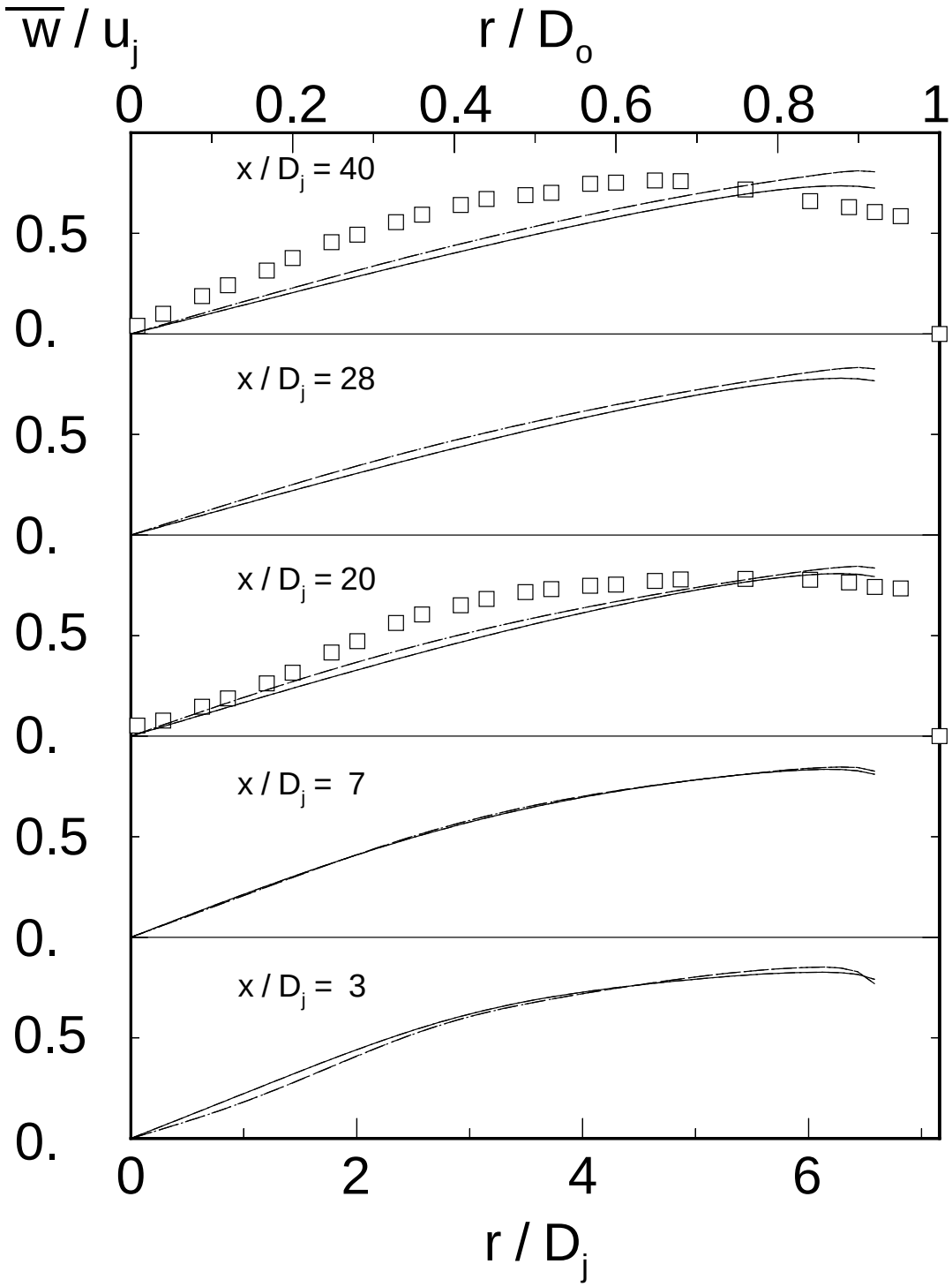

Figure 9: (TOP RIGHT)

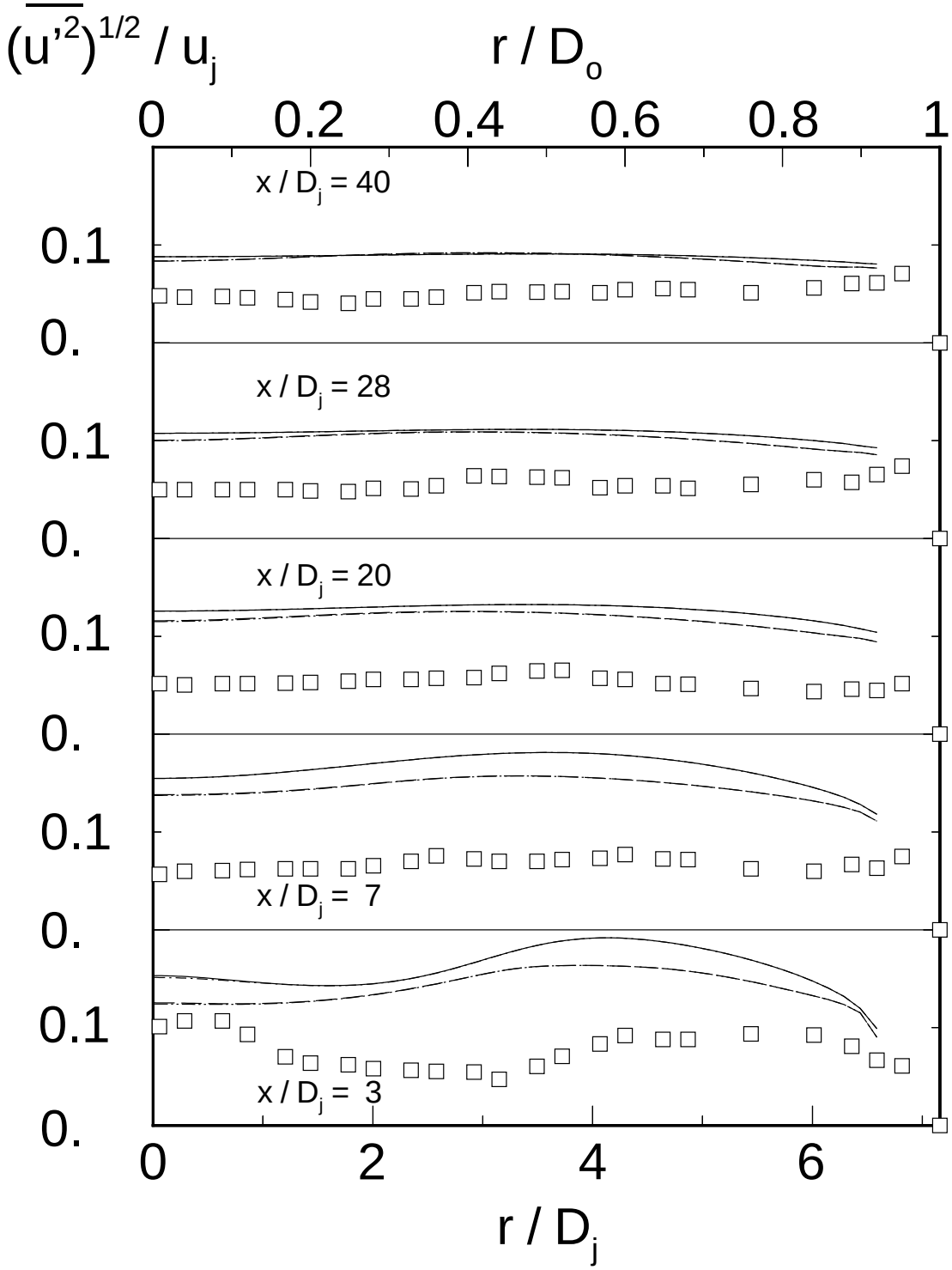

Figure 9: (BOTTOM LEFT)

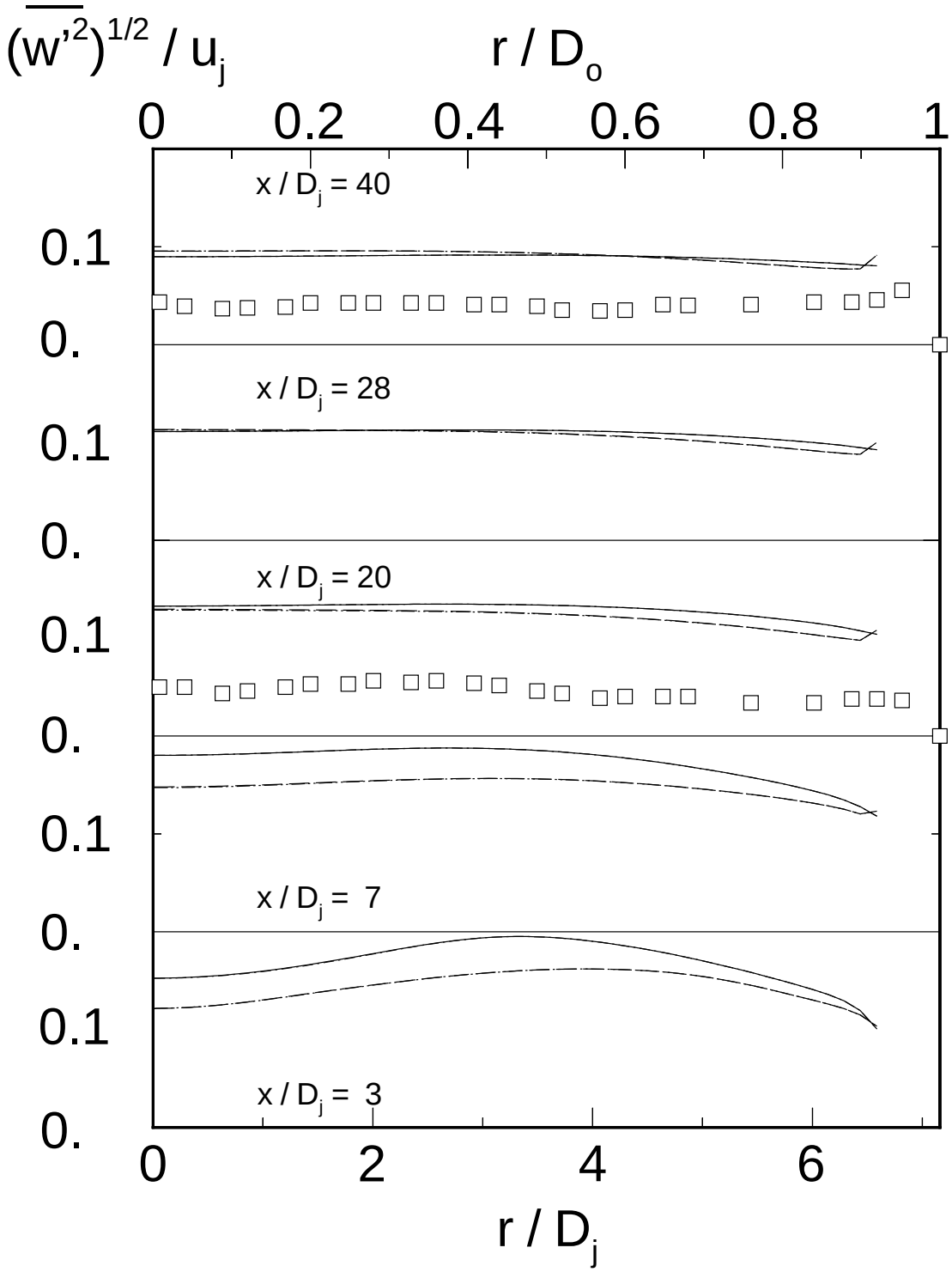

Figure 9: (BOTTOM RIGHT)

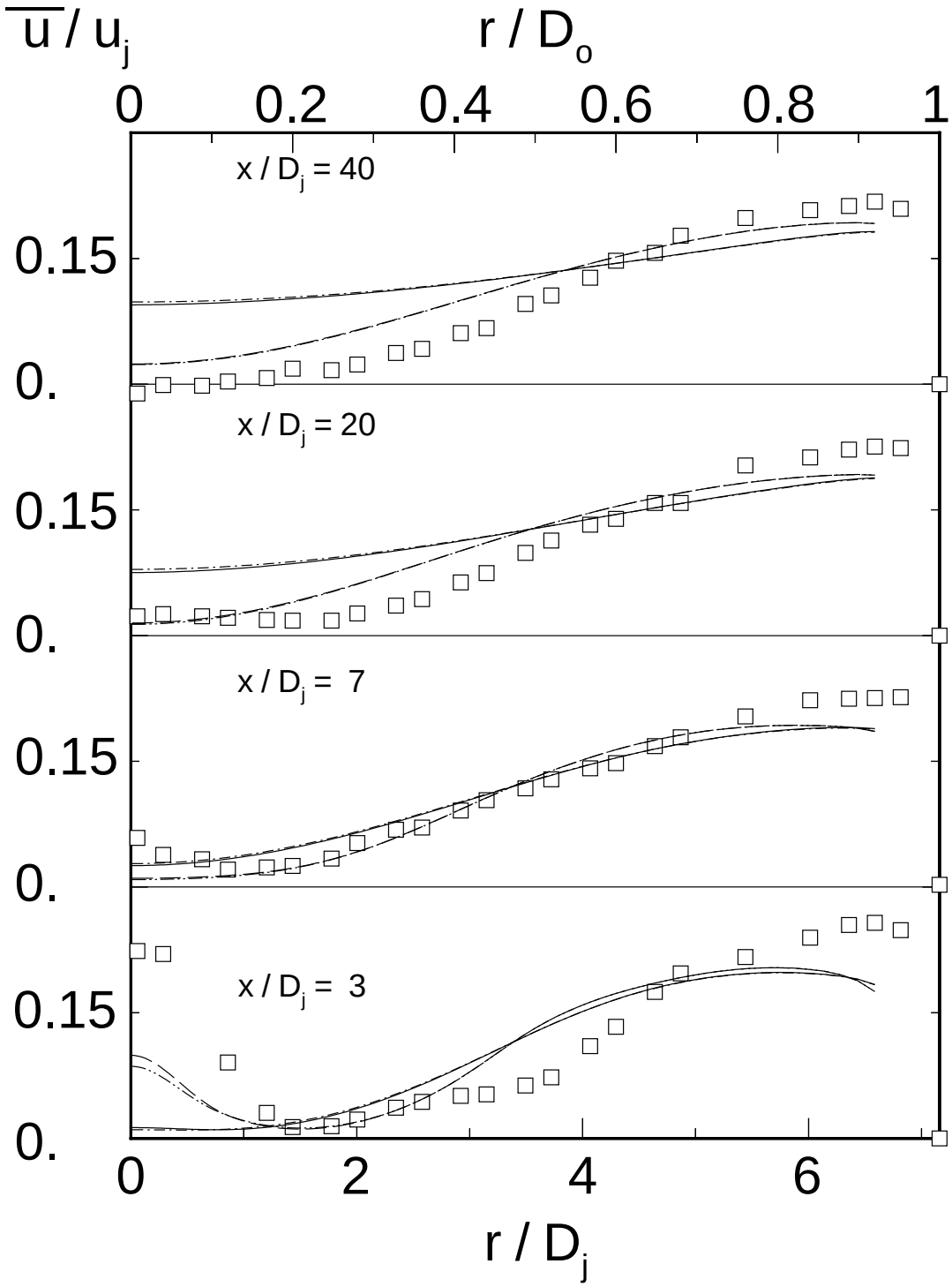

Figure 10: (TOP LEFT)

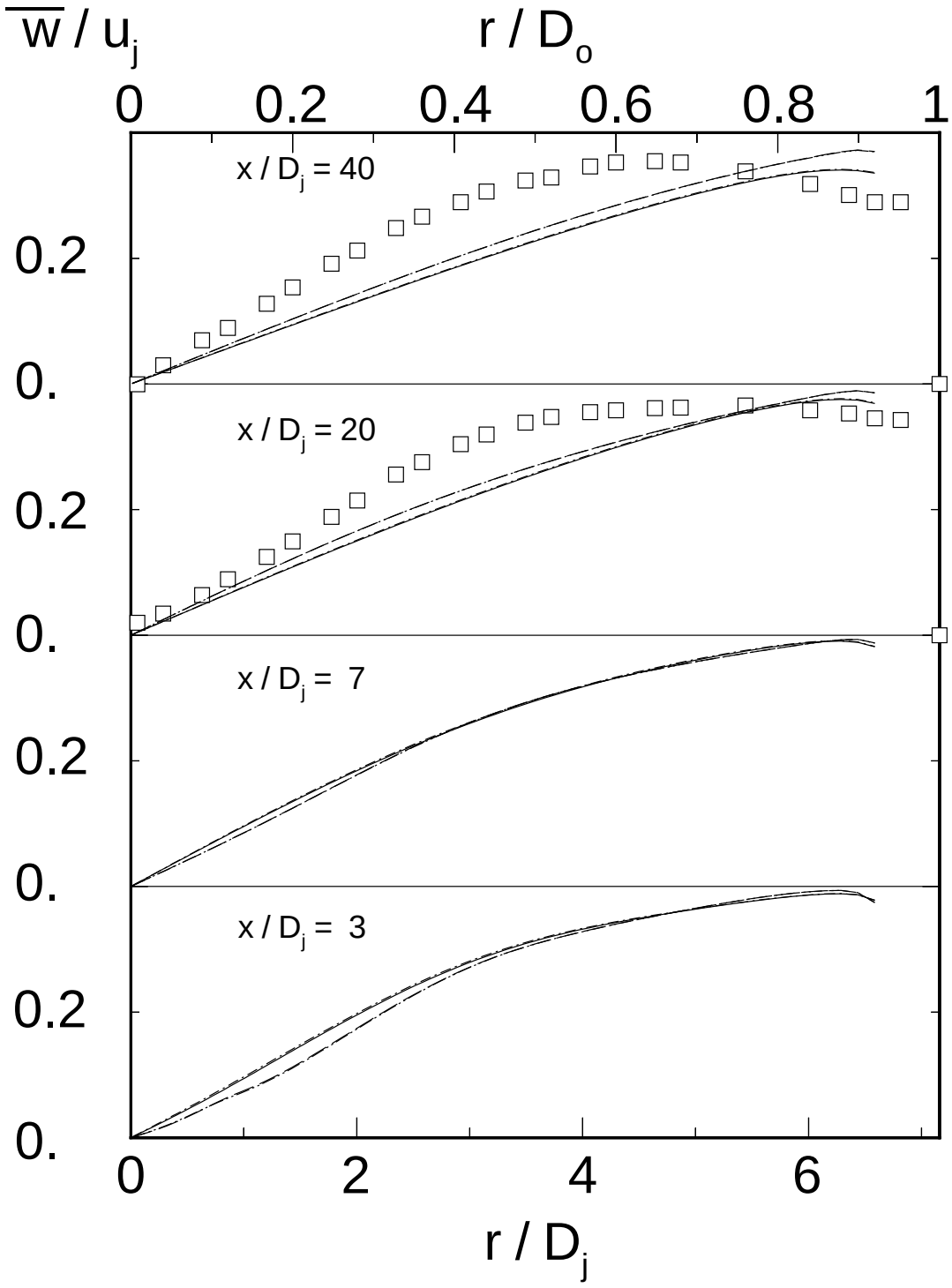

Figure 10: (TOP RIGHT)

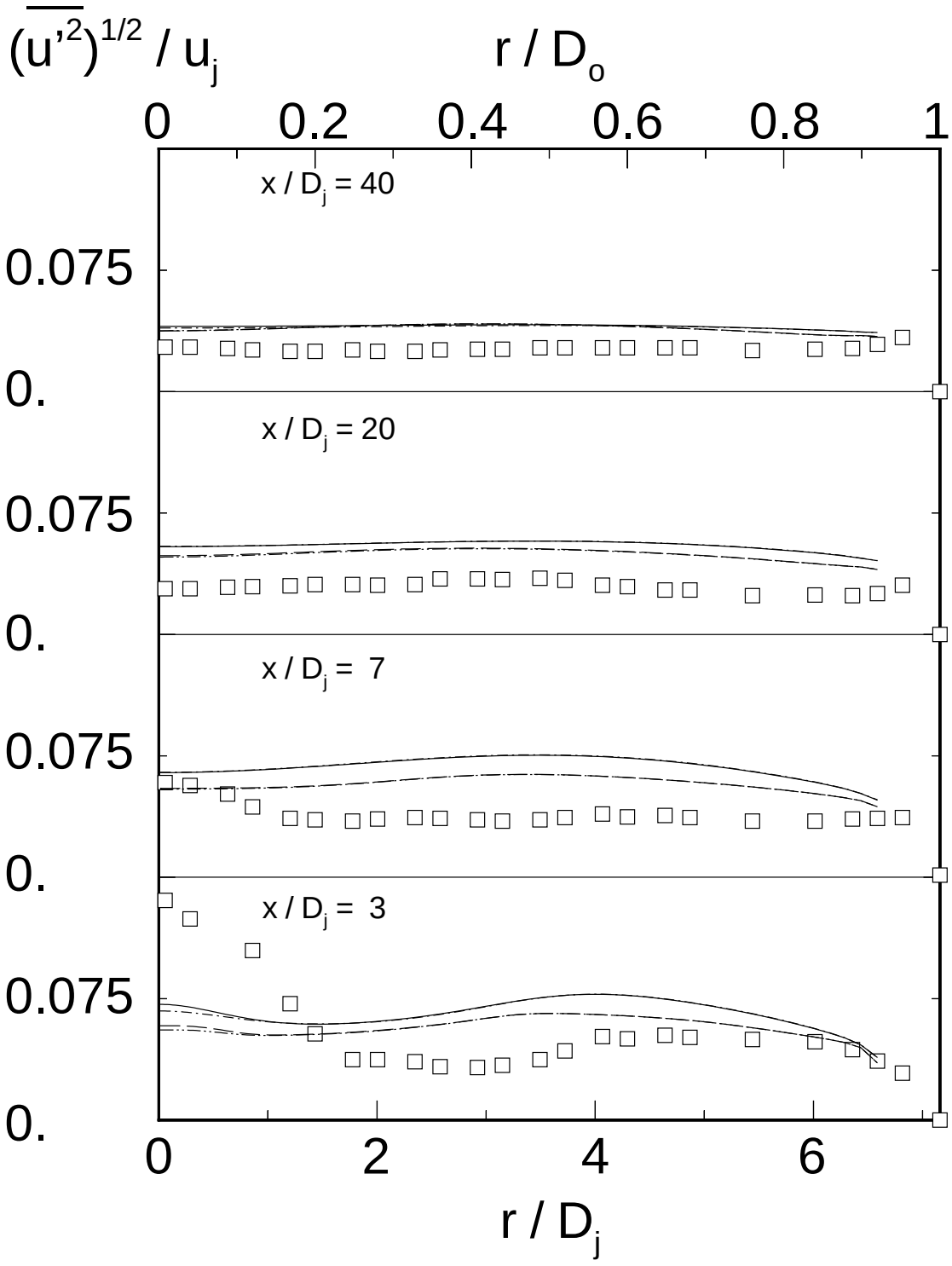

Figure 10: (BOTTOM LEFT)

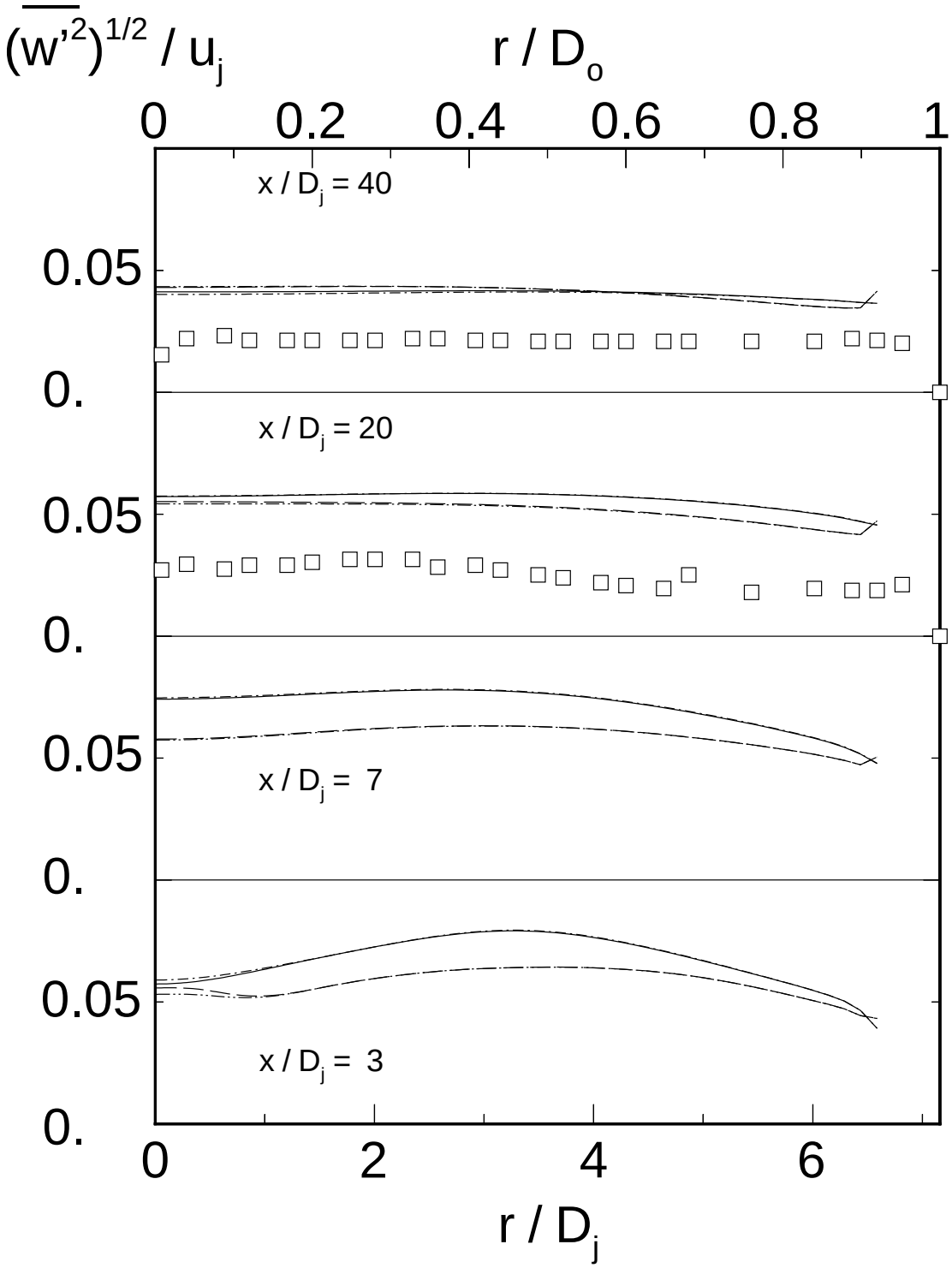

Figure 10: (BOTTOM RIGHT)

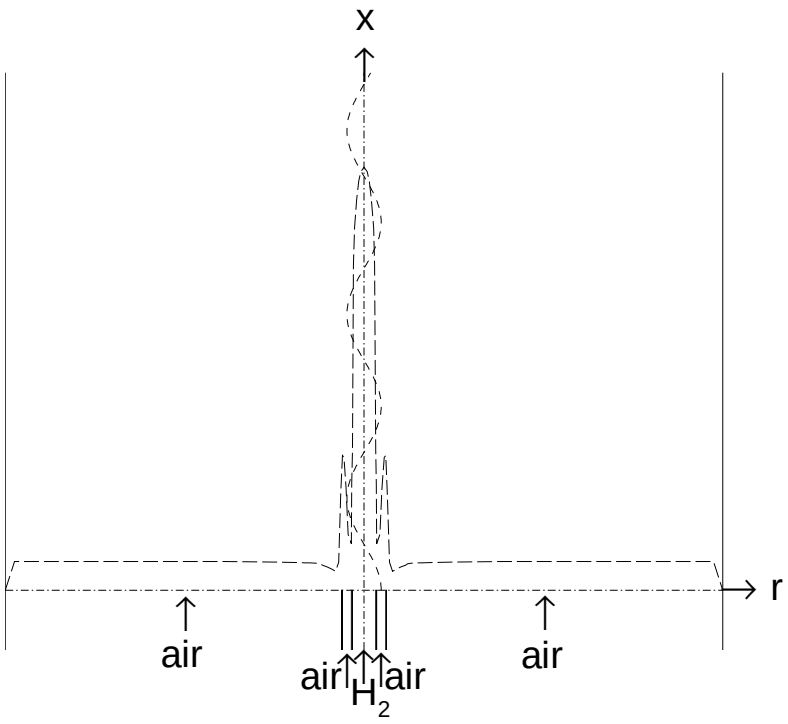

Figure 11:

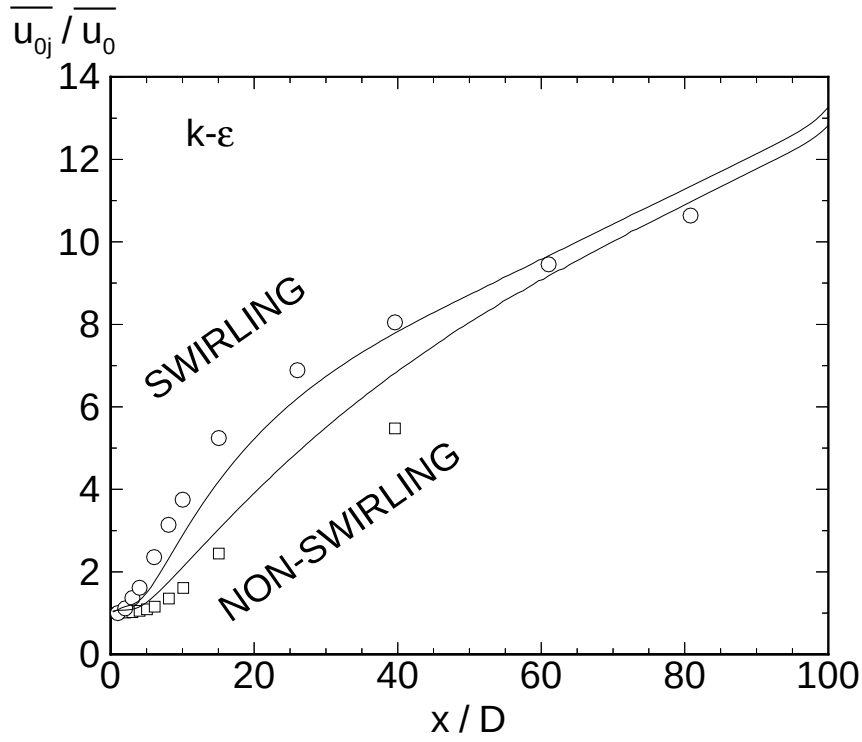

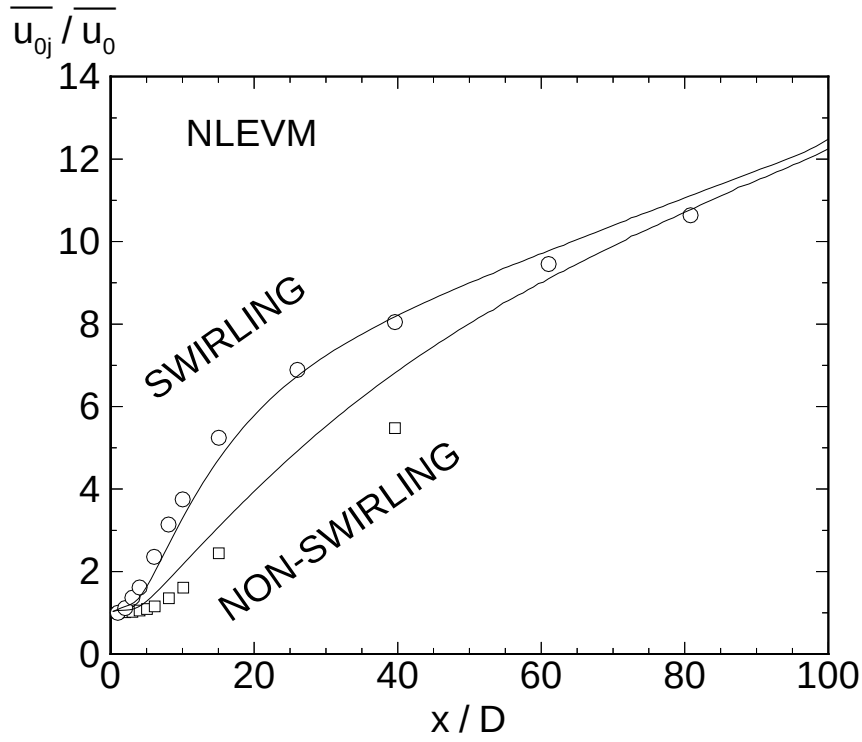

Figure 12: (FIRST PANEL)

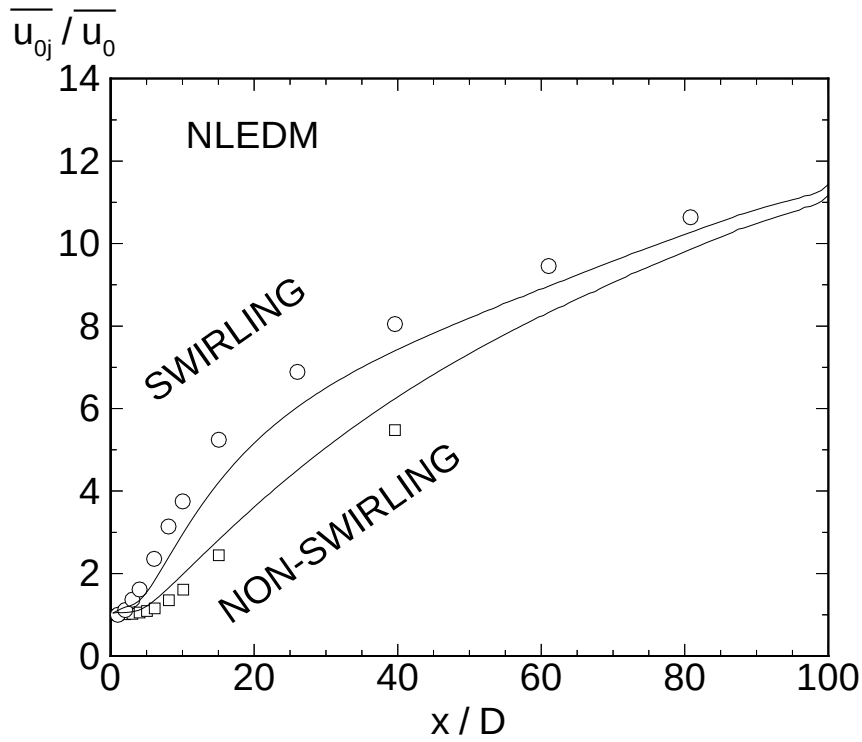

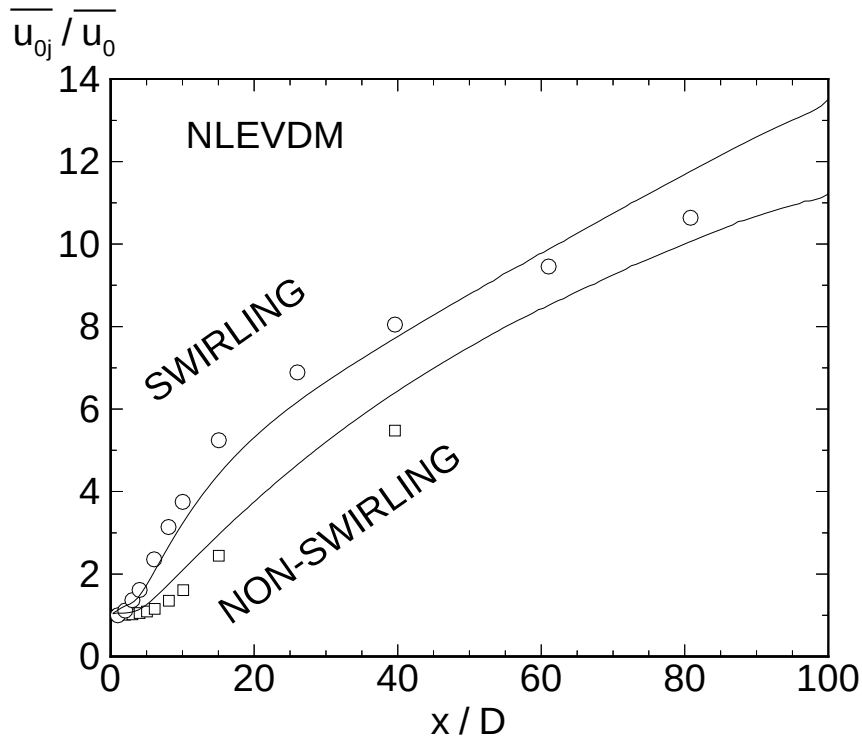

Figure 12: (SECOND PANEL)

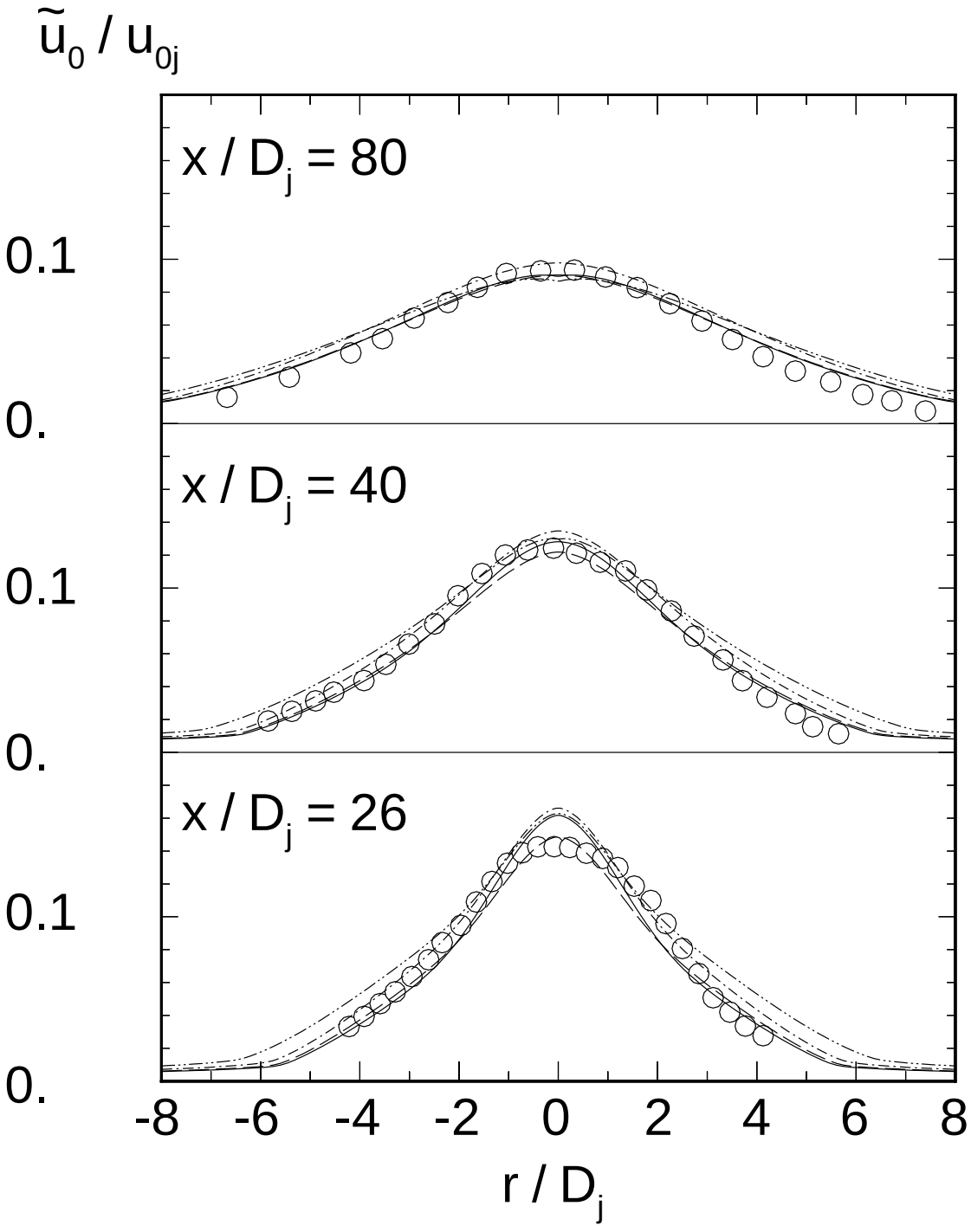

Figure 13: (TOP)

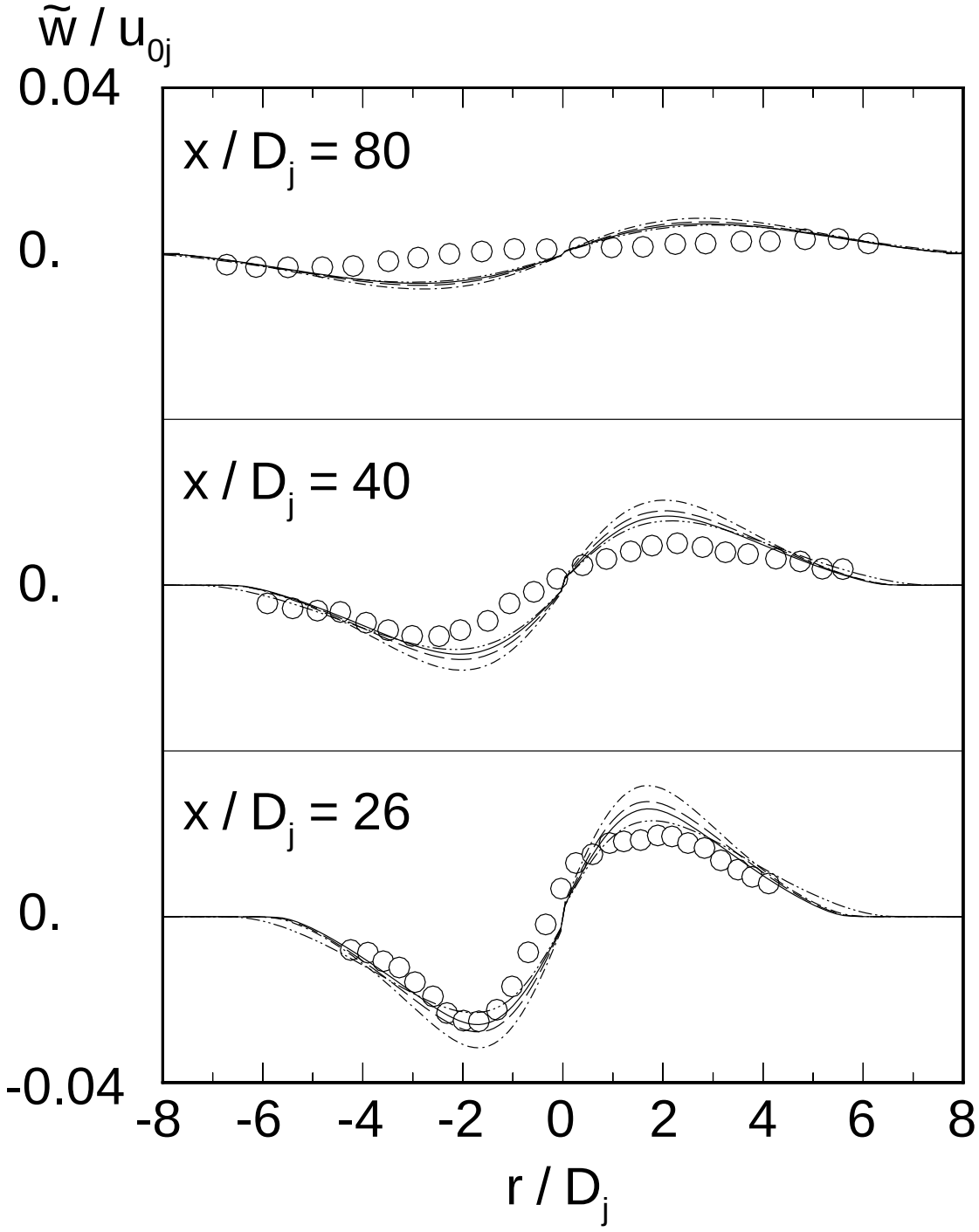

Figure 13: (BOTTOM)

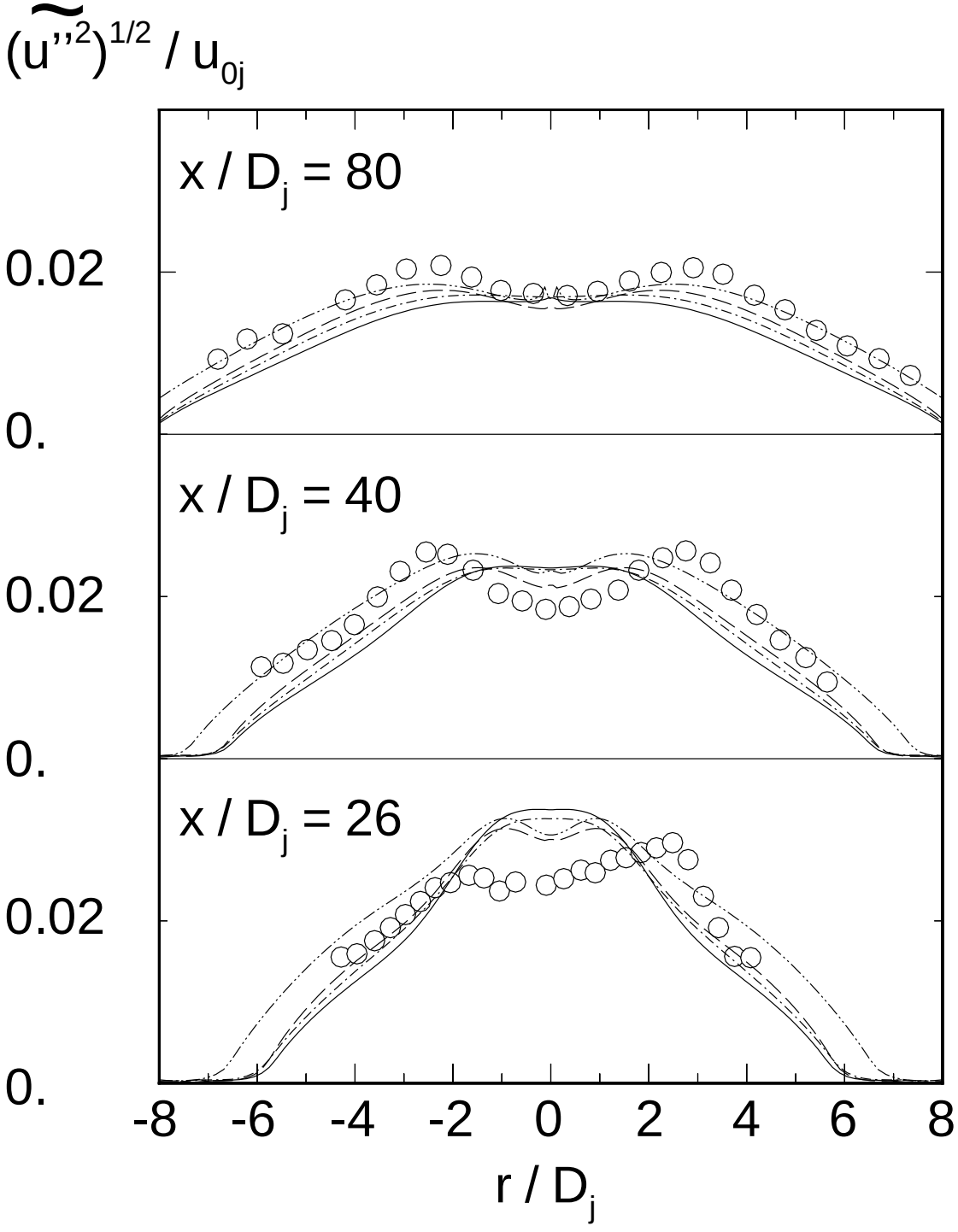
$(\widetilde{u''^2})^{1/2} / u_{0j}$
$x / D_j = 80$
$x / D_j = 40$
$x / D_j = 26$
0.02
0.
0.02
0.
0.02
0.
-8
-6
-4
-2
0
2
4
6
8
r / D_j

Figure 14: (a)

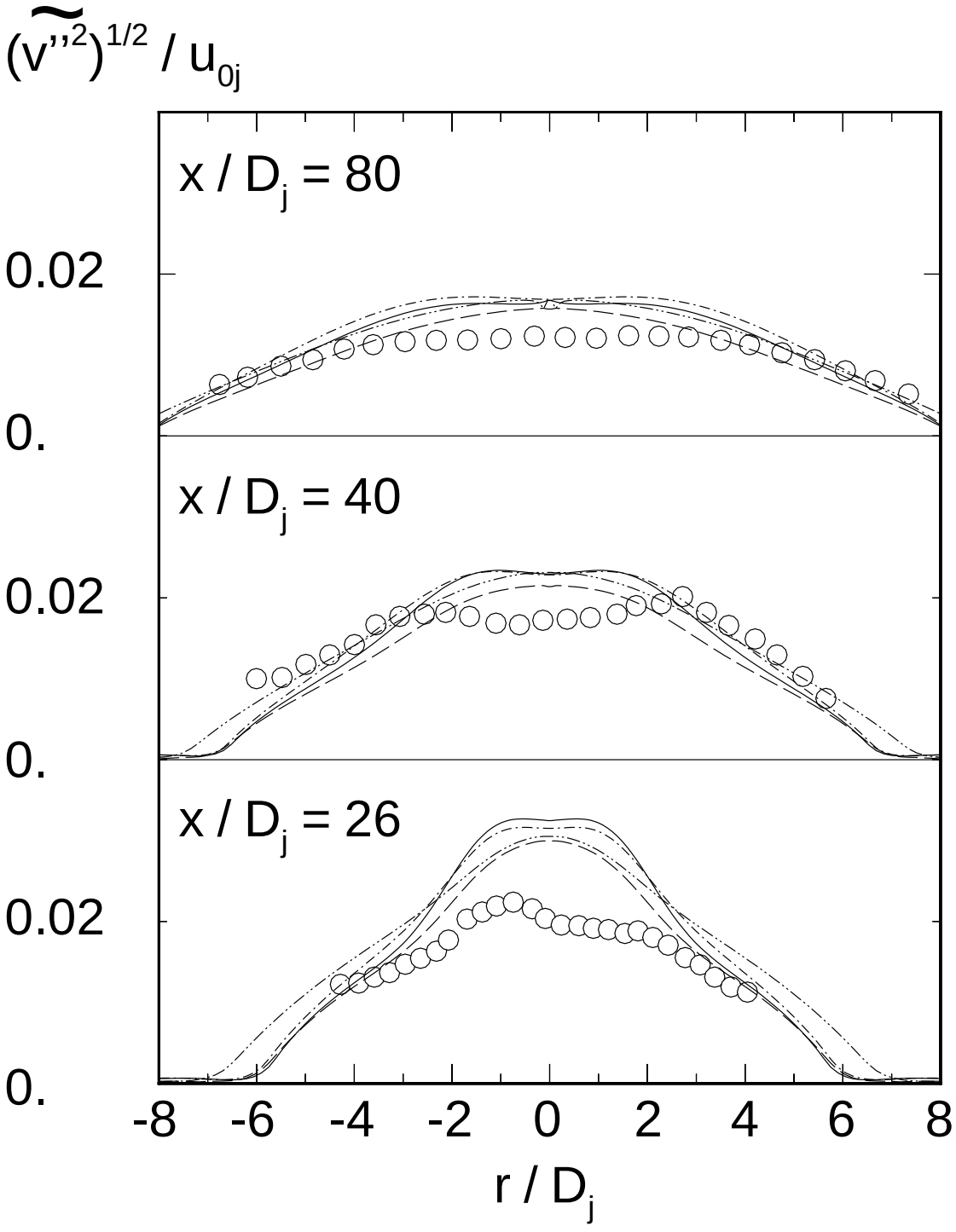
$(\widetilde{v''^2})^{1/2} / u_{0j}$
x / D_j = 80
x / D_j = 40
x / D_j = 26
0.02
0.
0.02
0.
0.02
0.
-8
-6
-4
-2
0
2
4
6
8
r / D_j

Figure 14: (b)

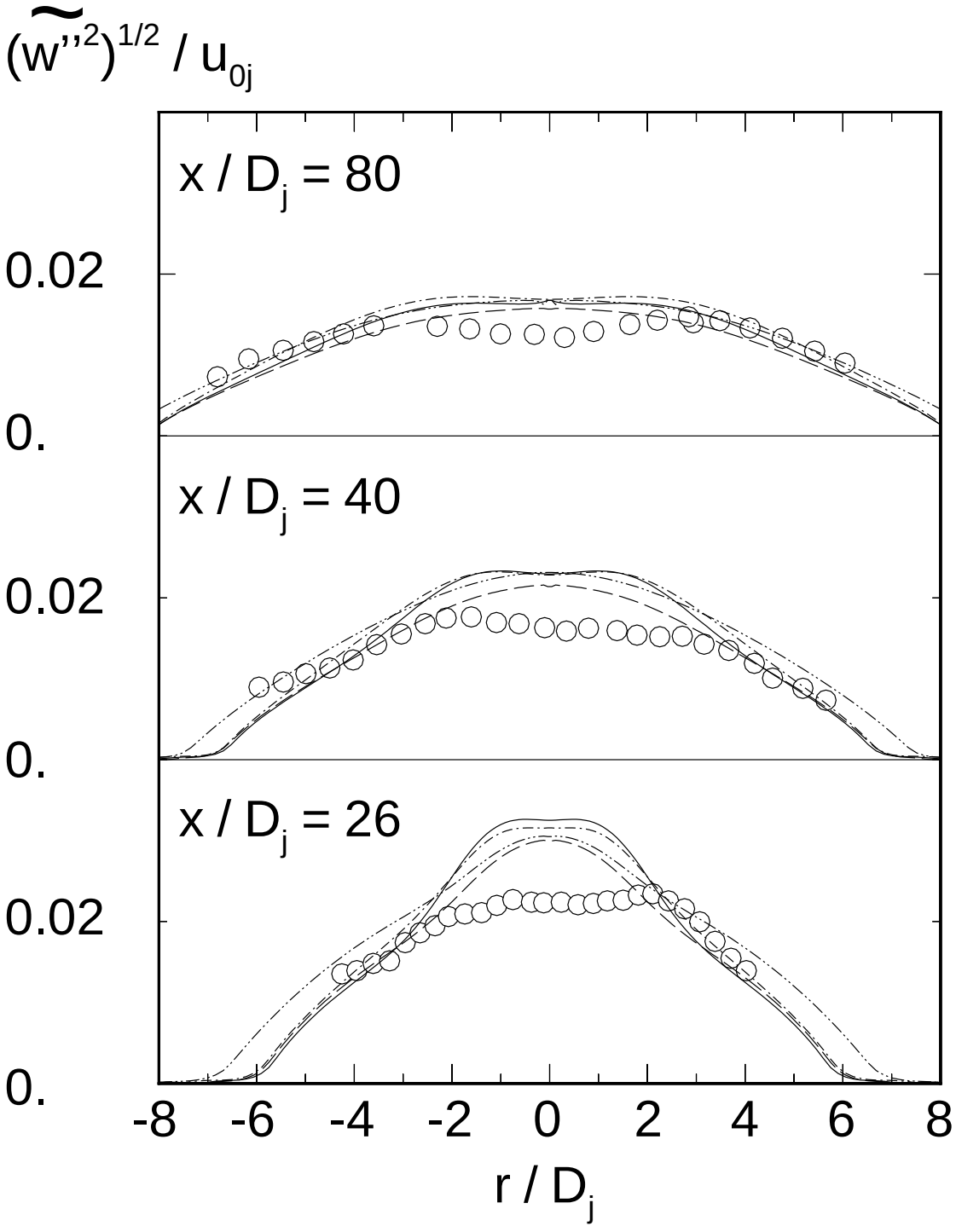
$(\widetilde{w''^2})^{1/2} / u_{0j}$
x / D_j = 80
x / D_j = 40
x / D_j = 26
0.02
0.
0.02
0.
0.02
0.
-8
-6
-4
-2
0
2
4
6
8
r / D_j

Figure 14: (c)

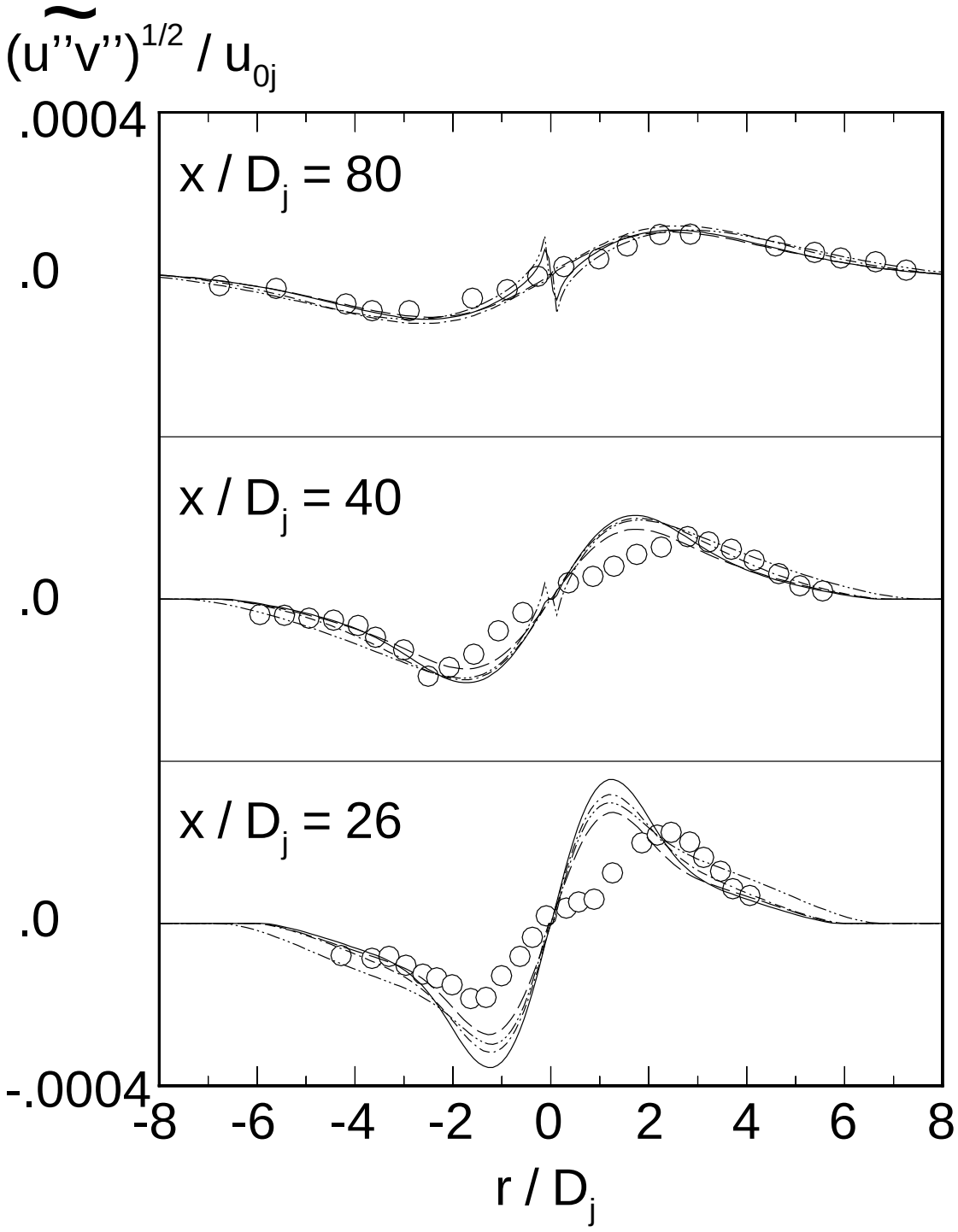
$(\widetilde{u''v''})^{1/2} / u_{0j}$
.0004
.0
-.0004
$x / D_j = 80$
$x / D_j = 40$
$x / D_j = 26$
.0
.0
-8
-6
-4
-2
0
2
4
6
8
r / D_j

Figure 14: (d)

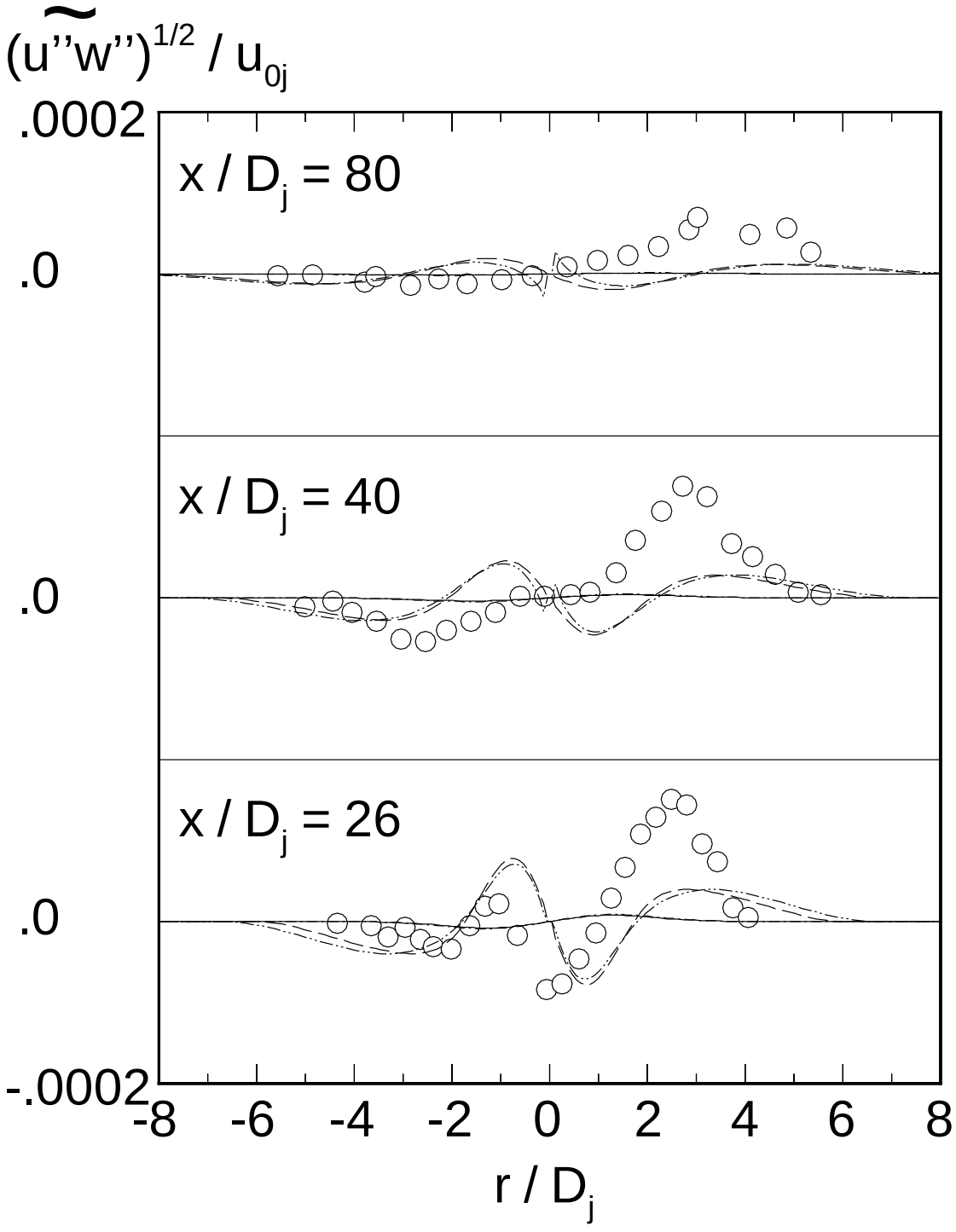
$(\widetilde{u''w''})^{1/2} / u_{0j}$
.0002
.0
-.0002
$x / D_j = 80$
$x / D_j = 40$
$x / D_j = 26$
.0
.0
-8
-6
-4
-2
0
2
4
6
8
r / D_j

Figure 14: (e)

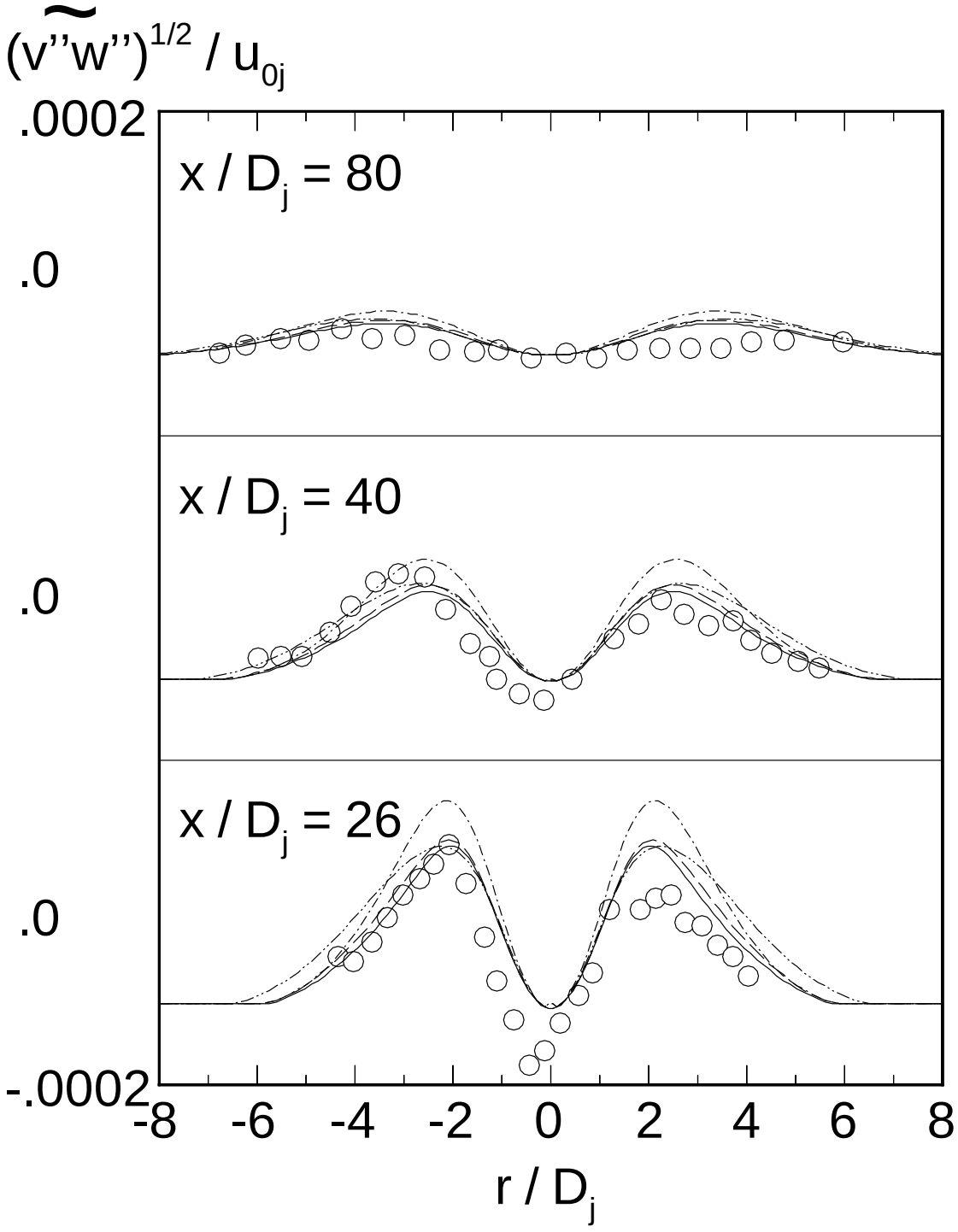
$(\widetilde{v''w''})^{1/2} / u_{0j}$
.0002
.0
x / D_j = 80
.0
x / D_j = 40
.0
x / D_j = 26
-.0002
-8
-6
-4
-2
0
2
4
6
8
r / D_j

Figure 14: (f)

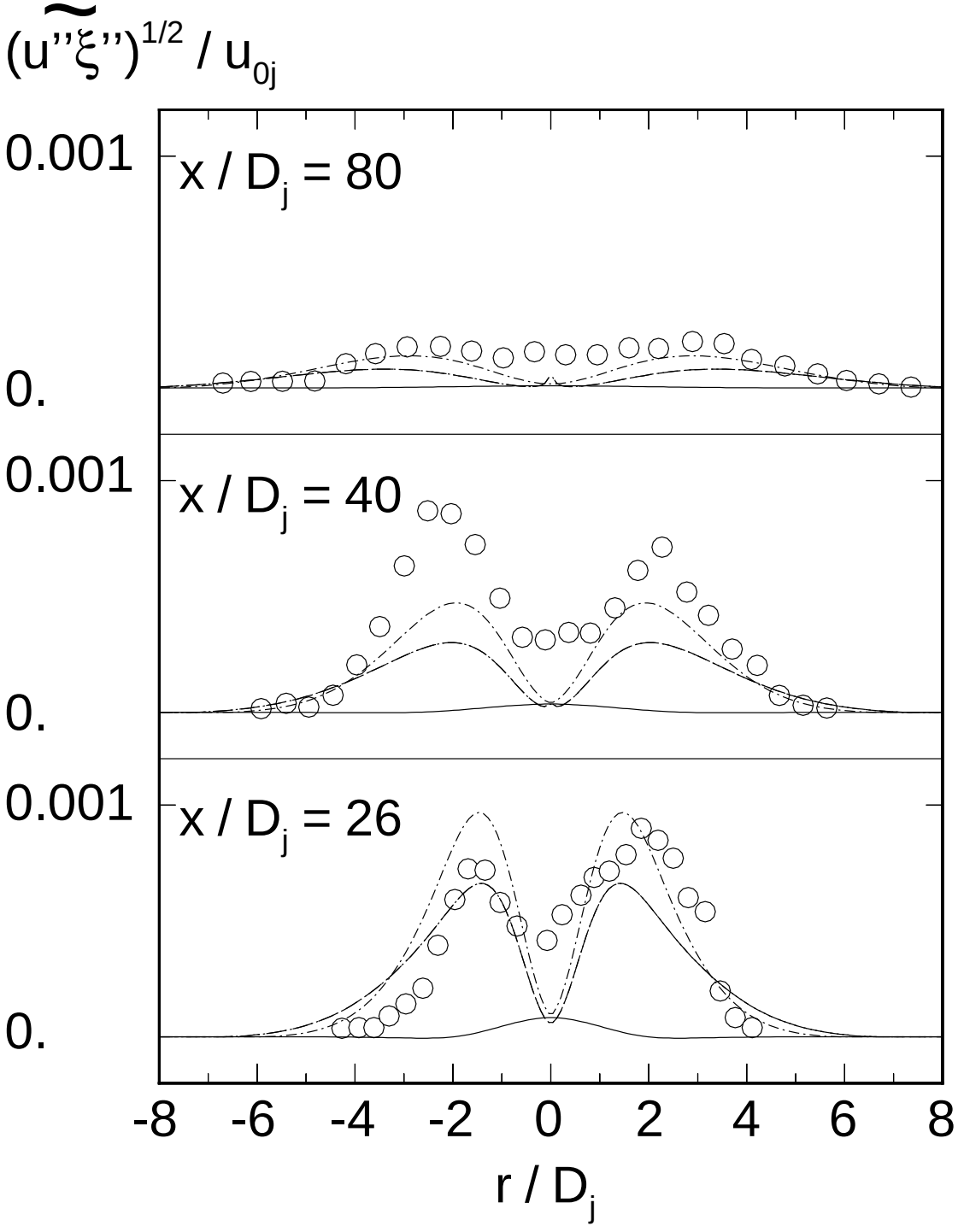
$(\widetilde{u''\xi''})^{1/2} / u_{0j}$
0.001
0.
0.001
0.
0.001
0.
$x / D_j = 80$
$x / D_j = 40$
$x / D_j = 26$
-8
-6
-4
-2
0
2
4
6
8
r / D_j

Figure 15: (a)

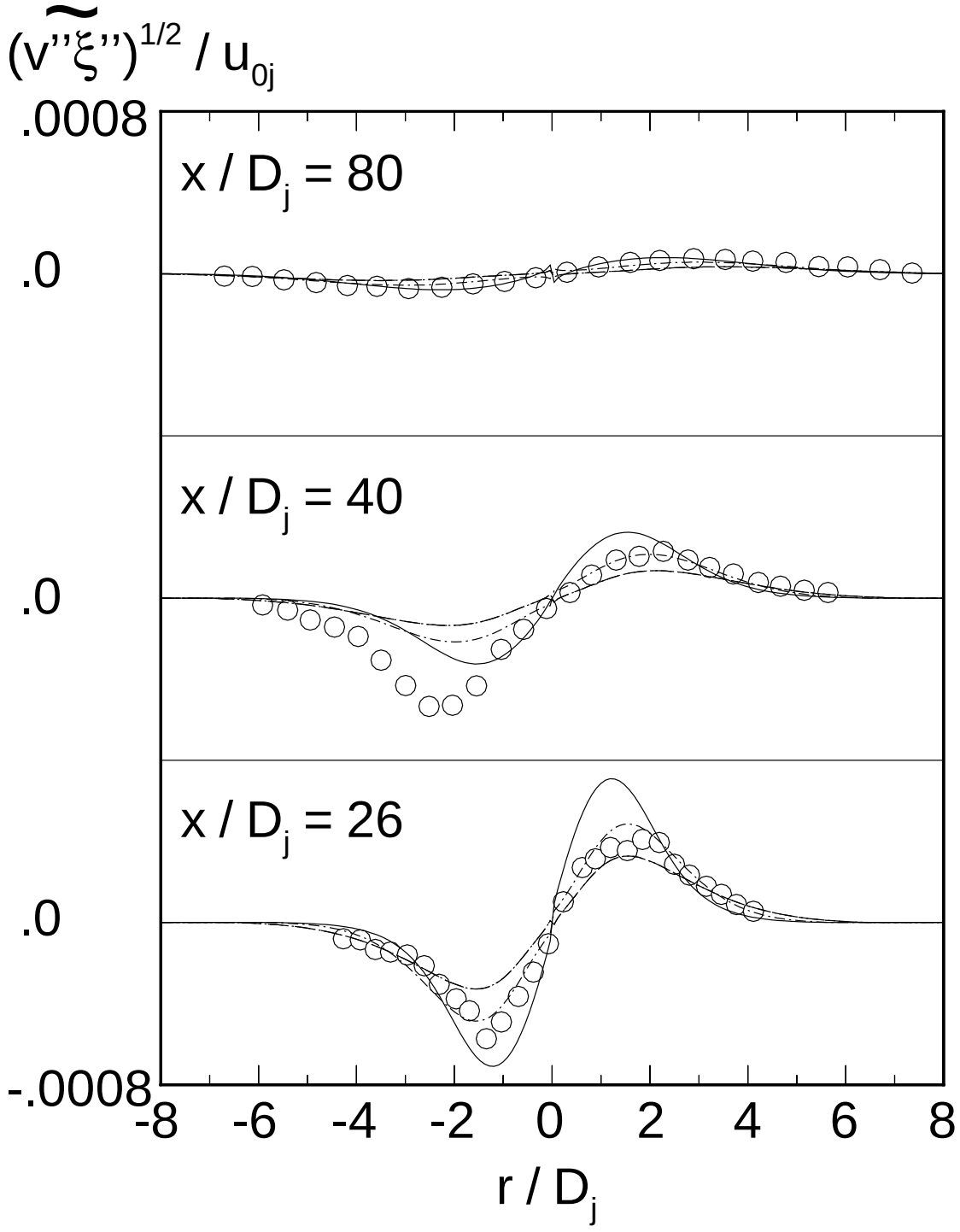
$(\widetilde{v''\xi''})^{1/2} / u_{0j}$
.0008
x / D_j = 80
.0
x / D_j = 40
.0
x / D_j = 26
.0
-.0008
-8
-6
-4
-2
0
2
4
6
8
r / D_j

Figure 15: (b)

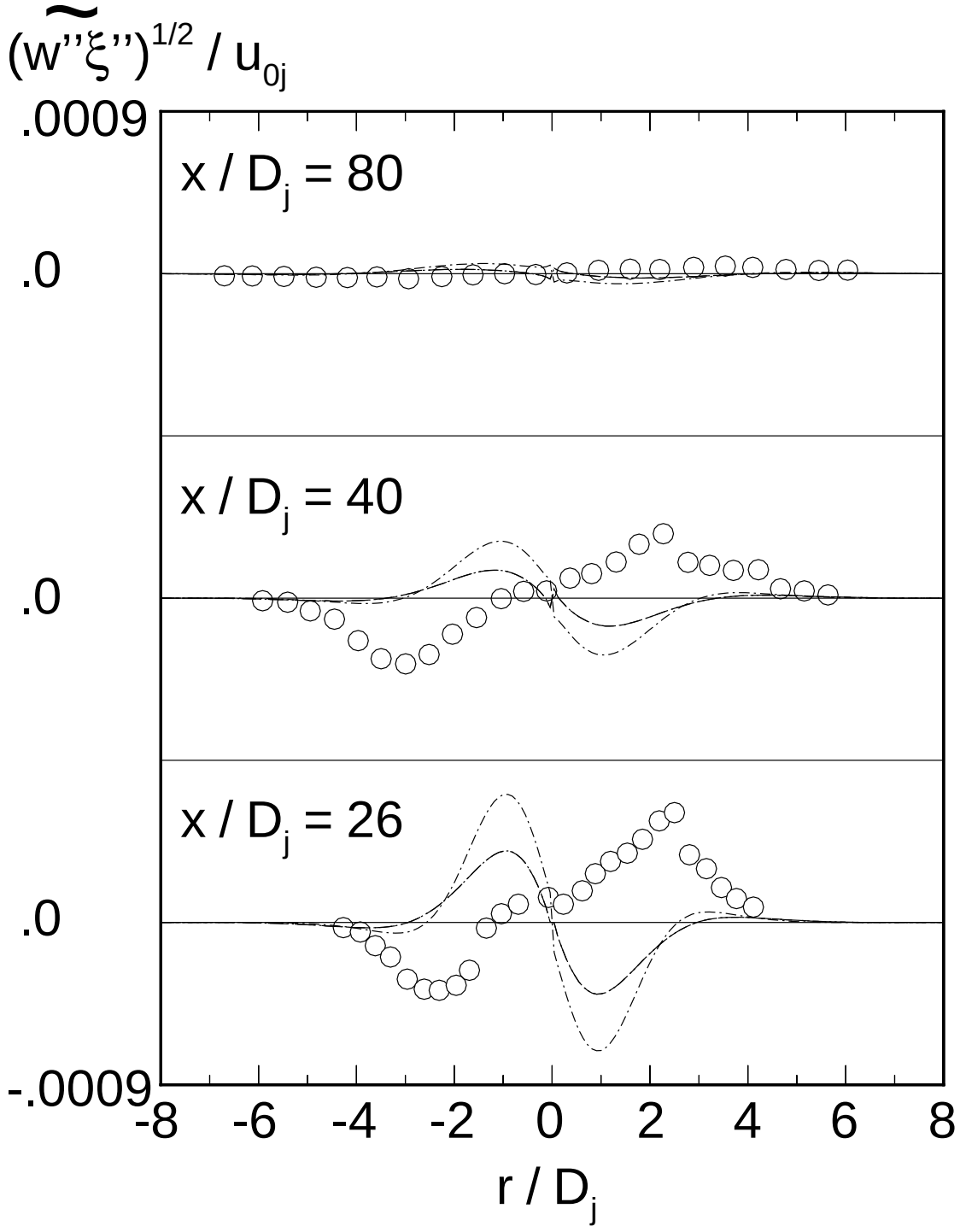
$(\widetilde{w''\xi''})^{1/2} / u_{0j}$
.0009
x / D_j = 80
.0
x / D_j = 40
.0
x / D_j = 26
.0
-.0009
-8
-6
-4
-2
0
2
4
6
8
r / D_j

Figure 15: (c)

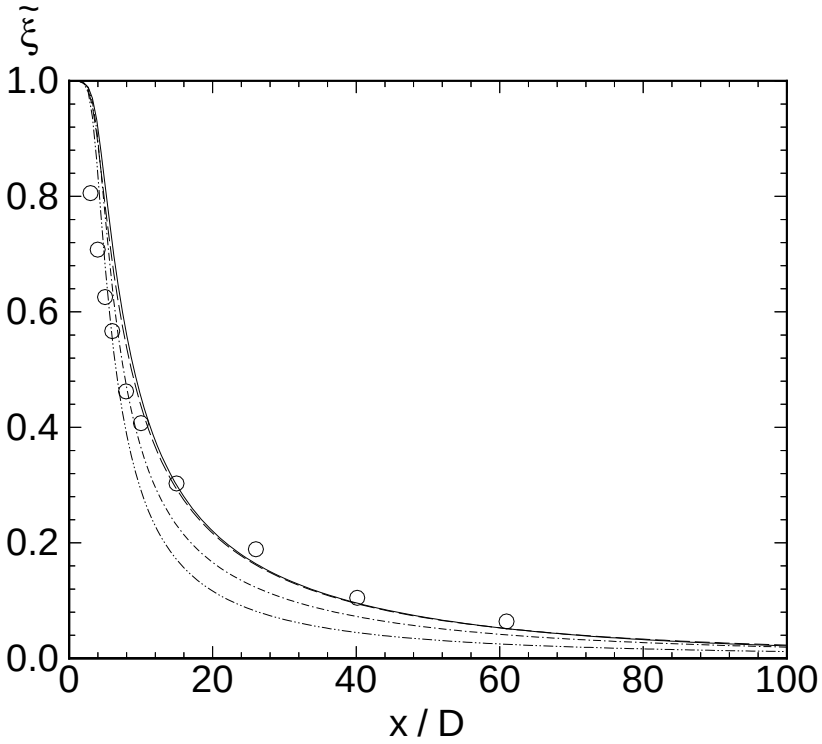

Figure 16: